SPECTROSCOPIC DETERMINATION OF GAS-WATER INTERACTIONS IN CLATHRATE HYDRATES

By

HUGH HILL RICHARDSON JR.

Bachelor of Science
Oral Roberts University
Tulsa, Oklahoma
1979

Master of Science
Oklahoma State University
Stillwater, Oklahoma
1982

Submitted to the Faculty of the Graduate College
of the Oklahoma State University
in partial fulfillment of the requirements
for the Degree of
DOCTOR OF PHILOSOPHY
July, 1985

SPECTROSCOPIC DETERMINATION OF GAS-WATER INTERACTIONS IN CLATHRATE HYDRATES

Thesis Approved:

J Paul Barker
Thesis Adviser

M E Rockley

Richard L Burrell

E J Evans

Norman N. Durham
Dean of the Graduate College

ACKNOWLEDGMENTS

There are many factors that contributed to my educational experience at Oklahoma State University and I wish to summarize some of them. I appreciate and am thankful for the facilities that the State of Oklahoma has provided so that the research undertaken in this thesis could be done. I realize that without the hard work on the part of my major adviser (Dr. Devlin) obtaining a quality research laboratory, that the completion of my Ph.D. degree would be seriously impaired. For this accomplishment, and for his mastery of the subject of chemistry, my thesis adviser has won my respect, but more than that, because of his genuine giving and friendship he has won my love and admiration.

I would like to express my gratitude to Gary Ritzhaupt for teaching me the "tricks of the trade". No problem was too small or question too dumb that I could not count on Gary's help. I would also like to thank Dr. Rockley for initiating me to the world of research. To my friends, M. P. Sudhakaran, Rick Snelling, Wayne Vinson and Charles Smith, thanks for helping me over some rocky roads.

Last of all, I would like to acknowledge the contribution that my family has made in helping me accomplish this goal. Without them this endeavor would not have been possible.

TABLE OF CONTENTS

LIST OF TABLES

LIST OF FIGURES

CHAPTER I

HISTORICAL PERSPECTIVE

Clathrate hydrates are a class of inclusive compounds in which guest molecules are entrapped in cages made up of hydrogen bonded water molecules. The entrapped molecules are not bonded to the hydrate lattice and only at low temperature are not freely rotating.

Hymphrey Davey in the Bakerian lecture to the Royal Society of London reported for the first time the existence of clathrate hydrates in 1810 (1). He observed that an aqueous solution of chlorine and water froze at a higher temperature than water did itself. This study was followed up by Faraday in 1823 (2). He speculated that the solid formed had the composition $Cl_2 \cdot 10.0\ H_2O$ but he realized that there was a possibility that the chlorine content was underestimated because of incomplete drying or loss of gas during the analysis. This was indeed the case because the hydration number of the chlorine clathrate hydrate is 7.05 (3). There was considerable controversy about the composition of the newly discovered clathrate hydrates because of the difficulty in obtaining accurate compositional information and the assumption of whole number stoichiometry (4).

In 1919 Scheffer and Meyer devised an accurate method of determining clathrate hydrate compositions (5). They applied the Clapeyron equation along both the hydrate-ice-gas (h-i-g) and hydrate-liquid-gas (h-l-g) curves to determine the hydrate composition at the intersection.

Despite a large volume of data which indicated non-whole number stoichiometry for the composition of the clathrate hydrate the tendency to assign the nearest whole number persisted as recently as 1950 when the composition of ethylene hydrate was assigned the composition of $C_2H_4 \cdot 7.0\ H_2O$ instead of $C_2H_4 \cdot 6.71\ H_2O$ which was determined experimentally (6).

Structure of the Clathrate Hydrate

There are basically two types of clathrate hydrates - type I and II. There are 46 water molecules in the unit cell for the type I hydrate and 136 water molecules in the type II hydrate. The oxygen are positioned in an orderly arrangement with Pm3n symmetry in the type I and Fd3m symmetry in the type II. The unit dimensions and geometry have been determined by x-ray crystallography and some of the parameters are presented in Table I (4). In contrast to this, the hydrogen positions do not follow an orderly arrangement and thus the clathrate hydrates are considered as disordered crystals. The positions of the hydrogen atoms are similar to the disordered arrangement that is found in cubic ice. The arrangement of the hydrogens in cubic ice as well as the clathrate hydrates are constrained to conform to the Bernal-Fowler rules (at least to a first approximation). Linus Pauling has summarized these rules in his discussion on the entropy in crystalline ice (7).

(1) In ice each oxygen atom has two hydrogen atoms attached to it at distances of about 0.95 $\mathring{A}$, forming a water molecule, the HOH angle being about 105^{o} as in the gas molecule.

TABLE I

GEOMETRY OF UNIT CELLS AND CAGES

	Structure I	Structure II
Space group, cell parameter	Pm3n, 12.03 Å	Fd3m, 17.31 Å
Number of H_2O molecules	46	136
Nonequivalent O sites	6(c), 16(i), 24(k)	8(a), 32(e), 96(g)
Oxygen site symmetry	$\bar{4}$2m, 3m, m	$\bar{4}$3m, 3m, m
Departure of O--O--O angle from tetrahedral:		
Average at O site	1.2°, 1.2°, 5.1°	0°, 2.1°, 3.6°
Average in structure	3.7°	3.0°
Average O--O length, Å	2.793	2.790
Small cages:		
Number, symmetry	2, m3	16, $\bar{3}$m
Oxygen sites	8(i), 12(k)	2(a), 6(e), 12(g)
Distance to center, Å	3.83, 3.96	3.748, 3.845, 3.956
Average cage radius, Å	3.91	3.902
Large cages:		
Number, symmetry	6, $\bar{4}$2m	8, $\bar{4}$3m
Oxygen sites	4(c), 8(i), 8(k), 4(k)	4(e), 12(g), 12(g)
Distance to center, Å	4.25, 4.47, 4.06, 4.645	4.729, 4.715, 4.635
Average cage radius, Å	4.33	4.683

(2) Each water molecule is oriented so that its two hydrogen atoms are directly approximately toward two of the four oxygen atoms which surround it tetrahedrally, forming hydrogen bonds.

(3) The orientation of adjacent water molecules are such that only one hydrogen atom lies approximately along each oxygen-oxygen axis.

(4) Under ordinary conditions the interaction of non-adjacent molecules is not such as to appreciably stabilize any one of the many configurations satisfying the preceding conditions with reference to the others.

Because there are many different configurations which will be possible using the above constraints no two adjacent unit cells will be alike and there is no long range order in the crystal. It is for this reason that cubic ice and the clathrate hydrates are considered disordered crystals.

Type II clathrate hydrates have compositions near $M \cdot 17\ H_2O$ whereas, type I hydrates have a variable composition starting at a hydration number of 5.75 which represents the composition in which all of the cages are filled with guest molecules and the hydration number decreases as the cages are depleted. Type II hydrates (see Table I) have 16 small cages (12 hedral) and 8 large cages (16 hedral) per unit cell. The hydration number of 17 represents the configuration in which 8 of the cages are filled. Since the guest molecules that form type II hydrates are larger than the average small cage radius (3.902 Å) only the large cages are filled and usually they are fully occupied. The type I hydrates have 2 small cages (12 hedral) and 6 large cages (14

hedral). If the clathrate hydrate theoretically loses all of the guest molecules but still remains in its crystalline form then it is in its metastable "empty lattice" configuration. The pressure at a particular temperature where the clathrate hydrate is in equilibrium with the guest vapor phase is known as the dissociation or decomposition pressure.

A definite correlation exists between the size of the guest molecule and the type of clathrate hydrate it will form. Guest molecules whose maximum molecular diameters are 5.3 Å or less still form type I clathrate hydrates whereas, molecular diameters in the range of 5.6-6.6 Å form type II clathrate hydrates. Not only is the type of clathrate hydrate determined by the size of the guest molecules but the composition of type I clathrate hydrates are as well. The H_2S molecule is small enough (4.1 Å) to fit into both the large and small cages. The H_2S clathrate hydrate has a hydration number of 6.119 which indicates that 94% of the large cages are filled and 94% of the small cages are filled (8). Ethylene oxide is a bigger molecule (maximum molecular diameter of 5.2 Å) and has trouble fitting into the small cages. This is reflected in a higher hydration number of 6.89 which was determined by freezing point measurements (9). The x-ray single crystal determination of the ethylene oxide hydrate showed that all of the large cages were filled and only 20% of the small cages were filled (10). In contrast to this, the freezing point measurements showed that 34% of the small cages are filled. The apparent discrepancy has been attributed to different concentrations of ethylene oxide solutions from which the hydrates were grown. One can see from the above discussion that the relative amounts of guest molecules which occupy the different

type of cages not only depends upon the size of the guest molecule, but the concentration or partial pressure of the guest molecules.

The average free space inside the cages has been calculated by Davidson (4) assuming the water molecule has a van der Waals radius of 1.4 Å. The 12 hedral small cages have a mean free diameter of 5.0 Å but the 14 hedral or 16 hedral large cages have a mean free diameter of 5.8 and 6.6 Å, respectively. This calculation shows why only 34% of the small cages are filled with ethylene oxide (molecular diameter 5.2 Å) but that 94% of the small cages are filled with H_2S (molecular diameter 4.1 Å). This correlation can be seen even more dramatically in the case of $CHClF_2$ (molecular diameter 5.4 Å) (8). The hydrate of $CHClF_2$ does not populate the small cages at all and has a hydration number of 7.939 at 0^oC (8).

The clathrate hydrate crystalline structure has many similarities to crystalline ice (I_c or I_h). Each water molecule is hydrogen bonded to its four nearest neighbors as in ice and the average departure from the tetrahedral angle (O-O-O) found in ice is only 3.7 and 3.0^o for the type I and II hydrates, respectively (4). In addition, the O-O bond lengths in the hydrate vary by only 1% from that which is found in cubic or hexagonal ice. The obvious difference between the clathrate hydrate and ice is the presence of cages in the hydrate. The cages appear to have almost spherical symmetry. The type II large cages have a variation in the cage radius from spherical symmetry of only 2% whereas the type II large cage shows a 14% deviation (11). Another structural difference between the clathrate hydrate and ice is the presence of planar (type II) and near planar (type I) five membered rings. The six membered rings are planar in the type I hydrates and

near planar in the type II hydrate. Cubic and hexagonal ice do not have any planar rings: all of the rings are puckered. The five membered rings are much more plentiful in the clathrate hydrate than are the six membered rings. The ratio of five to six membered rings in the type I and II hydrates are 8:1 and 9:1, respectively. If all the faces were exactly planar then this ratio should be 8.26:1 to make the average angle tetrahedral (4).

Theoretical Calculations

One of the first attempts to model the thermodynamic properties of the clathrates in general and clathrate hydrates in particular was detailed by van der Waals and Platteeuw (vdW and P) in 1959 (12). By using statistical mechanics and treating the guest molecules as solutes dissolved in solvent cages they were able to reproduce the known thermodynamic properties of noble gas clathrate hydrates. A brief synopsis of this theory will be presented because it is the framework from which much of the clathrate hydrate theory of today is built. Working through the grand partition function and classical thermodynamics they were able to relate the observed variables (P_K and U_Q) to two equations (1 and 2). It should be noted that the gas molecules have been treated as ideal gases.

$$(1)\quad P_K = y_{ki}/(C_{ki}*(1-\Sigma_J y_{Ji}))$$

$$(2)\quad U_Q = U_Q^{\beta} + KT*\Sigma_i v_i \ln(1-\Sigma_k y_{ki})$$

The following list defines the above variables.

N_Q => number of solvent molecules (Q => H_2O)

P_k => partial pressure of the K type of gas

C_{ki} => Langmuir constant, measure of the equilibrium constant which describes the distribution of the solute molecules between the gas and cages

y_{Ki} => the probability of finding a gas molecule K in a cavity of type i

Y_{Ji} => the probability of finding any solute molecule in a cavity of type i

U_a => chemical potential of the clathrate

U_Q^β => chemical potential of the empty clathrate lattice

v_i => number of cavities of type i per solvent Q

For the specific example of type I clathrate hydrate there are two types of cavities - small (i=1) and large (i=2). If these assumptions are made: (1) that an equilibrium exists between the ice, clathrate and gas and (2) there are only one type of solute gas A, then equations 1 and 2 can be cast into the form of equations 3 and 4.

$$(3)\quad y_{Ai} = C_{Ai}P_A/(1 + C_{Ai}P_A)$$

$$(4)\quad \sum_i v_i \ln(1 - y_{Ai}) = -\Delta U/kT$$

where ΔU is $U_Q^\beta - U_Q^\alpha$ and U_Q^α is the chemical potential of crystalline ice. The total solute content (Y_A) in moles of A per moles of Q in terms of the variables above is given by equation 5.

$$(5)\quad Y_A = \sum_i v_i y_{Ai}$$

For the two types of cavities in the type I clathrate hydrate these equations reduce to 6, 7, 8a and 8b.

$$(6)\quad y_{A1} = C_{A1}P_A/(1 + C_{A1}P_A);\quad y_{A2} = C_{A2}P_A/(1 + C_{A2}P_A)$$

$$(7)\quad v_1 \ln(1 - y_{A1}) + v_2 \ln(1 - y_{A2}) = \Delta U/kT$$

(8a) $Y_A = v_1 y_{A1} + v_2 y_{A2}$

(8b) $n = 46/(6y_{A2} + 2y_{A1})$

where n is the hydration number. Y_A and P_A can be determined experimentally but if the solute molecules can fit into both cages then there exists an infinite number of solutions to equation 7. If, however, the probability of observing a solute molecule in one type of cage can be eliminated, i.e. the molecule is too big to fit into the small cage, then equation 7 can be solved. This has been done in the case of Bromine clathrate hydrate in which only the large cages are populated. The hydration number has been found to be 8.47. Therefore, Y_{A2} is equal to 1/8.47 and the probability of observing a solute molecule in the large cage (y_{A2}) is 46/8.47*6. From this probability ΔU can be calculated and is equal to 167 cal/mole. The preceding ΔU value of 167 cal/mole was a much quoted value until it was shown that Bromine does not form a type I clathrate hydrate (4). Davidson has argued that a value of 265 cal/mole should be used instead of the old ΔU value. This value is based on more recent type I clathrate hydrate data (4). As was stated earlier, if the solute molecules occupy both type of cages then there exists an infinite set of solutions which satisfy equation 7. But if the Langmuir constant (C_{Ai}) can be theoretically calculated then the thermodynamic behavior of the clathrate hydrate relative to the empty lattice can be predicted. In order to calculate this constant the partition function of the gas molecules in the cages must be calculated. Van der Waals and Platteeuw did this by assuming that the interaction of the solute with the "spherical" cage wall could be described by equation 9.

$$(9) \quad V(r) = 4\varepsilon[(\sigma/r)^{12} - (\sigma/r)^{6}]$$

The resulting field (w(r)) within the spherical cage can be calculated by summing these interactions over the water molecules which are distributed along the surface of the sphere (12). The partition function for solute molecule is represented by equation 10.

$$(10)\quad h_{Ji} = \phi(T)\exp(-w(0)/kT)\int_{cell}\exp[(-w(r)-w(0))/kT]4\pi r^2 dr$$

where $\phi(T)$ is the molecular partition function of the K type of gas less the volume factor. This molecular partition function represents the translational motion and internal degrees of freedom of the solute molecules. From equation 10 the Langmuir constant can be calculated remembering that $C_{Ki} = h_{Ki}(T,V)/\phi(T)kT$.

Cady (8) attempted to verify equation 3 (Langmuir's isotherm) by determining the hydration number of different clathrate hydrates as a function of the gas pressure at constant temperature (0^oC). The hydration number was determined by forming the hydrate at a constant gas pressure and weighing the sample after the gas has been evacuated. Davidson's ΔU value of 265 cal/mole was assumed to be reasonable and the Langmuir constants were calculated using this value. Implicit in the derivation of equation 4 is the assumption that the system is existing in an equilibrium between the ice, hydrate and gas. Equation 4 determines the minimum cage occupancy or the minimum partial pressure of the gas for the clathrate hydrate stability. If Davidson's value of ΔU is substituted into equation 4 and it is noted that the hydration number is given by equation 8b then y_{A1} and y_{A2} can be calculated if n could be determined experimentally at 0^oC. It is at this temperature that the gas is existing in equilibrium with the hydrate and ice. Once y_{A1} and y_{A2} are known, from equation 6, C_{A1} and C_{A2} can be calculated.

If the Langmuir constants are known then one has a working equation that can predict the hydration numbers of the clathrate hydrate at any pressure. At this point in time it is impossible to determine directly an accurate hydration number of a hydrate in equilibrium with gas and ice at $0^{o}C$ (8). Cady estimated this hydration number by working the above procedure backwards. P_0 (the vapor pressure above the g-h-i mixture) was determined by extrapolating P vs T data of an equilibrium h-i-g mixture to $0^{o}C$. The partial pressure of the gas was determined by subtracting from P_0 the vapor pressure above pure ice at $0^{o}C$. Then by an iterative process the value of n at P_0 was calculated so that the theoretical value of n at $3P_0$ agreed with the experiment. Some of Cady's results are presented in Table II. After the Langmuir constants for each of the clathrate hydrates have been calculated, then the hydration number at a particular gas pressure can be determined. Cady was able to experimentally verify that the statistical theory of van der Waals and Platteeuw correctly predicted the pressure versus compositional relationships for type I clathrate hydrates.

Barrer and Edge (13) calculated the interaction energy (e) of an inert gas molecule as a function of distance in each cavity of type i. They summed the individual interactions between the guest molecule and the water molecules forming the clathrate hydrate using a Lennard-Jones 12:6 potential. For the specific case of the type I hydrate the cavity of type i was situated in the center of a 27 unit cell block and the sum was carried out over this block. Figure 1 and 2 shows the interaction energies of inert gases in the small and large cages, respectively, taken from the published results of Barrer and Edge (13). It should be noted that the potential minimum is not in the center of the

TABLE II

LANGMUIR CONSTANTS FOR STRUCTURE I HYDRATES AT $0^{o}C$

gas	P_0, atm	ref	n^a	$\theta_1{}^b$	$\theta_2{}^b$	$K_1{}^c$	$K_2{}^c$
H_2S	0.955	12	6.119	0.940	0.940	16.42	16.42
Xe	1.46	13	6.478	0.651	0.9664	1.28	19.78
SO_2	0.323	15	7.240	0.255	0.9739	1.08	118
Cl_2	0.320	18, 17	7.503	0.140	0.9751	0.518	125
CH_3Cl	0.386	d	7.717	0.052	0.9759	0.146	107
CH_3Br	0.241	11	7.829	0.0090	0.9763	0.039	175
$CHClF_2$	0.870	7	7.839	0.0050	0.9763	0.0058	47.7

[a]Estimated when $P = P_0$.

[b]Calculated when $P = P_0$.

[c]Langmuir constants.

[d]This work.

Figure 1. Interaction Energies, ε (kcal/mole) for Guest Molecules in Pentagonal Dodecahedral Cavities of Type 1 Hydrates.
(a) Variations of E as guest moelcule moves along an axis joining the centres of two opposite water molecules.
(b) The same as the guest moves along an axis joining the mid-point of two opposite pentagons of water molecules.
The abscissae measure distances (Å) of the centre of the guest from the cavity centre. (Taken from reference 13.)

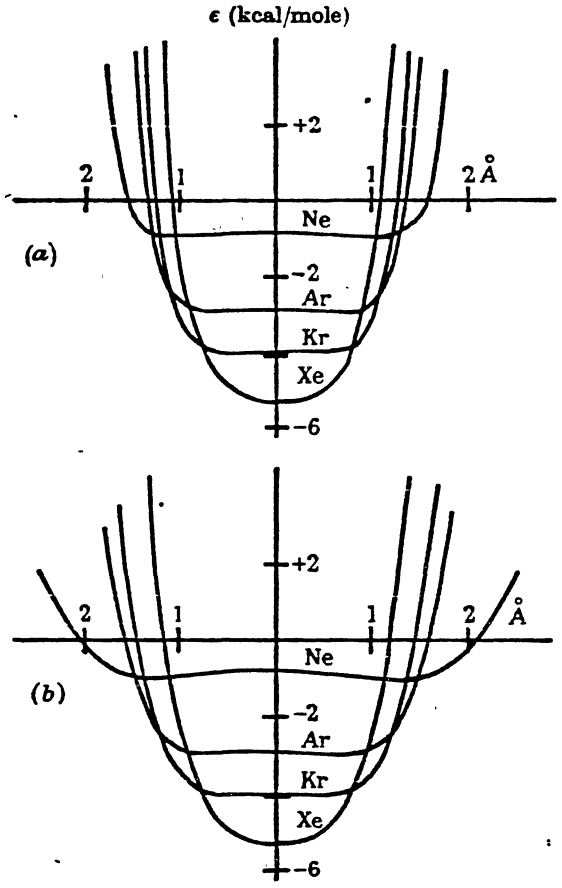
ε (kcal/mole)
+2
2
1
1
2 Å
Ne
(a)
-2
Ar
Kr
Xe
-6
+2
2
1
1
2
Å
Ne
(b)
-2
Ar
Kr
Xe
-6

Figure 2. Interaction Energies, ε (kcal/mole) for Guest Molecules in Tetrakaidecahedral Cavities of Type I Hydrates. (a) Variations of E as guest molecule moves through the cage centre along an axis normal to that joining the centres of two opposite hexagonal faces, and parallel to the line joining two opposite water molecules of one of the hexagonal faces. (b) The same as guest moves along the axis of the cavity joining the centres of two opposite hexagonal faces. (Taken from reference 13.)

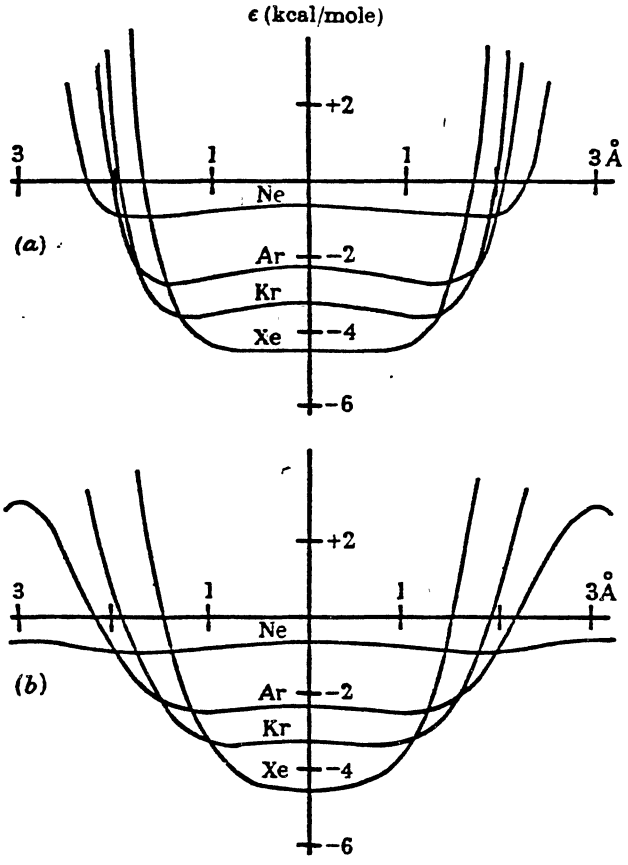
ϵ (kcal/mole)
+2
3
1
1
3Å
Ne
(a)
Ar
−2
Kr
Xe
−4
−6
+2
3
1
1
3Å
Ne
(b)
Ar
−2
Kr
Xe
−4
−6

cage for inert molecules incorporated in the large cages but is located at a position which brings the guest molecules in Van der Waals contact with the water molecules forming the cage. At low temperature it is expected that guest molecules will occupy off center positions and that there will be a finite barrier to rotation of polyatomic molecules.

Experimental Results of Clathrate Hydrates

There have been four main types of probes used to generate experimental information concerning clathrate hydrates: (1) dielectric measurements, (2) NMR, (3) infrared/Raman and (4) calorimetry. Of these, the majority of the accent has been on the first three. D. W. Davidson's group (14-19) has done most of the work with dielectric and NMR measurements while J. E. Bertie, E. Whalley and G. P. Johari (20-28) have done some vibrational analyses of clathrate hydrates. Because of the vast amoung of experimental information that has been generated on different types of hydrates, only experimental information pertinent to the type of clathrate hydrates that were studied in this thesis research will be reviewed, i.e., the type I clathrate hydrates of H_2S and ethylene oxide.

Dielectric Measurements

The dielectric properties of ethylene oxide and H_2S clathrate hydrates have been determined by D. W. Davidson and co-workers (14). The polarization and dielectric loss curves with constant applied field of 1 kHz for the ethylene oxide clathrate hydrate at low temperature obtained by Davidson (14) is shown in Figure 3. He

Figure 3. Absorption and Dispersion in EO·7.0 H_2O at 1 kHz at Low Temperatures. (Taken from reference 14.)

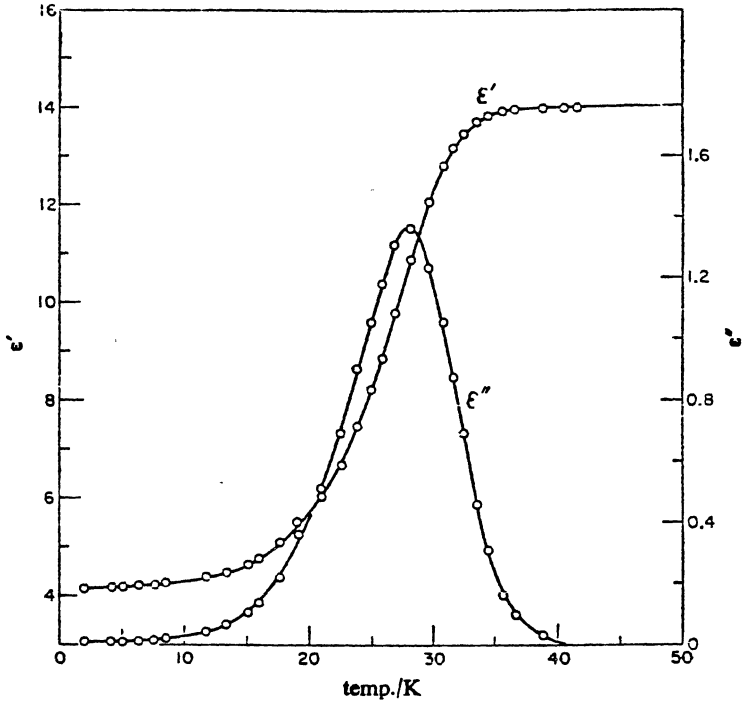
ε'
ε''
ε'
ε''
temp./K
16
14
12
10
8
6
4
1.6
1.2
0.8
0.4
0
0
10
20
30
40
50

concluded for the specific case of the ethylene oxide clathrate hydrate that the dispersion curves were much broader than what a single Debye relaxation time would give. A correlation was made between the observed low temperature dielectric properties and the skewed arc behavior found in liquid systems (19). This broadness at low temperatures was attributed to the anisotropic orientation of the guest molecules in the cage (14). This anisotropy can give rise to a continuous distribution of relaxation times because each preferred orientation will have a particular relaxation time. If there is a continuous distribution of orientations in the cages then there will be a continuous distribution of relaxation times. It is this distribution of different cage orientations which leads to peak broadening of the dielectric loss ε'' at low temperatures. Not only can the motion of the guest molecules which occupy the different cages be determined by dielectric measurements, but the water molecules which make up the lattice for the different clathrate hydrates can be probed with this technique as well. Davidson has obtained the difference in permittivity between the lattice molecular reorientation and guest molecular reorientation as a function of the applied frequency, and it is shown in Figure 4, as well as the difference between the dielectric absorption ε'' of type I and II clathrate hydrates shown in Figure 5. In general, the type I water molecules can reorient themselves at a faster rate than can the water molecules of type II hydrates. This can be attributed to the fact that the type I clathrate hydrate has a structure which is more distorted than the type II hydrate from the crystalline ice structure. As can be seen from the results of Davidson (14) presented in Table III, hexagonal ice reorientations rates are much

Figure 4. Schematic Representation of the Dielectric Dispersion and Absorption Shown by Clathrate Hydrates of Dipolar Guest Specie. (Taken from reference 14.)

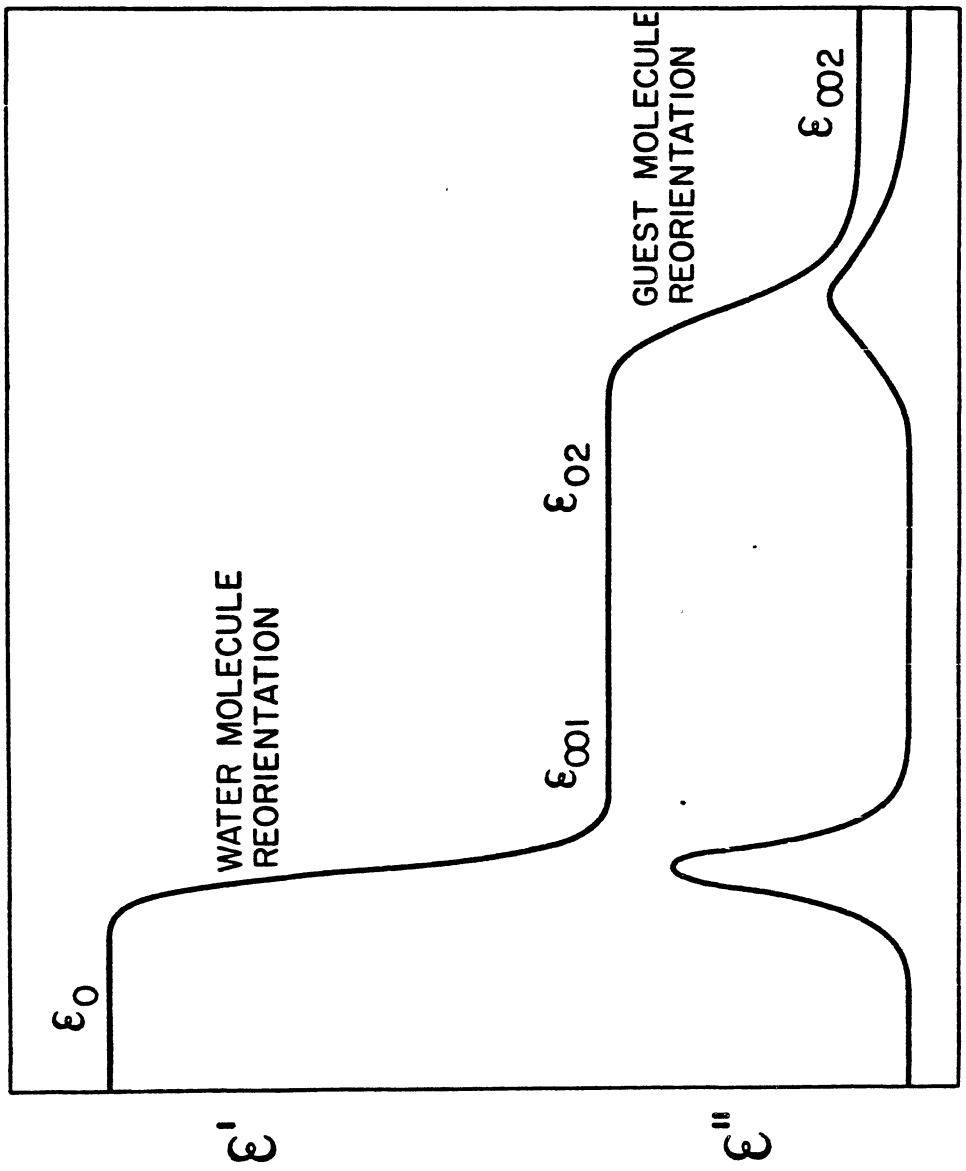
ε'
ε"
ln f
ε0
WATER MOLECULE REORIENTATION
ε001
ε02
GUEST MOLECULE REORIENTATION
ε002

Figure 5. Dielectric Absorption by Water Molecules in Structure I and Structure II Hydrates of Trimethylene Oxide at 158 K. (Taken from reference 14.)

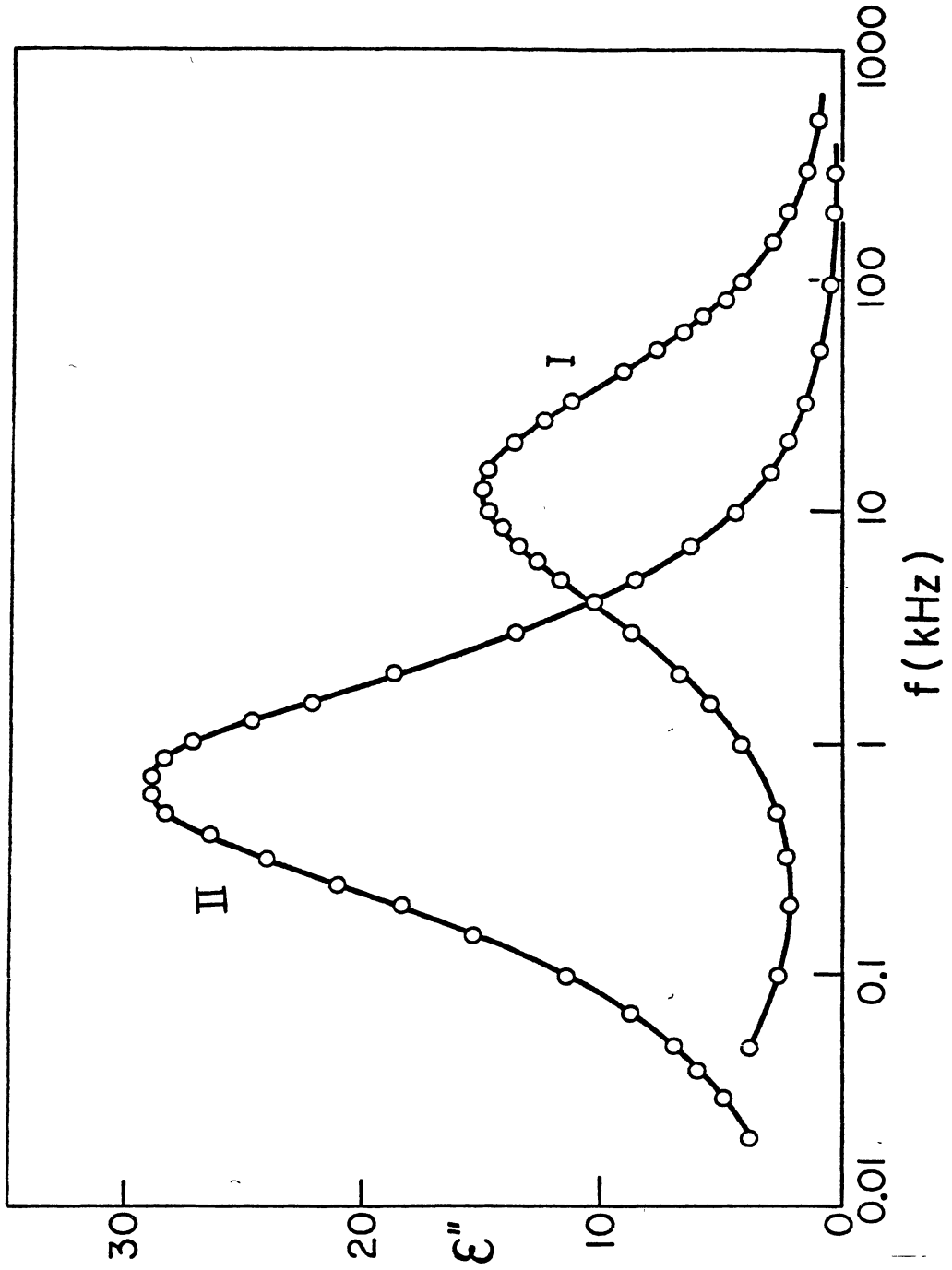
30
20
10
0
ε''
0.01
0.1
1
10
100
1000
f (kHz)
I
II

TABLE III

WATER MOLECULE DIELECTRIC RELAXATION TIMES AND ACTIVATION ENERGIES

	Guest (ref.)	τ_0 at 233.2K (μs)	E_D[a] (kcal/mole)	μ[b] (debye)
Ice Ih		1420	13.2	
Structure I	Xe	330	12	0
	cyclopropane	310	11.4	0
	N_2	180(1.2kbar)		0
	Ar	96(2.0kbar)[c]		0
	CH_3Cl		(10.5)	1.87
	ethylene oxide	0.33	7.7 (8.15)	1.90
	trimethylene oxide	0.03[d]	5.8	1.93
Structure II	SF_6	780	12.3	0
	CCl_3F	~450		0.46
	CCl_2F_2	~230		0.51
	$CClF_3$	~160		0.50
	$CHCl_2F$	~130		1.30
	$CBrClF_2$	~60		-
	1,3-dioxolane	5.4	8.7	1.47
	1,4-dioxane	4.6	9.1	0
	propylene oxide	2.0	8.0	2.00
	1,3-dioxane	1.7	7.7	2.06
	2,5-dihydrofuran	1.5	7.5	1.54
	tetrahydrofuran	1.0	7.4 (7.2)	1.63
	isoxazole	0.88	7.1	2.90
	dimethyl ether	0.78	6.8	1.31
	acetone	0.57	6.5	2.88
	cyclobutanone	0.49	6.5	2.89
	trimethylene oxide	0.48	7.0	1.93
Tetragonal Structure				
	dimethyl ether	0.087[d]	5.9	1.31

[a]Bracketed values are from T_1 measurements.

[b]Dipole moment of guest molecule.

[c]Extrapolated from higher temperatures.

[d]Extrapolated from lower temperatures.

slower than either of the two types of clathrate hydrates. This reorientation rate in ice has been linked to the diffusion of Bjerrium defects through the crystal. In this respect, the Bjerrium defect migration is expected to be faster in either type I or II clathrate hydrates than is observed in ice at comparable temperatures. Davidson's dielectric results (17) for the H_2S clathrate hydrates were surprising because the reorientation rate of H_2S in the clathrate hydrate is greater than 1 MHz at 1.8 K. This extremely fast rate is unique among the polar guest molecules that they have studied.

Infrared Measurements of the Ethylene Oxide Clathrate Hydrate

J. E. Bertie and co-workers (20-22) have measured the infrared spectrum of the ethylene oxide (E.O.) clathrate hydrate. The clathrate hydrate structure was first confirmed by x-ray photographs which characterized the sample as type I clathrate hydrate. The infrared spectrum of the hydrate showed little change from that which is obtained for hexagonal or cubic ice. The HOD impurity that was formed in the hydrate by 5% doping of D_2O in the hydrate gave a very sensitive test of ice formation. At 100 K the V_{OH} band in pure clathrate hydrate was determined to be at 2427 ±3 cm^{-1} with a half band width of 80 ± 10 cm^{-1}. But with an ice impurity the band shifted to 2419 cm^{-1} with a half band width of only 65 cm^{-1}. A simple model is presented by Bertie for comparing the clathrate hydrate infrared spectrum with that of crystalline ice (20). In hexagonal ice at 100 K, all of the hydrogen bond lengths are 2.75 Å. However, in the hydrate only 52% of the hydrogen bonds are 2.75 Å with 26% of 2.79 Å. The remainder of the hydrogen

bond lengths are 2.74 and 2.82 Å. Since the band positions in the hydrate are nearly the same as I_h, the assumption is made that the infrared band frequencies of the clathrate hydrate lattice are determined by the 2.75 Å hydrogen bonds while the breadth of these peaks are due to the hydrogen bonds of length 2.79 Å. Qualitatively this can be seen by the fact that the V_{OH} band in hydrate resembles a poorly resolved V_{OH} band in hexagonal ice. The infrared absorption from the guest molecule (ethylene oxide) is similar to that which is found for crystalline ethylene oxide (29). However, the bands are very sharp and lack the factor group splittings that are observed in crystalline ethylene oxide (20). The liquid ethylene oxide peaks are much broader than the corresponding bands in the E.O. clathrate hydrate (30) so differentiating the hydrate from its liquid or crystalline counterparts was easy. There have been no infrared absorption measurements of the H_2S clathrate hydrate reported in the literature.

Proposed Research

The first attempt to prepare the clathrate hydrate from the amorphous deposit and subsequent annealing is attributed to K. B. Harvey and co-workers (31). They attempted to prepare the $SO_2 \cdot H_2S$ and the Kr clathrate hydrate. However, in a subsequent article (32) they refuted the earlier claims and concluded instead that the amorphous material had been obtained instead of the clathrate hydrate. They pointed out that the sample had only been annealed at 110 K for 2-3 minutes and this annealing is not extensive enough to give the clathrate hydrate. This technique of forming the clathrate hydrate laid dormant until Bertie and Devlin (33) resurrected it to prepare

the ethylene oxide clathrate hydrate.

The analysis of different clathrate hydrates has been greatly facilitated by the technique of low temperature gas deposition. The correct stoichiometric amounts of gas and water for clathrate hydrate formation are mixed in the vapor phase, and stored in a gas bulb. The gas-water vapor is condensed on a cold CsI window ($\sim$50 K) to form an amorphous film. Annealing the sample at approximately 120 K causes formation of the crystalline clathrate hydrate. This phase can be monitored by FTIR. The clathrate hydrate gives a characteristic infrared spectrum which is different from either of its amorphous or crystalline counterparts. Once the hydrate has been formed then its different physical properties can be probed with infrared techniques. Some of these physical properties are outlined below and the elucidation of these properties using the above technique is really the subject of this thesis.

The proton mobility through the lattice of the clathrate hydrate under conditions that produce mobile protons (temperature, irradiation and photostimulation) can be determined by replacing some of the H_2O in the lattice with D_2O. This is accomplished by co-condensing molecular beams of H_2O, D_2O and guest molecules on the cold substrate window. Annealing the amorphous sample to form the crystalline clathrate hydrate can leave the D_2O molecules unreacted. Once the D_2O has become incorporated into the hydrogen bonded lattice the mobility of the proton through the lattice can be determined by observing the conversion of D_2O into HOD as a function of time and temperature. Comparison of these rates with the values for crystalline cubic ice can give some insights into the Bjerrum defect migration and proton transfer rates

of the clathrate hydrate. The effect that different guest molecules have on the proton mobilities in the clathrate hydrate lattice can also be probed with this technique. The incorporation of D_2O into the lattice enhances the possibility of studying the effect that an acidic guest molecule has on proton transfer. If different guest molecules do effect the transfer rates then it is hoped that this mechanism might be uncovered by studying whether or not the guest molecule itself undergoes isotopic substitution with the D_2O in the lattice. One would expect that if it was completely decoupled from the lattice, i.e. no bonding with the lattice, that no isotopic substitution should occur. If the guest molecules do effect the proton transfer rates but do not undergo isotopic substitution, then one might postulate that the interaction of the guest molecules with the cell walls might be of a van der Waals type.

Both small and large cages can be populated, as is the case of H_2S type I clathrate hydrate. One would expect the fundamental frequencies of the H_2S molecules that are trapped in the different cages to reflect the different environments that they assume. This interaction could be explored by studying the infrared spectrum of the H_2S hydrate as a function of temperature. As the H_2S hydrate is cooled (< 80 K) the rotational motion of the guest molecules in differently sized cages are frozen out at different temperatures. The degree of rotational mobility of the guest molecule in the different cages can be explored by studying the effect of cooling the sample on the infrared spectrum of the clathrate hydrate.

The formation of low temperature clathrate hydrates via gas deposition will greatly facilitate the acquisition of scientific

knowledge concerning clathrate hydrate formation, structure and energetics. The physical and chemical interactions of the guest molecules with the lattice can be probed, and the effect of different guest molecules on the proton transfer rates through the hydrogen bonded lattice of different hydrates can be determined.

CHAPTER II

EXPERIMENTAL PROCEDURE

In this first section I hope to present the basic format for all of the experiments that were run in the laboratory and then deal in the subsequent sections with the different variations on this theme for each particular clathrate hydrate that was explored.

All of the samples were first mixed in the vapor phase and stored in bulbs inside a vacuum system which is discussed in detail in Appendix A. The guest molecules, i.e. H_2S or ethylene oxide were mixed with water vapor such that the partial pressure of the water was between 3-8 times greater than the guest molecules' partial pressure. This mixture was stored in a 3 liter bulb designated as bulb #1 and in another 3 liter bulb (bulb #2) was stored D_2O vapor. The total pressure in either bulb was rarely over 20 torr. Both bulbs were connected to different needle valves (see Appendix A) that were calibrated to give a known flow rate as a function of micrometer setting. Needle #2 (needle valve from bulb #2) was set so that the D_2O that was being deposited was about 5% of the amount that was being deposited from bulb #1. The flow rate from bulb #1 was set to give approximately a .3 microns per minute film on a CsI substrate which was housed inside a vacuum shroud and cooled by a closed cycle cooler (Appendix B). Molecular beams of the guest-water mixture from bulb #1 and D_2O vapor from bulb #2 were deposited on this cold (50 K) CsI substrate to give a 7-8 micron film

deposited over a time of 20-50 minutes. The experimental conditions could be changed to insure good optical quality films which were initially (before annealing) amorphous mixtures of guest-water-D_2O. The samples were then annealed to the clathrate hydrate crystallization temperature which depended on the type of hydrate being examined but was usually found to be between 100-140 K. The vacuum shroud (which houses the substrate) and the close cycle cooler were disconnected from the vacuum line and the sample was placed in the beam path of a Digilab FTIR FTS-20C spectrometer (see Appendix C). The annealing temperature was controlled by an Air Products APD-8 Displex Controller with a precision of ± 0.5 K and was monitored using a chromel vs gold-iron thermocouple that was sandwiched between the deposition side of the substrate and the copper substrate holder (Appendix B). By observing the change in the potential of the chromel vs gold-iron thermocouple with a Rubicon Instruments potentiometer the substrate temperature could be determined. The appropriate annealing temperature was deduced by observing the infrared spectrum of the sample as the amorphous mixture changed into the clathrate hydrate. When clathrate hydrate crystallization was complete then either the proton mobility through the lattice or the effect of lattice temperature upon the guest molecules could be probed using the Fourier transform infrared spectrometer.

H_2S Clathrate Hydrate

The number of guest molecules (H_2S) to water molecules contained in bulb #1 varied but usually there were 5 times as many water molecules as there were guest molecules. A representative gas mixture was made on

September 16, 1983 in which 3.0 torr of H_2S was let into the bulb and then water vapor was admitted until the total pressure in the bulb was 18.30 torr. The partial pressure of the water was 15.30 torr which gives a hydration number of 5.1 if just the contents of bulb #1 were deposited on the substrate. However, approximately 5% of the water vapor (.7 torr) must be included in the hydration number to account for the D_2O vapor that is co-deposited from bulb #2. This changes the hydration number to 5.4 instead of 5.1 calculated above. On the 3rd of October 1983, a 20 minute deposit was made in which needle #1 and #2 were opened to .23 and .03, respectively. These needle settings allowed only about 5% D_2O to be cocondensed with the guest-water mixture on the 50 K CsI substrate. An amorphous film was obtained which was confirmed by the infrared spectrum of the film. By observing the red Newton's ring as a function of time the sample thickness could be approximated. The films were usually 7 microns in depth. The deposition area consisted of a circle with a radius of 0.9 cm giving a total sample deposition of 1.8×10^{-3} cm^3. This particular sample was first annealed at 100 K for 2 hrs and observation of the infrared spectrum at 10 K showed that the sample still had recognizable "glassy" characteristics. So annealing was continued at 100 K for another 3 hrs. Dropping the temperature again to 10 K and observing the infrared spectrum showed little change from the preceding spectrum. At this time the sample was annealed for 30 minutes at 130 K and upon subsequent cooling to 10 K showed what is now recognized as the characteristic infrared spectrum for the H_2S clathrate hydrate.

Ethylene Oxide Clathrate Hydrate

The ethylene oxide clathrate hydrate was prepared by two different methods: 1) amorphous annealing and 2) epitaxial growth. The first method is virtually identical to that which was used to prepare the H_2S clathrate hydrate. The second method is different and will be dealt with in detail here. A mini deposit which is a shortened main deposit was made at 50 K using similar conditions as were used in the amorphous annealing procedure with the exception that only the vapor from bulb #1 was deposited. After the mini deposit for which the deposition time was usually 4 minutes, the sample was annealed at 120 K for 30 minutes and at 130 K for an hour. This annealing time converted the mini deposit to the clathrate hydrate crystal and when the main deposit was made at 100 K on top of the mini deposit the crystalline ethylene oxide clathrate hydrate was obtained. Thus, the crystals were grown epitaxially and no subsequent annealing of the sample had to be done. The second method used to grow the clathrate hydrate (epitaxial growth) had the added advantage that the D_2O did not convert to HOD when the crystal was formed so it was possible to study the kinetics of the D_2O conversion into HOD at specified temperatures in the ethylene oxide clathrate hydrate.

CHAPTER III

ETHYLENE OXIDE CLATHRATE HYDRATE

The first part of this chapter will be centered around the proof that clathrate hydrates can be formed by the method of vapor deposition and annealing. Then the rest of the chapter will deal with the results obtained for the ethylene oxide clathrate hydrate as well as the interpretation of these results. Much of the proof of clathrate hydrate crystallization rests largely upon the published results of J. E. Bertie on the ethylene oxide clathrate hydrate (24). Bertie and co-workers have published the infrared spectrum of the x-ray characterized bulk crystals of type I clathrate hydrate of ethylene oxide, while Bertie and Devlin (33) have published the infrared spectroscopic proof of ethylene oxide clathrate hydrate formation from the annealed low temperature condensate. Since the sample temperature of the clathrate hydrate characterized by Bertie was 100 K, the infrared comparison of Bertie's samples with the vapor deposited samples will also be made at 100 K. It should be noted that the infrared spectrum of the x-ray characterized hydrate was obtained by mulling the hydrate in three different types of mull, i.e. propane, propylene and freon, but the samples grown from the vapor required no mulling agents. The peak to peak comparison of the characterized clathrate hydrate and the vapor deposited hydrate is presented in Table IV. The almost identical matching of the infrared peaks between the vapor deposited samples

TABLE IV

ASSIGNMENTS OF ETHYLENE OXIDE CLATHRATE HYDRATE

Characterized	Vapor Deposited	Δν	Assignment	Crystalline Ethylene Oxide	Liquid Ethylene Oxide
3400 sh					
3220 vs br			ν_{OH} (H_2O)		
3100 sh					
3066 w	3065	1	E.O. ν_{13},ν_6	3073.7 3062.3 3051.3	3072
3009 w	3005	4	E.O. ν_1	3024.5	3014
2998 w	2996	2	E.O. ν_9	3005.7 2996.0	3003
2957 w	2955	2	E.O. $2\nu_2$	2950.5	
2920 w	2919	1	E.O. $\nu_2 + \nu_{10}$	2915.7	
2913 vw	2913	0	E.O. $2\nu_{10}$	2904.3	
2427 bl	2427	0	ν_{OD} (HOD)		
2250 ± 15	2255	5	$\nu_2 + \nu_R$ $3\nu_R$ (H_2O)		
1605 ± 20	1600	5	ν_2 (H_2O)		
1489 w	1489	0	E.O. ν_2	1494.7 1480.7	1492
1466 w	1466	0	E.O. ν_{10}	1467.3 1460.3	1468
1282 w	1281	1	E.O. small cage ν_3		
1270 m	1269	1	large cage E.O. ν_3	1266	1268
1268 vs	1267	1	large cage E.O. ν_3		
1255 vw	1253	2	C_{13} large cage E.O.	1253.3	
1147 w	1147	0	E.O. ν_{11},ν_{14}	1169.5 1166.5 1160.8 1147	1150

TABLE IV (Continued)

Characterized	Vapor Deposited	Δν	Assignment	Crystalline Ethylene Oxide	Liquid Ethylene Oxide
1123 vw	1123	0	E.O. ν_4	1119	1124
890 sh	890	0	ν_R (H_2O) + E.O. ν_{12}		
864 i	875		ν_R (H_2O) + E.O. ν_5		
845 sbr			ν_R (H_2O)		
808 sh			E.O. ν_8	837	815
805 s	803	2	E.O. ν_{15}	797.5 794	799
630 wsh					
590 wsh			ν_R (H_2O)		
560 wsh					
530 wsh					

and the x-ray characterized samples along with the mismatching of these peaks with the liquid ethylene oxide bands as well as the lack of factor group splitting which is observed for crystalline ethylene oxide (see Table IV) strongly supports the conclusion that the vapor deposited samples are indeed the ethylene oxide clathrate hydrate.

Another factor which adds credence to this conclusion is the observation of peak enhancement and narrowing of the guest molecule bands upon cooling. This effect can be qualitatively ascribed to the following: At low temperature ($\sim$10 K) the cage of the hydrate encroaches upon the guest molecules and forces the guest molecules to assume preferred orientations inside the cage. As a result, the range in the vibrational density of states available to the guest molecules is small at low temperatures so the peaks are sharp and intense. However, as more energy is put into the clathrate hydrate the guest molecules can assume a greater spectrum of orientations, and the vibrational density of states is broadened. This leads to bands that are more diffuse at higher temperatures. Thus, in the clathrate hydrates the peaks associated with the guest molecules tend to intensify and sharpen anomalously with cooling.

Another factor that was used to infer clathrate hydrate crystallization was the frequency of the O-D stretching mode of an isolated HOD molecule in the hydrogen bonded lattice of the hydrate. This characteristic frequency showed a 10 cm^{-1} shift to higher frequencies in clathrate hydrates from what is obtained for cubic ice and a 13 cm^{-1} shift to lower frequencies from what is obtained in the amorphous material (see Table V and Figure 6). Thus, it was possible to tell from both the position of the isolated HOD frequency and its half band

TABLE V

O-D STRETCHING FREQUENCY OF ISOLATED HOD AS A FUNCTION OF TEMPERATURE

Temp K	ν_{OH} ice	ν_{OH} E.O. C.H. 8/9/84	FWHM E.O. C.H.	ν_{OH} E.O. C.H. 8/15/84	ν_{OH} E.O. C.H. 9/6/84	ν_{OH} Amorphous Ice
170	2427.0					
160	2425.5					
150	2424.0	2432.0	85.94			
140	2422.5	2433.2	85.55	2433	2430.5	
130	2421.0	2432.0	85.94	2432	2429.5	
120	2419.9	2431.8	86.33	2430	2428.5	
110	2418.5	2430.2	83.59	2429	2427	
100	2417.0	2429.8	84.38	2428	2426	
90	2416.0	2427.0	82.03	2427	2425	2434
80	2414.8	2426.0	82.03	2426	2424	
70	2413.5	2424.0	82.03	2425	2423	
60	2412.8	2423.4	79.30	2424	2422	
50	2411.5	2422.4	79.30	2423	2421	
40	2410.5	2420.9	78.13	2422	2420	
30	2410.0	2419.3	76.95	2421	2419.5	
20	2409.5	2419.6	80.86	2420	2419	
10	2409.25	2419.3	77.34	2420	2419	

Figure 6. O-D Stretching Absorption of Isolated HOD in Cubic Ice (●) and in the Ethylene Oxide Clathrate Hydrate (⊙). The frequency has been adjusted by a 10 cm^{-1} additive constant.

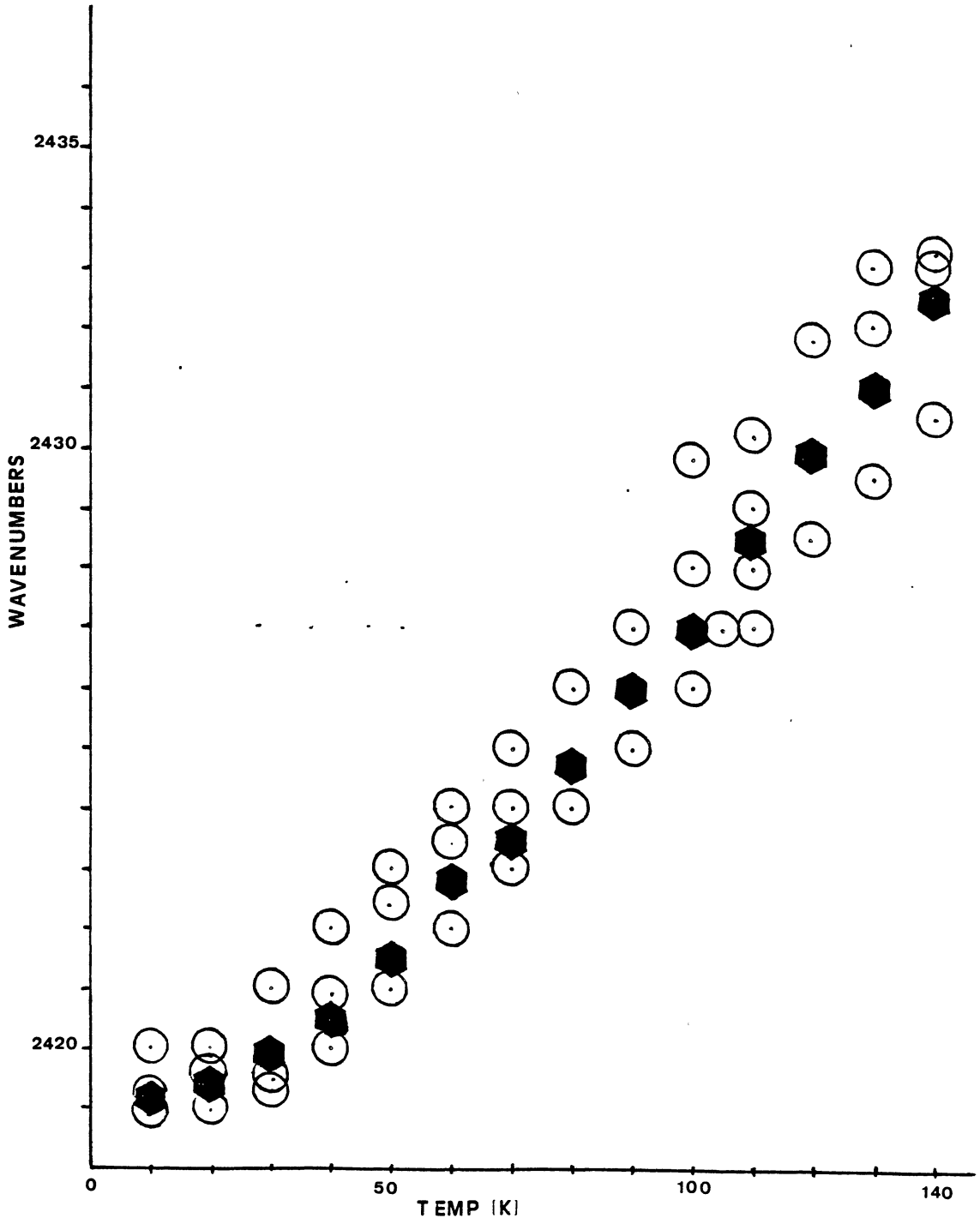
2435
2430
2420
WAVENUMBERS
0
50
100
140
TEMP [K]

width whether the samples were amorphous mixtures, clathrate hydrates or cubic ice. Not only was it possible to isolate HOD in the clathrate hydrate lattice but D_2O as well. Both HOD and D_2O absorption bands, as a function of temperature, are presented in Figures 7-9 and Table 5. Some of the representative spectra that were obtained for the ethylene oxide clathrate hydrate are presented in Figures 10-14.

Proton Transfer Kinetics of Ethylene Oxide Clathrate Hydrate

With the use of epitaxial deposition (see Chapter II) it was possible to isolate in the lattice of the clathrate hydrate D_2O joined by H_2O molecules. As a proton moves through the hydrogen bonded network of the clathrate hydrate it will convert the D_2O into isolated HOD. A mechanism has been worked out in great detail for cubic ice (34) and, it was hoped that this mechanism could be used to interpret the kinetic data that were obtained for the ethylene oxide clathrate hydrate. The conversion of D_2O into HOD as a function of time was monitored by infrared spectroscopy at various temperatures (105, 107, 110, 115, 118 and 120 K) and the raw data from these measurements is presented in Tables VI-XII, while the data from a representative experiment is presented in Figure 15. Because the ν_{OH} and D_2O frequencies were broad (FWHM > 80 cm) detailed observation of intermediates such as coupled HOD was futile. In cubic ice it is believed that the proton moves through the three dimensional hydrogen bonded chains by a two step mechanism. First, the proton hops from oxygen to neighbor oxygen with essentially zero activation energy and secondly, a Bjerrum defect will migrate through this site flipping the proton into another

Figure 7. O-D Stretching Absorption of Isolated HOD in the Ethylene Oxide Clathrate Hydrate. A - 10 K; B - 20 K; C - 30 K; D - 40 K; E - 50 K; F - 60 K; G - 70 K; H - 80 K; I - 90 K; and J - 100 K.

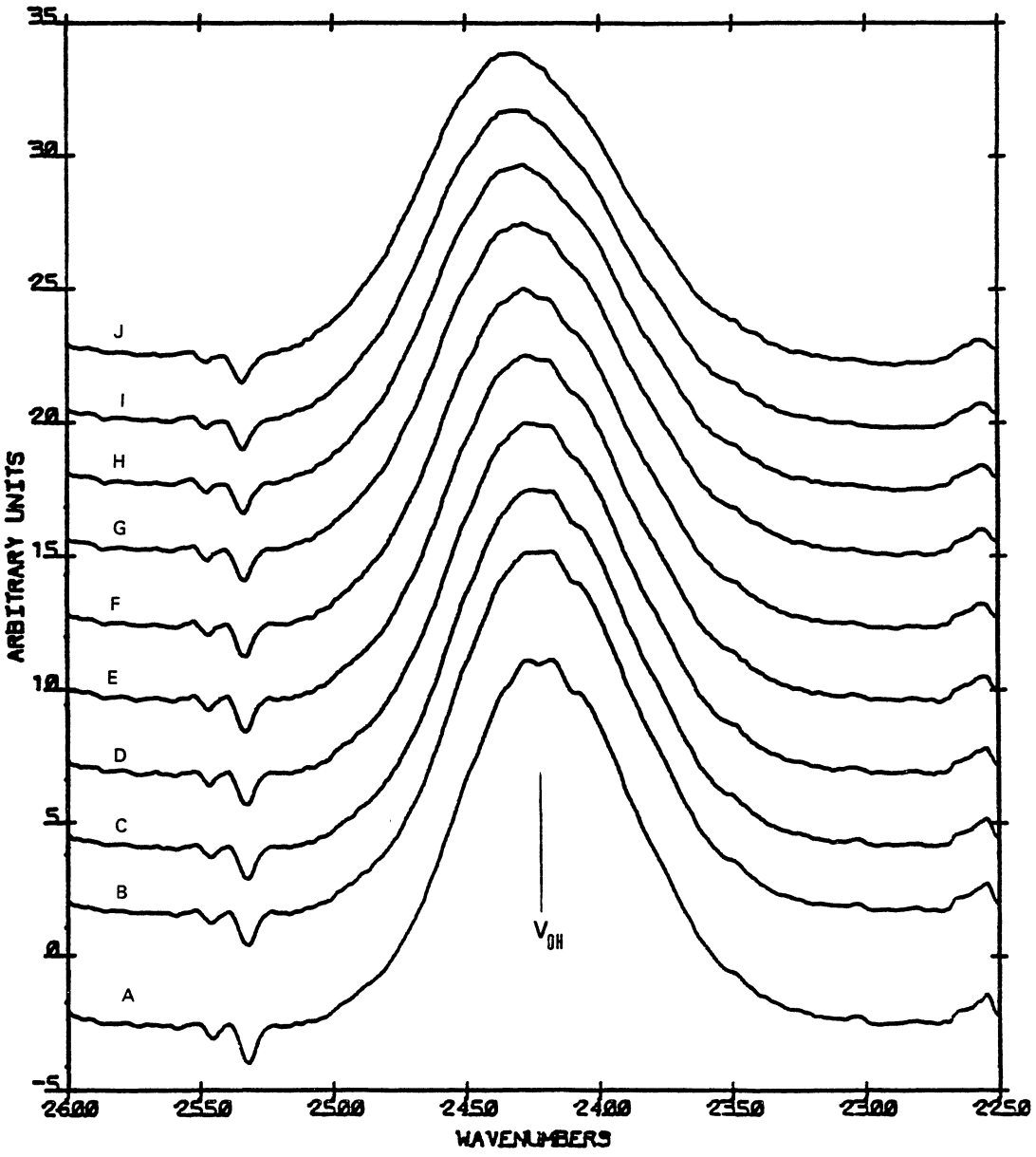
35
30
25
20
15
10
5
0
-5
ARBITRARY UNITS
J
I
H
G
F
E
D
C
B
A
V_{OH}
2600
2550
2500
2450
2400
2350
2300
2250
WAVENUMBERS

Figure 8. O-D Stretching Absorption of Isolated HOD in the Ethylene Oxide Clathrate Hydrate. A - 110 K; B - 120 K; C - 130 K; D - 140 K; and E - 150 K.

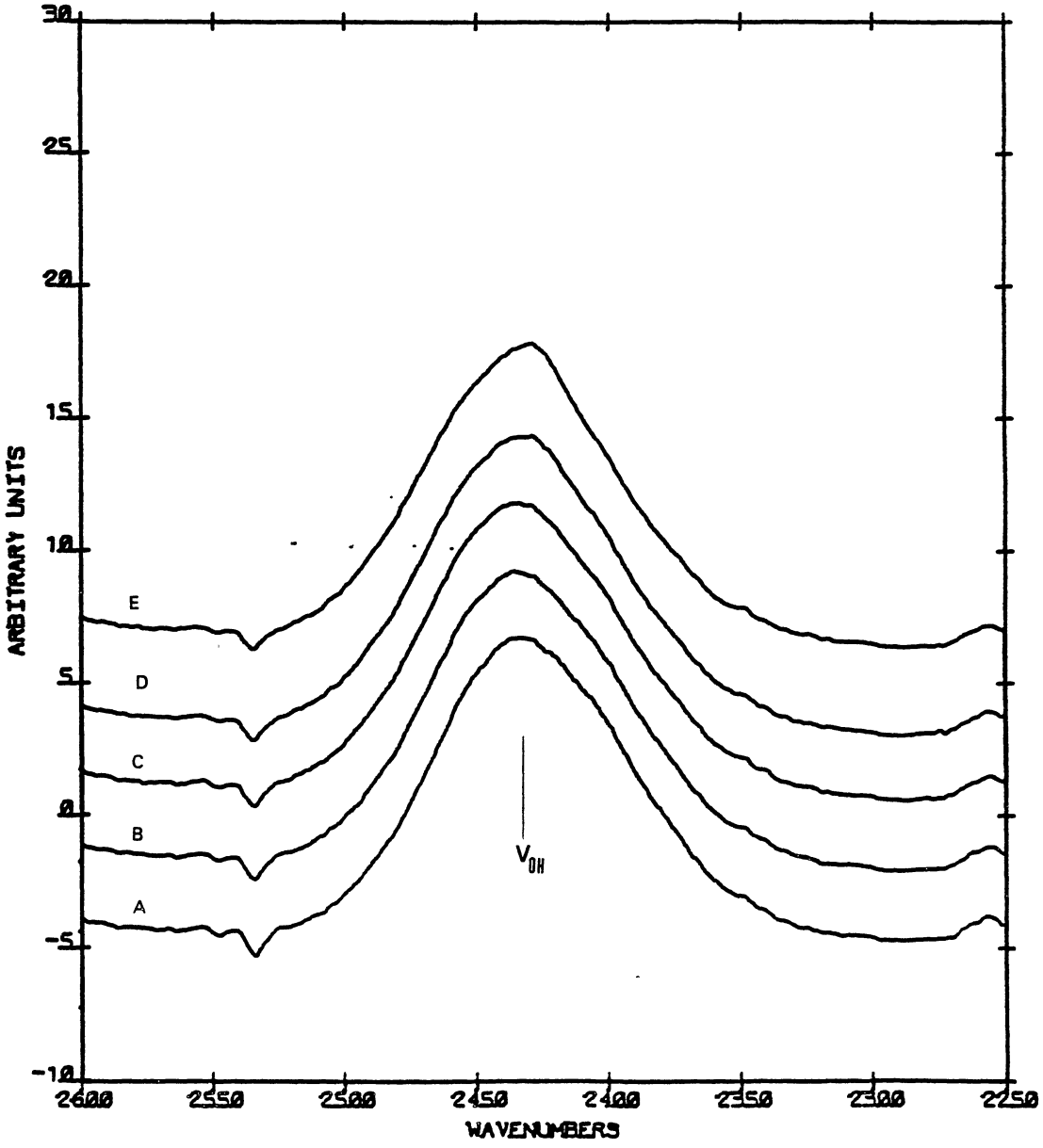
30
25
20
15
10
5
0
-5
-10
ARBITRARY UNITS
E
D
C
B
A
V_{OH}
2600
2550
2500
2450
2400
2350
2300
2250
WAVENUMBERS

Figure 9. Isolated D_2O Absorption in the Ethylene Oxide Clathrate Hydrate. A - 10 K; B - 20 K; C - 30 K; D - 40 K; E - 50 K; F - 60 K; G - 70 K; H - 80 K; I - 90 K; and J - 100 K.

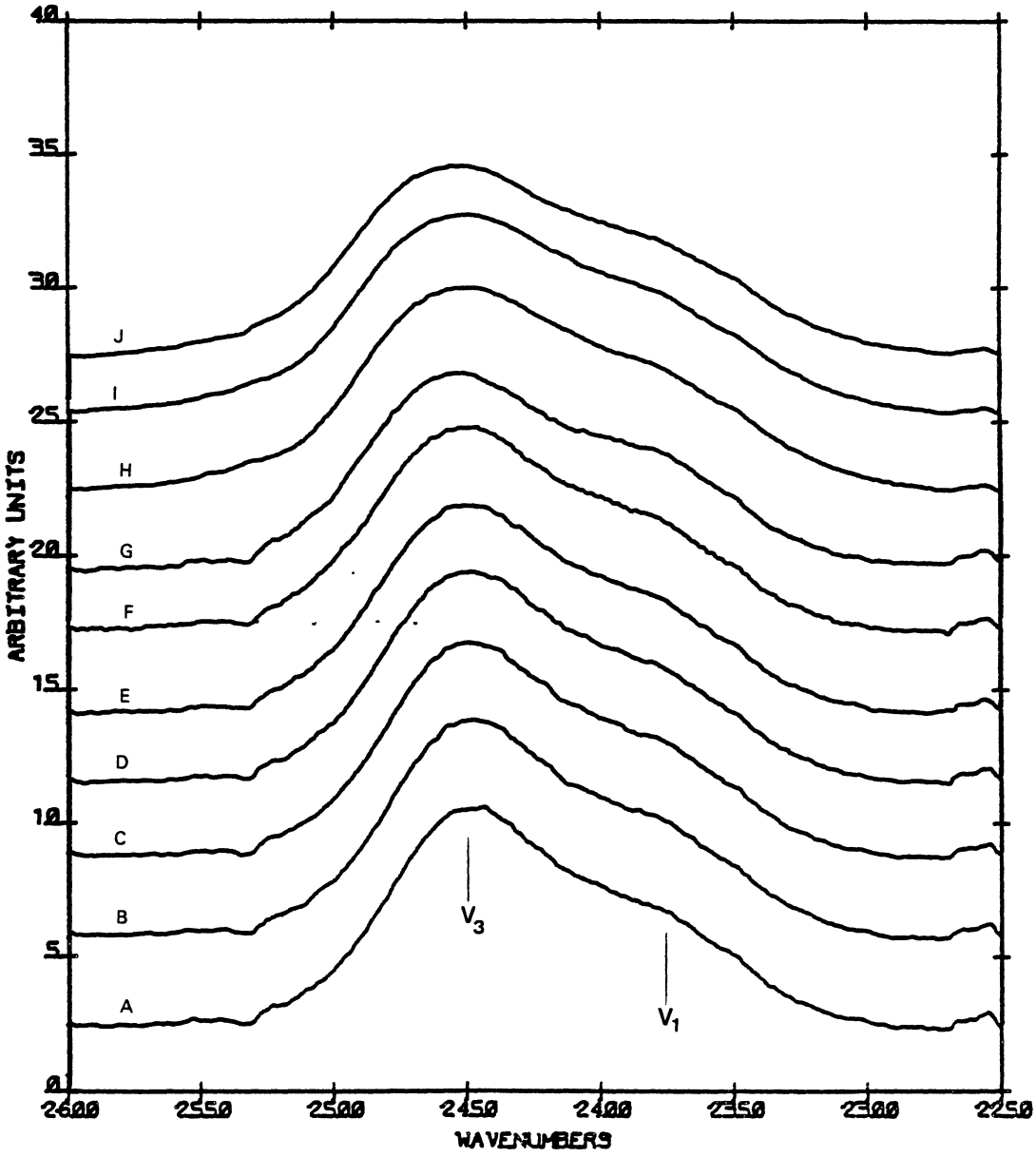
40
35
30
25
20
15
10
5
0
ARBITRARY UNITS
J
I
H
G
F
E
D
C
B
A
V_3
V_1
2600
2550
2500
2450
2400
2350
2300
2250
WAVENUMBERS

Figure 10. C-H Stretching Absorption of the Ethylene Oxide Molecule in the Clathrate Hydrate. A - 80 K and B - 10 K.

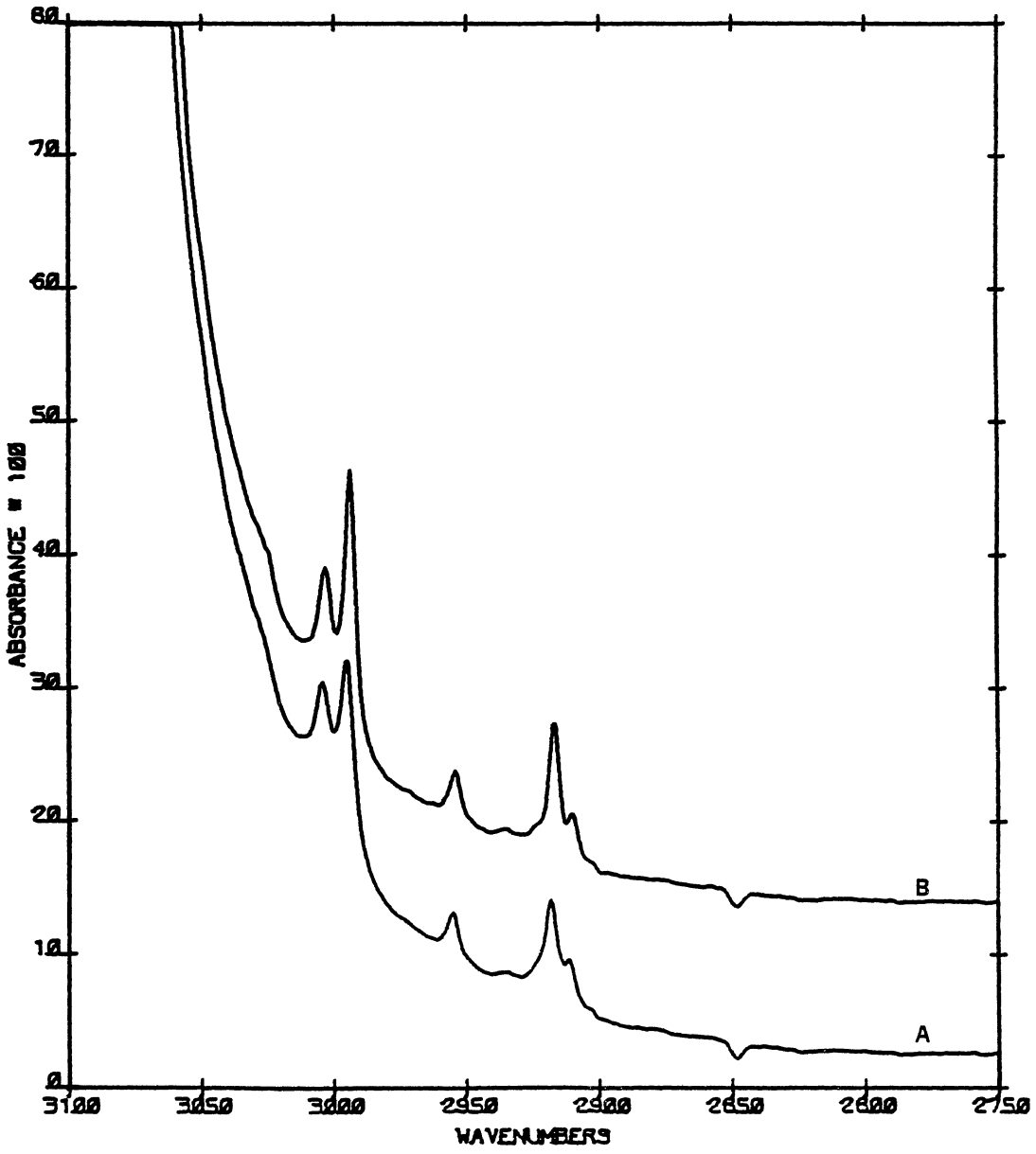
80
70
60
50
40
30
20
10
0
ABSORBANCE * 100
3100
3050
3000
2950
2900
2850
2800
2750
WAVENUMBERS
B
A

Figure 11. Ethylene Oxide Clathrate Hydrate. A - 80 K and B - 10 K.

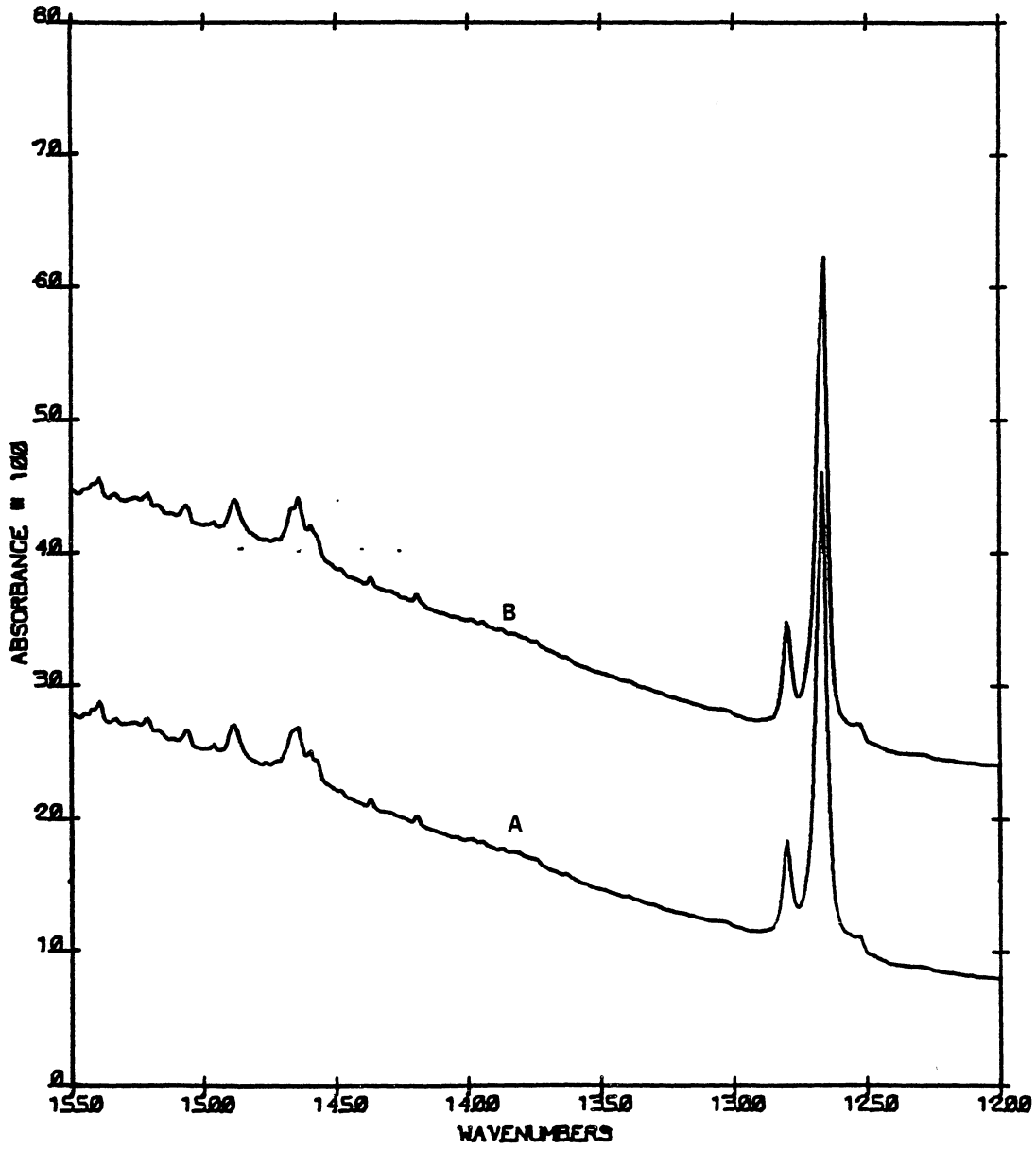
80
70
60
50
40
30
20
10
0
ABSORBANCE * 100
B
A
1550
1500
1450
1400
1350
1300
1250
1200
WAVENUMBERS

Figure 12. High Resolution (0.5 cm^{-1}) of Ethylene Oxide Clathrate Hydrate at 10 K.

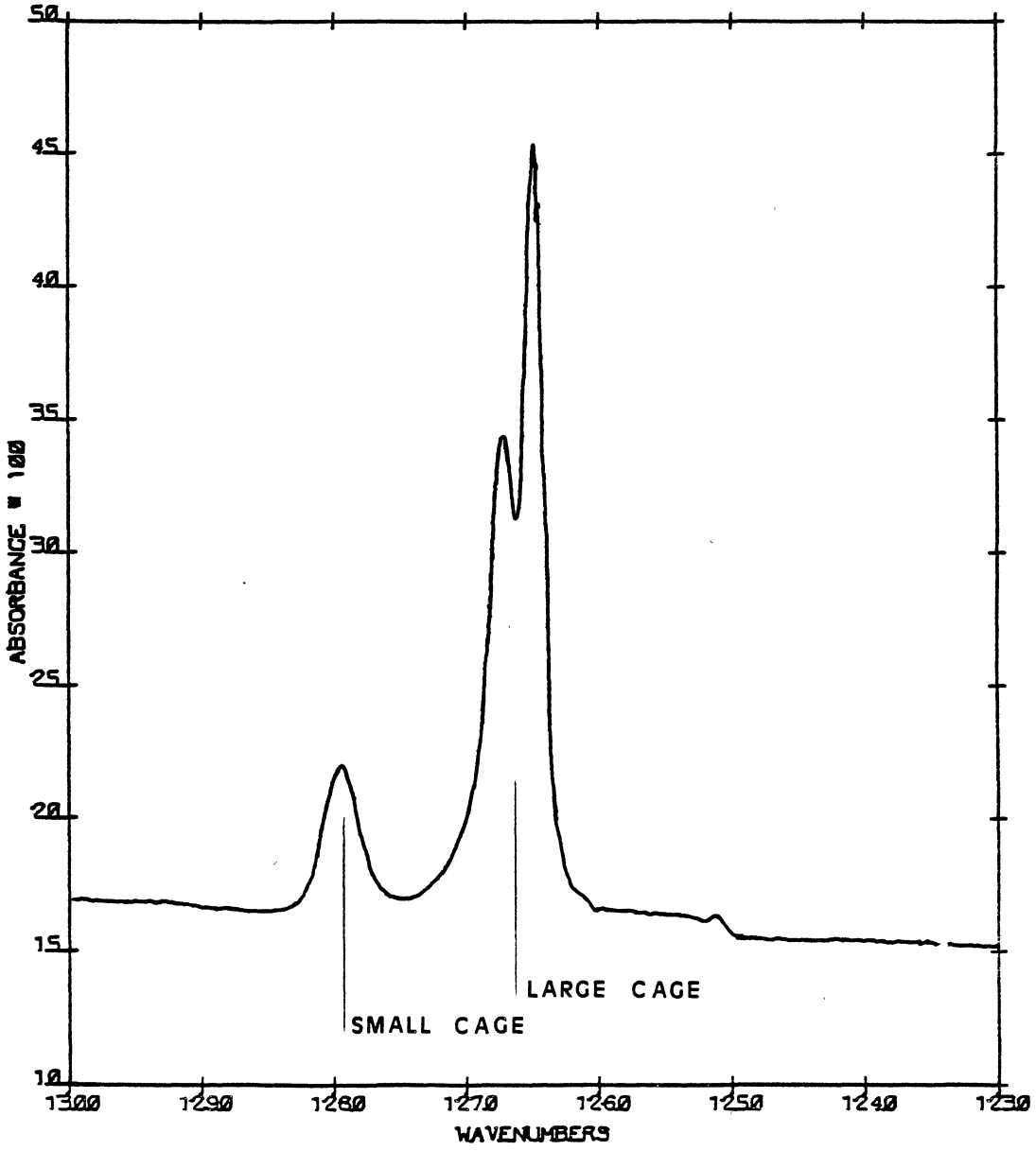
50
45
40
35
30
25
20
15
10
ABSORBANCE * 100
SMALL CAGE
LARGE CAGE
1300
1290
1280
1270
1260
1250
1240
1230
WAVENUMBERS

Figure 13. Ethylene Oxide Clathrate Hydrate. A - 80 K and B - 10 K.

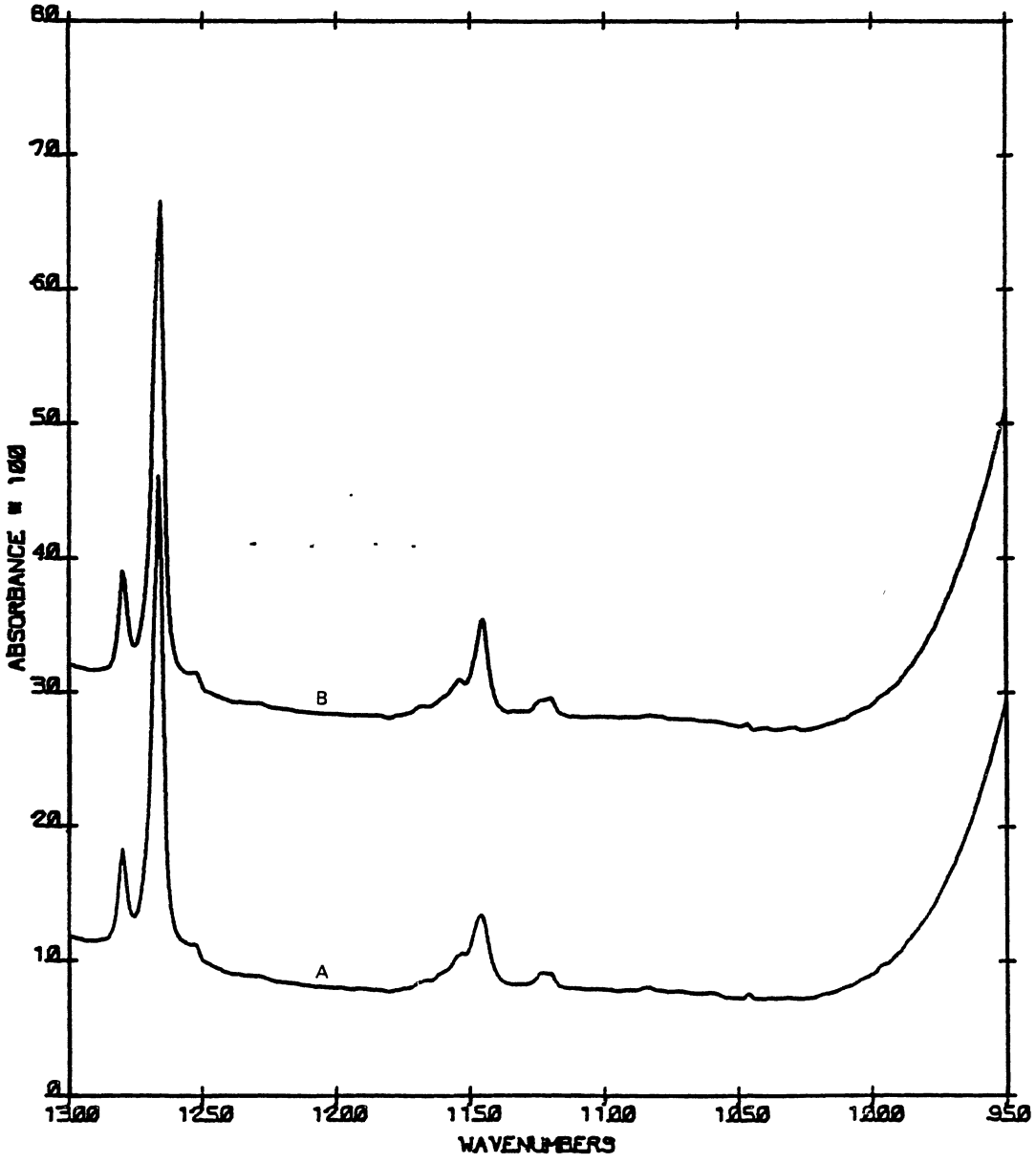
80
70
60
50
40
30
20
10
0
ABSORBANCE = 100
B
A
1300
1250
1200
1150
1100
1050
1000
950
WAVENUMBERS

Figure 14. Ethylene Oxide Clathrate Hydrate. A - 80 K and B - 10 K.

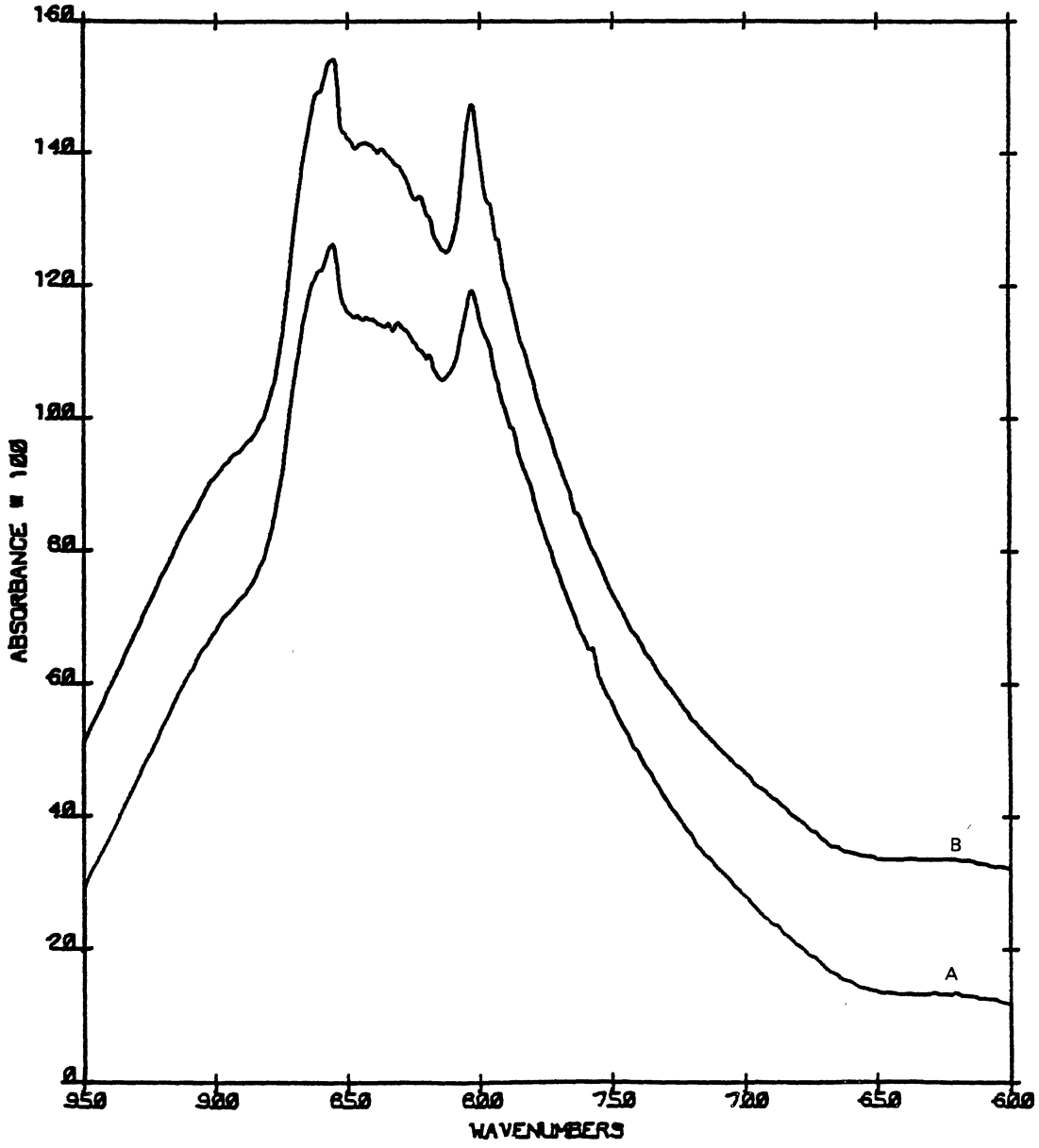
160
140
120
100
80
60
40
20
0
ABSORBANCE * 100
950
900
850
800
750
700
650
600
WAVENUMBERS
B
A

TABLE VI

KINETICS AT 105 K 8/23/84

Time (min)	Peak Height ν_3	Peak Height ν_1	Fitted ν_3	Fitted ν_1	ln Fitted 3	ln Fitted ν_1	HOD Scaling Parameter
0	17	11.5	17	11.4	2.83	2.44	.22
10	16	10.5	16.1	10.8	2.78	2.38	.28
20	15.5	10.25	15.4	10.2	2.73	2.32	.30
30	13.5	9.75	14.6	9.8	2.68	2.28	.34
40	13.5	9.25	13.9	9.3	2.63	2.23	.38
50	13.5	9.25	13.3	8.8	2.59	2.17	.38
60	13.0	8.5	12.8	8.5	2.55	2.14	.42
70	12.5	8.5	12.3	8.15	2.51	2.10	.44
80	12.0	8.25	12.0	7.9	2.48	2.07	.46
90	11.80	8.0	11.7	7.75	2.46	2.05	.48
100	12.0	7.5	11.4	7.65	2.43	2.03	.49
110	10.5	7.5	11.3	7.65	2.42	2.03	.49

TABLE VII

KINETICS AT 107 K 9/11/84

Time (min)	Peak Height ν_3	Peak Height ν_1	Fitted ν_3	Fitted ν_1	ln Fitted ν_3	ln Fitted ν_1	HOD Scaling Parameter
0	17	12	17.3	13.3	2.85	2.59	.20
10	17	12	16.8	12.7	2.82	2.54	.20
20	16	11.5	16.3	12.0	2.79	2.48	.26
30	15.5	11.25	15.7	11.4	2.75	2.43	.28
40	15.5	11.5	15.2	10.9	2.72	2.39	.28
50	15.0	11.0	14.6	10.3	2.68	2.33	.30
60	14.5	10.5	14.1	9.8	2.65	2.28	.34
70	14.0	9.5	13.5	9.4	2.60	2.24	.38
80	13.0	9.25	13.0	9.0	2.56	2.20	.40
90	12.5	8.75	12.4	8.6	2.52	2.15	.42
100	11.5	8.0	11.9	8.3	2.48	2.12	.46
111	11.5	8.0	11.3	8.1	2.42	2.09	.46

TABLE VIII

KINETICS AT 110 K 8/19/84

Time (min)	Peak Height ν_1	Peak Height ln	Peak Height Fitted Line	ln P.H. S.L. f.h.	HOD Scaling Parameter
0	8	2.08	-	-	.30
2	8	2.08	-	-	.30
4	8	2.08	7.7	2.04	.35
6	7	1.95	7.0	1.95	.39
8	6.75	1.91	6.5	1.87	.41
10	6.25	1.83	6.1	1.81	.45
12	6.0	1.79	5.8	1.76	.47
14	5.75	1.75	5.6	1.72	.50
16	5.25	1.66	5.38	1.63	.53
18	5.15	1.64	5.2	1.65	.55
20	5.00	1.61	5.02	1.61	.55
30:40	4.5	1.39	4.0	1.39	.65
37	4.0	1.39	4.0	1.39	.65
44	3.75	1.32	3.7	1.31	.67

TABLE IX

KINETICS AT 110 K 8/26/84

Time (min)	Peak Height ν_3	Peak Height ν_1	Fitted ν_3 line	Fitted ν_1 line	ln Fitted ν_3	ln Fitted ν_1	HOD Scaling Parameter
0	16.25	10.00	16.25	10.00	2.79	2.30	.22
2	15.75	9.50	15.60	9.60	2.75	2.26	.26
4	14.75	9.00	15.10	9.20	2.71	2.22	.32
6	14.75	8.75	14.60	8.90	2.68	2.19	.34
8	13.50	8.00	14.15	8.60	2.65	2.15	.38
10	13.00	7.75	13.65	8.30	2.61	2.12	.40
12	13.00	8.00	13.20	8.00	2.58	2.08	.40
14	12.75	8.00	12.80	7.80	2.55	2.05	.42
16	12.75	7.75	12.40	7.60	2.52	2.03	.42
18	11.50	7.50	12.10	7.40	2.49	2.00	.48
20	11.25	7.25	11.75	7.15	2.46	1.97	.48
22	11.50	7.50	11.50	7.00	2.44	1.95	.48
24	11.50	7.00	11.25	6.80	2.42	1.92	.48
34	11.00	6.50	10.60	6.20	2.36	1.82	.50
44	10.00	6.00	10.20	6.10	2.32	1.81	.55

TABLE X

KINETICS AT 115 K 8/29/84

Time (min)	Peak Height ν_3	Peak Height ν_1	Fitted ν_3	Fitted ν_1	ln Fitted ν_3	ln Fitted ν_1	HOD Scaling Parameter
0	12		-		-		.34
4	11		10		2.30		.40
6	10		9.1		2.21		.45
8	9		8.3		2.12		.50
10	8		7.7		2.04		.55
12	7.25		7.2		1.97		.60
14	6.5		6.7		1.90		.64
16	6.5		6.35		1.85		.64
20	5.25		5.75		1.75		.70
22	5.5		5.5		1.70		.70
24	5.0		5.23		1.65		.72
35	4.5		4.0		1.39		.75
43	3.5		3.25		1.18		.80
51	2.5		2.55		0.94		.85
60	2.0		1.85		0.62		.88

TABLE XI

KINETICS AT 118 K 9/5/84

Time (min)	Peak Height ν_3	Peak Height ν_1	Fitted ν_3	Fitted ν_1	ln Fitted ν_3	ln Fitted ν_1	HOD Scaling Parameter
0	17.25	11.75	17.25	11.6	2.85	2.45	.26
2	15.5	10.75	15.6	10.6	2.75	2.36	.32
4	14.0	9.25	14.1	9.5	2.65	2.25	.40
6	13.0	8.50	12.6	8.5	2.53	2.14	.46
8	11.0	7.5	11.3	7.6	2.42	2.03	.52
10	9.5	6.5	10.0	6.7	2.30	1.90	.58
12	8.5	5.75	8.8	5.9	2.17	1.77	.62
14	7.75	5.25	7.7	5.1	2.04	1.63	.66
16	6.75	4.5	6.75	4.5	1.91	1.50	.70
18	6.25	4.25	6.0	3.9	1.79	1.36	.72
22	5.75	4.0	5.1	3.4	1.63	1.22	.74
24	5.0	3.5	4.9	3.25	1.59	1.18	.76
40	3.25	2.0	-	-	-	-	-

TABLE XII

KINETICS AT 120 K 8/13/84

Time (min)	Peak Height ν_3	Peak Height ν_1	Fitted ν_3	Fitted ν_1	ln Fitted ν_3	ln Fitted ν_1	HOD Scaling Parameter
0	18.5	11.5	18.5	11.5	2.92	2.44	.38
2	13.0	7.5	13.6	7.8	2.61	2.05	.58
4	10.0	6.0	10.7	5.9	2.37	1.77	.68
6	8.5	4.0	8.9	4.6	2.19	1.53	.74
8	7.0	3.75	7.6	3.7	2.03	1.31	.78
10	7.0	3.5	6.6	3.2	1.89	1.16	.78
12	6.5	3.25	5.7	2.6	1.74	0.96	.80
14	6.0	3.0	5.2	2.3	1.65	0.83	.82
16	4.75	2.5	4.8	2.15	1.57	0.77	.86
18	4.0	2.0	4.4	2.0	1.48	0.69	.88

Figure 15. Isolated D_2O in the Ethylene Oxide Clathrate Hydrate at 118 K. A - 0 min; B - 2 min; C - 4 min; D - 6 min; E - 8 min; F - 10 min; G - 12 min; H - 14 min; I - 16 min; J - 18 min; K - 22 min; L - 24 min; and M - 40 min. (Isolated HOD has been subtracted out of the spectra in Figure 15.)

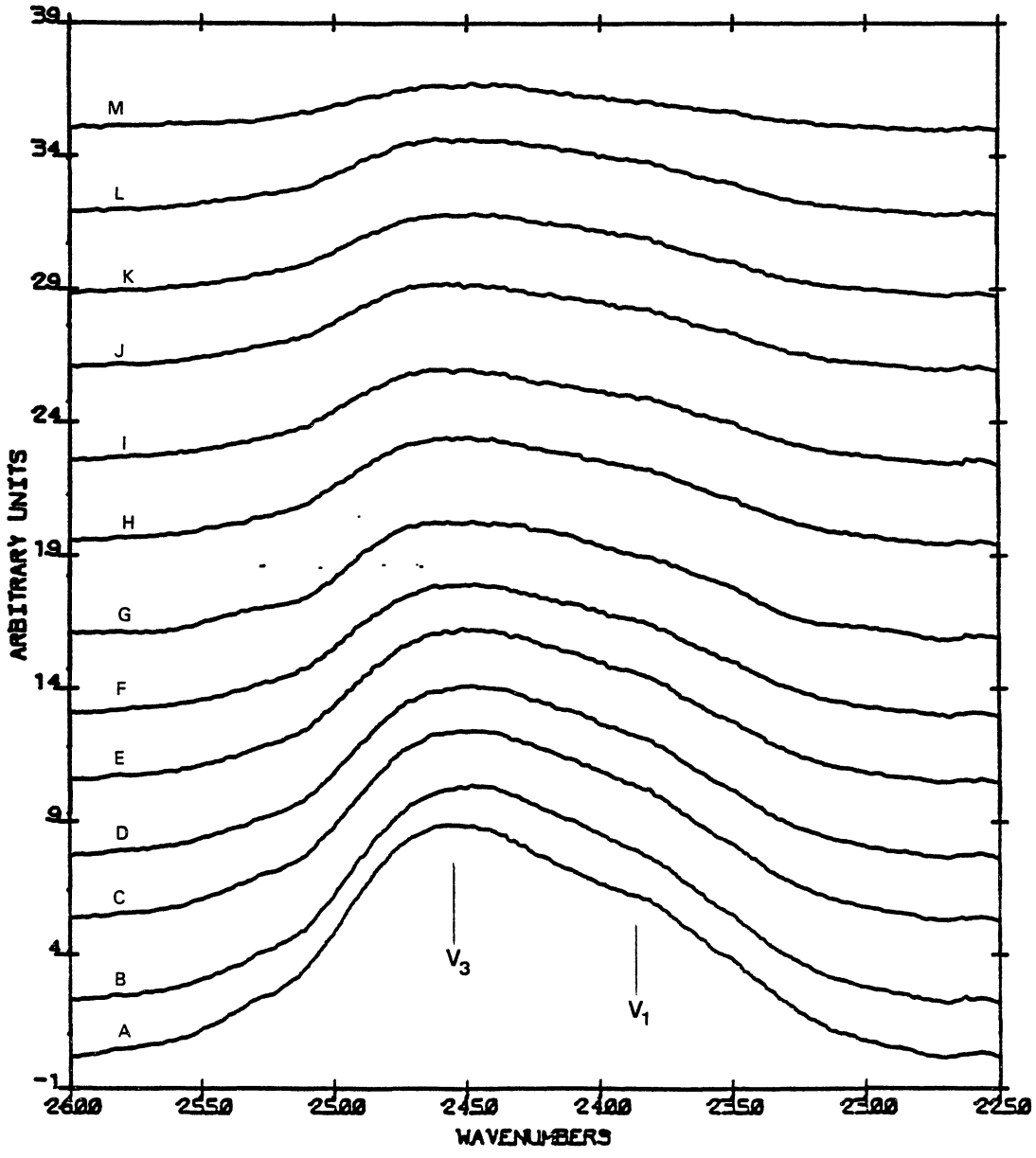
39
34
29
24
19
14
9
4
-1
M
L
K
J
I
H
G
F
E
D
C
B
A
ARBITRARY UNITS
V_3
V_1
2600
2550
2500
2450
2400
2350
2300
2250
WAVENUMBERS

proton transfer channel. The chain is now in the same configuration as it was when the hopping process began and is ready to start another "hopping step". In ethylene oxide clathrate hydrate, it can be postulated from Davidson's activation energy for the reorientation rate of the water molecules in ethylene oxide clathrate hydrate of 7.7 Kcal/mole (ice 13.2 Kcal/mole) that the Bjerrum defects remain mobile at a lower temperature in the clathrate hydrate than they do in ice (14). If this is indeed the case, then at temperatures (130 K in cubic ice) where the proton migration rate is affected by the diminishing number of protons, the Bjerrum defects will be mobile because there is not a deficiency of Bjerrum defects and/or their migration rate is not affected by the lack of energy to cross the rotational bond breaking barrier. To test this assumption the ethylene oxide clathrate hydrate with D_2O isolated was irradiated with 1.7 MeV electrons at low temperatures ($\sim$80 K). At 80 K there is normally no proton migration in the ethylene oxide clathrate hydrate which is shown by the fact that D_2O in the lattice does not convert to HOD at 80 K. This lack of proton migration is attributed to the lack of protons not the fact that protons are less mobile at these temperatures than they are at higher temperatures. Irradiation of samples similar to clathrate hydrates (cubic ice) produced a sizeable concentration of protons; therefore, it was anticipated that radiolysis of clathrate hydrates with 1.7 MeV electrons should produce a proton concentration above the regular thermal concentration of protons. If enough protons are produced so that their effect can be measured spectroscopically (definition of sizeable), then two different results might be anticipated: 1) The Bjerrum defects are not mobile at 80 K (there is not enough energy

available for these defects to migrate) then only coupled HOD [(HOD)] should be the final product; and 2) The Bjerrum defects have a low activation energy so as to be mobile. Then isolated HOD will be the final product. The results are shown in Figure 16. Because only isolated HOD was formed at 80 K (see Figure 17), it is possible to draw the conclusion that the Bjerrum defects are indeed mobile at temperatures as low as 80 K where the thermal proton concentration is essentially non-existent (<< 1E-18 M) and it is expected that in the absence of irradiation the rotational rate constant (K_r) will be much larger than the hopping rate constant (K_h) in this temperature range. Therefore, at temperatures around 100 K it is expected that the rate determining step is the hopping step shown in equations 3.1-3.

(3.1) $D_2O \xrightarrow{K_h} (HOD)_2$ slow rate determining step

(3.2) $(HOD)_2 \xrightarrow{K_r} 2HOD$ fast step

(3.3) $D_2O \xrightarrow{K_h} 2HOD$ overall reaction

The proton concentration at a particular temperature is assumed to be constant, i.e. an equilibrium exists between H_2O and the ionic defects H^+ and OH^-, and has been incorporated into the hopping rate constant. Therefore, the reaction in 3.1 is pseudo first order with the hopping rate constant proportional to the proton concentration. The conversion of D_2O into HOD should follow first order kinetics, and a plot of the $\ln[D_2O]$ versus time gives a straight line; the slope of which is the hopping rate constant (see Figure 18). The peak height of the ν_3 and ν_1 modes of D_2O were used instead of the concentration of D_2O and the peaks heights were assumed to be proportional to the D_2O

Figure 16. D_2O Isolated in the Ethylene Oxide Clathrate Hydrate Before (A) and After (B) Irradiation with 1.7 MeV Electrons.

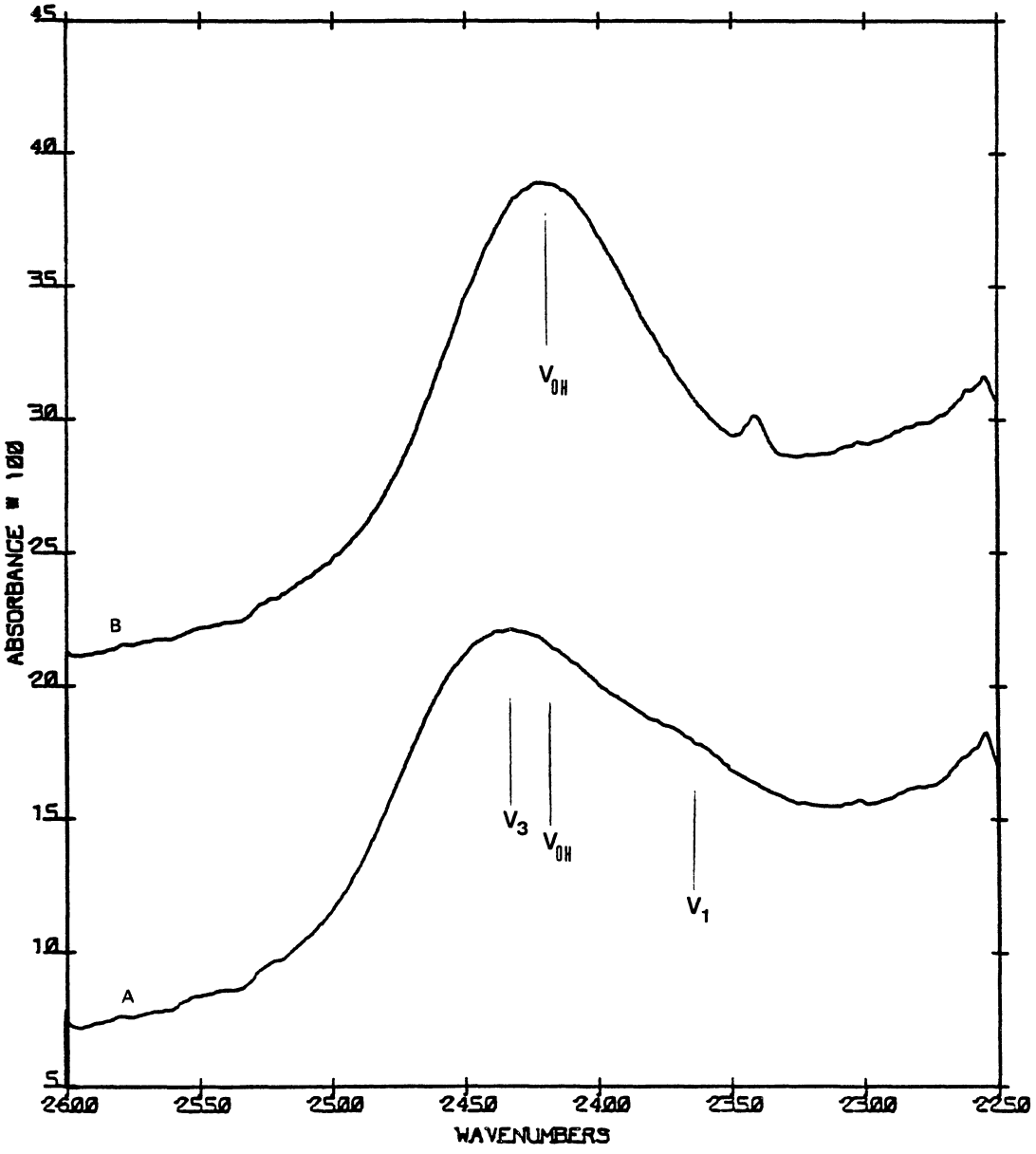
45
40
35
30
25
20
15
10
5
ABSORBANCE = 100
B
A
V_{OH}
V_3
V_{OH}
V_1
2600
2550
2500
2450
2400
2350
2300
2250
WAVENUMBERS

Figure 17. Isolated HOD Subtracted from the After Irradiation of Ethylene Oxide Clathrate Hydrate with 1.7 MeV Electrons.

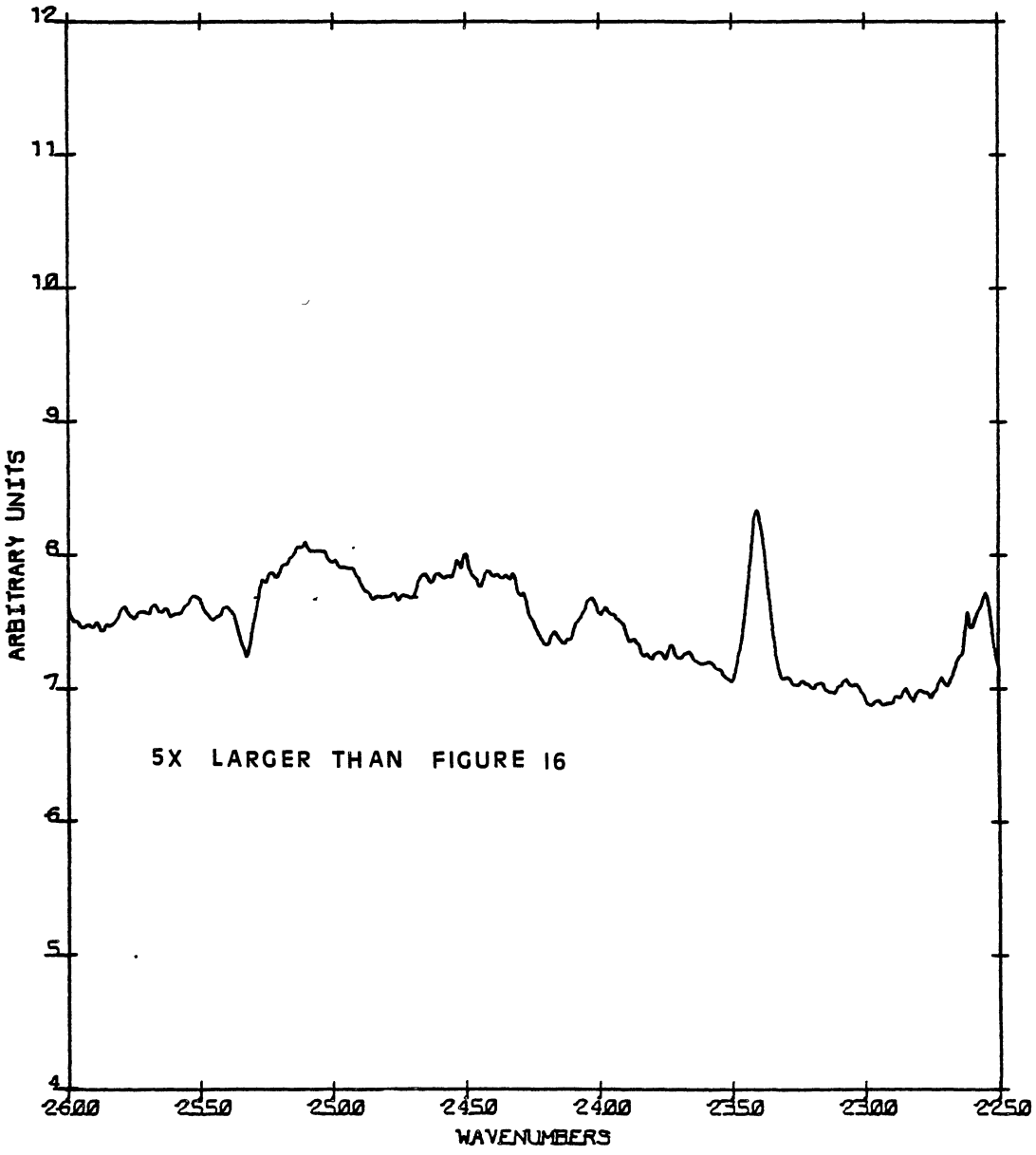
12
11
10
9
8
7
6
5
4
ARBITRARY UNITS
5X LARGER THAN FIGURE 16
2600
2550
2500
2450
2400
2350
2300
2250
WAVENUMBERS

Figure 18. Graph of the Rate Data Obtained at 118 K for D_2O Isolated in Ethylene Oxide Clathrate Hydrate.

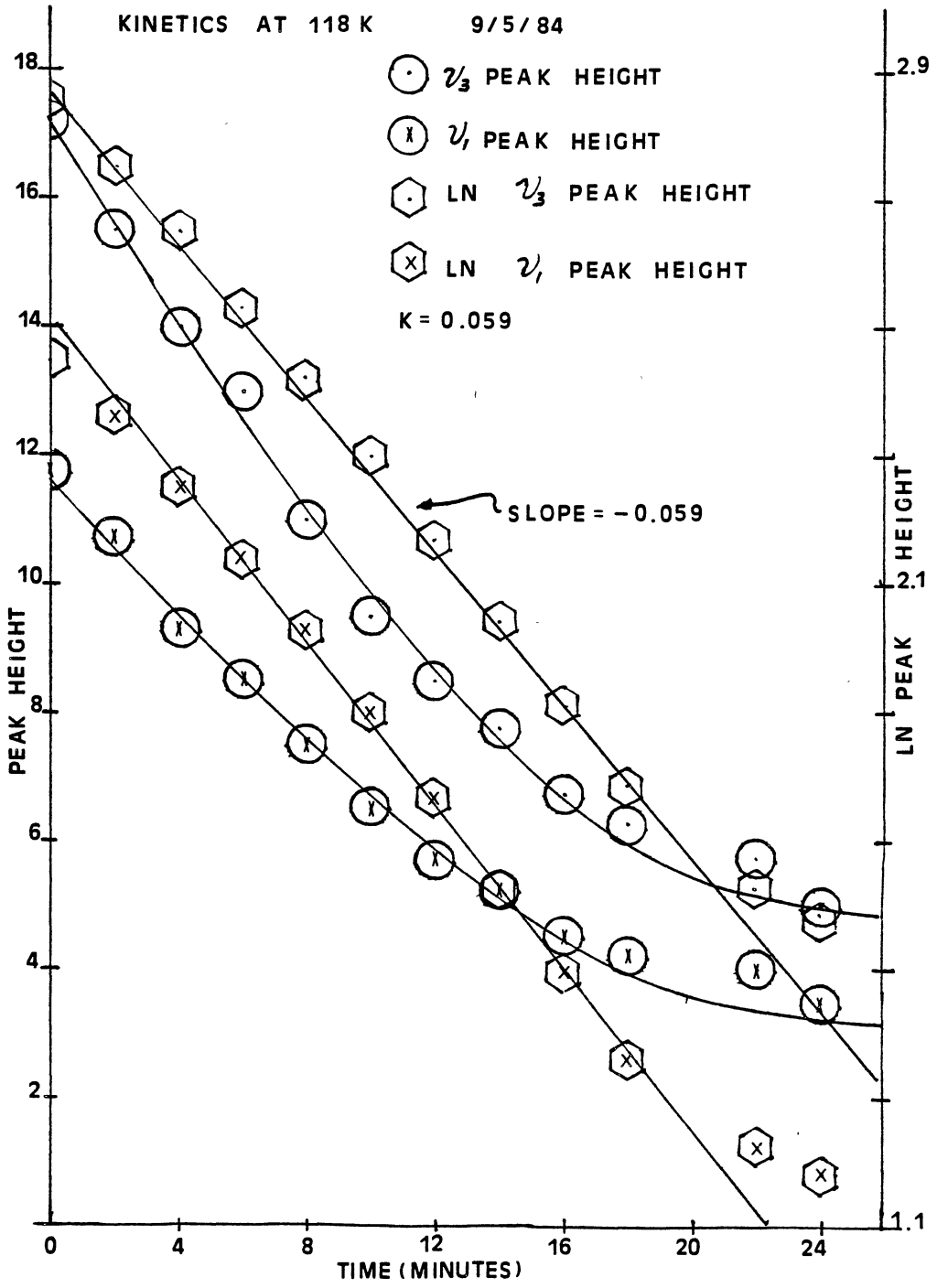
KINETICS AT 118 K 9/5/84
ν_3 PEAK HEIGHT
ν_1 PEAK HEIGHT
LN ν_3 PEAK HEIGHT
LN ν_1 PEAK HEIGHT
K = 0.059
SLOPE = −0.059
PEAK HEIGHT
LN PEAK HEIGHT
TIME (MINUTES)
18
16
14
12
10
8
6
4
2
0
4
8
12
16
20
24
2.9
2.1
1.1

concentration. This assumption should not affect the rate constants that were calculated from the above mentioned slope. An Arrhenius plot, made from rate constants determined at different temperatures, yielded an activation energy of 4.5 ± 1.8 Kcal/mole (see Figure 19 and Table XIII). These results are very different from similar experiments that were carried out in cubic ice. First, irradiation of cubic ice at temperatures around 90 K produced only coupled HOD, and secondly, the activation energy determined from the hopping rate constant in cubic ice was 9.5 Kcal/mole. This activation energy was attributed to the ionic defect formation energy, as it was assumed that the hopping step proceeded with essentially zero activation energy. Therefore, in cubic ice the picture at this point is that at temperatures less than 130 K there are essentially no ionic defects (< 1E-18 M) and the Bjerrum defects are non-mobile because there is not enough energy available to these defects so that they can cross the rotational bond-breaking barrier. In order for the L defects to move through the crystal, a hydrogen bond must be broken and the water molecule must rotate, flipping one of its hydrogens into the hole that has been created by the L defect. This is an activated process and the barrier to this process is the rotational bond breaking barrier. In the ethylene oxide clathrate hydrate, however, the Bjerrum defects are obviously mobile at temperatures as low as 90 K, and there must be protons present at a concentration level such that their effect can be measured spectroscopically (conversion of D_2O into HOD) at any temperature in excess of 100 K. It is also doubtful that the activation energy determined for clathrate hydrates is the energy needed to form ionic defects in the hydrate because the hydrogen bonded chains

Figure 19. Arrhenius Plot of the LN Hopping Rate Constant Versus 1/T in the Ethylene Oxide Clathrate Hydrate.

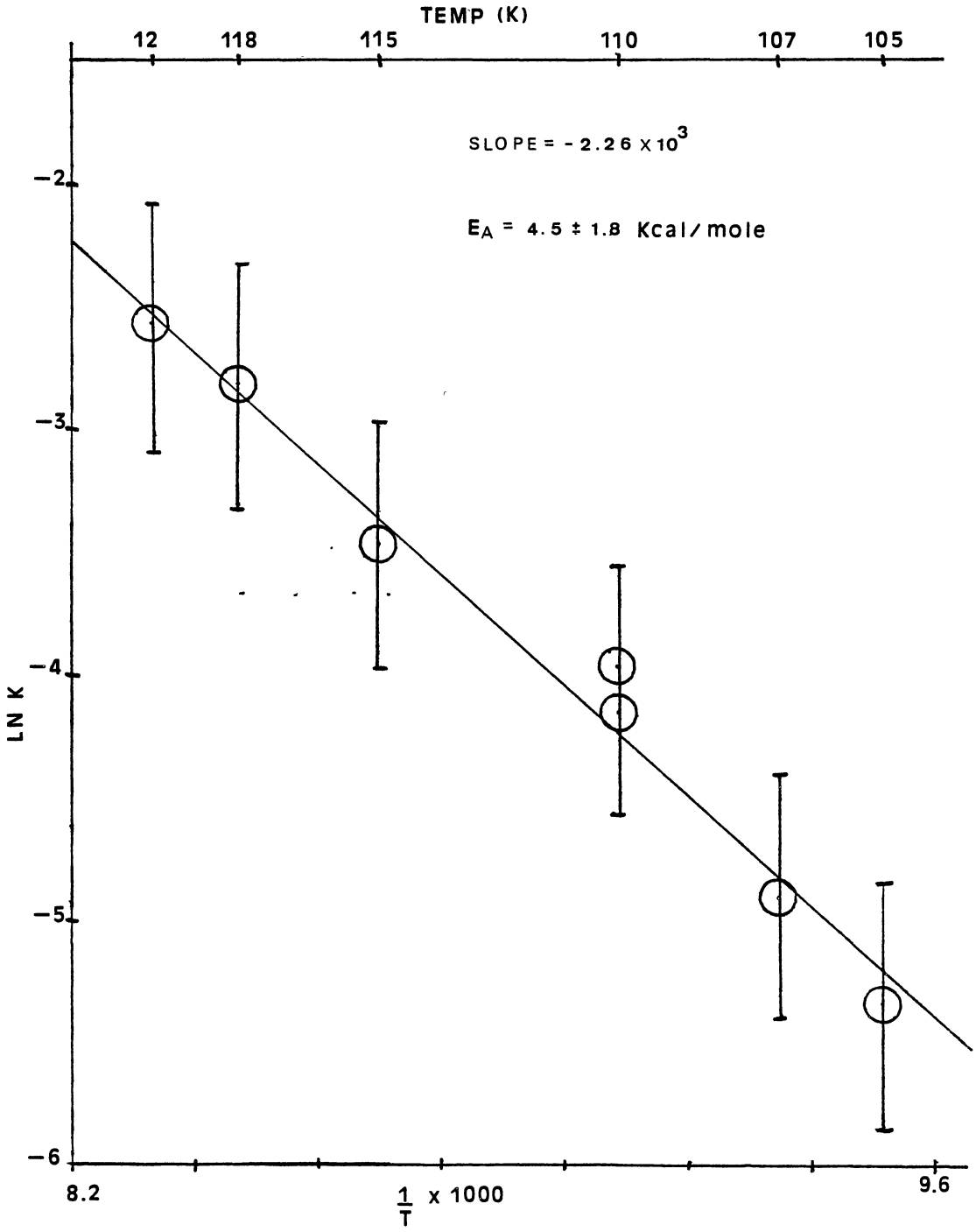
TEMP (K)
12
118
115
110
107
105
SLOPE = - 2.26 X 10^3
E_A = 4.5 ± 1.8 Kcal / mole
-2
-3
-4
-5
-6
LN K
8.2
1/T x 1000
9.6

TABLE XIII

ETHYLENE OXIDE RATE DATA-CONVERSION OF D_2O TO ISOLATED HOD

Date Data Taken	Temp (K)	K	ln K	1/T x 1000	$t_{1/2}$ (min)
8/23/84	105	0.0048	-5.34	9.52	144
8/19/84	110	0.0188	-3.97	9.09	37
8/26/84	110	0.016	-4.14	9.09	43
8/29/84	115	0.031	-3.47	8.70	22
8/12/84	120	0.076	-2.58	8.33	9
9/5/84	113	0.059	-2.83	8.47	12
9/11/84	107	0.0074	-4.91	9.35	94

in the hydrate are very similar to the chains in cubic ice. One would expect the formation energy for ionic defects in the two crystals to be similar, if in fact not higher in the clathrate hydrate for which the hydrogen bond lengths are longer. If the activation energy determined does not represent the formation energy of the ionic defects in the hydrate then what does it represent? Some of the possible answers to this question will be explored in the following sections following what is felt to be the most reasonable picture for proton transfer in clathrate hydrates.

A back-of-the-envelope calculation using the proton transfer potential of Steve Scheiner (35) presents one possibility. Scheiner has calculated a double well potential for proton transfer within a $H_9O_4^+$ complex. This complex has four water molecules joined together by hydrogen bonds with an ionic defect (H^+) on the second water molecule (see Figure 20). The barrier against proton transfer that he calculated for an oxygen-oxygen (O-O) bond distance of 2.75 Å (ice 2.75 Å and clathrate hydrate 2.77 Å) was 7.9 Kcal/mole. Figure 21 shows a Morse potential fitted to the Scheiner potential. The various vibrational energy levels were then calculated from the fitted Morse parameters in which a zero point energy of 4.9 Kcal/mole was determined. The energy that is needed to cross the barrier is 3 Kcal/mole (7.9-4.9 Kcal/mole). The barrier height for an O-O bond distance of 2.8 Å was determined by Scheiner to be 8.6 Kcal/mole. The activation energy of 4.5 ± 1.8 Kcal/mole determined from the rate data of the ethylene oxide clathrate hydrate could be the energy needed to cross this proton transfer barrier if the probability is low for the proton to tunnel through the barrier. It should be noted that in cubic ice it

Figure 20. The $Hg_2O_4^+$ Complex of Scheiner (35) in Which the Proton Transfer Barrier Was Determined.

Figure 21. Morse Potential (A) Fitted to the Proton Transfer Potential (B) of Scheiner (35).

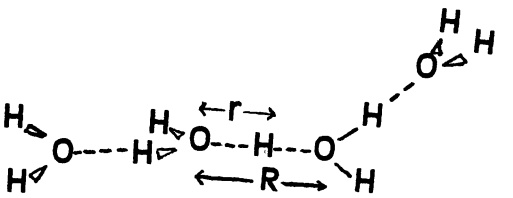
H
O
H
H
O
H
O
H
H
O
H
H
r
R
H
O
H
H

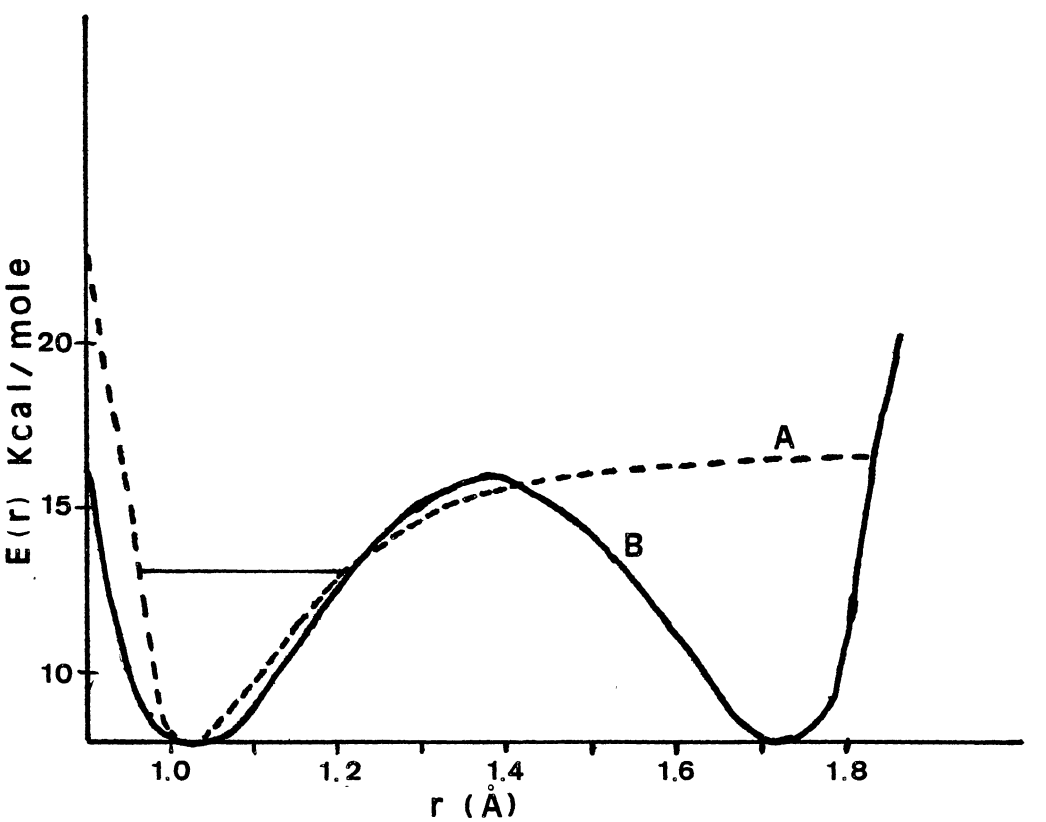
E(r) Kcal/mole
20
15
10
A
B
1.0
1.2
1.4
1.6
1.8
r (Å)

is assumed that the proton transfer step occurs with zero activation energy, i.e. the proton tunnels through the barrier. This probability (tunnelling coefficient) can be calculated using the potential of Scheiner by first calculating the probability of finding the proton at point b (see Figure 22) and dividing this result by the probability of finding the proton at point a.

$$(3.4) \quad t = | \phi_2(b) |^2 / | \phi_2(a) |^2$$

The wavefunctions used are those of Wentzel, Kramers, Brillouin and Jeffreys (WKBJ) approximation, and are given by 3.5.

$$(3.5) \quad \phi_2(x) = A[2m(V-E)]^{\frac{1}{4}} * (\exp -1/h \int_x^b [2m(V-E)]^{\frac{1}{2}} dx + i\exp 1/h \int_x^b [2m(V-E)]^{\frac{1}{2}} dx$$

The numerator in equation 3.4 is 2, while the denominator is given by equation 3.6. Notice that the constant $A[2m(V-E)]^{\frac{1}{4}}$ cancels out in equation 3.4.

$$(3.6) \quad \text{Denominator} = \exp -2/h \int_a^b [2m(V-E)]^{\frac{1}{2}} dx + \exp 2/h \int_a^b [2m(V-E)]^{\frac{1}{2}} dx$$

The tunnelling coefficient is given by equation 3.7

$$(3.7) \quad t = 2[\exp -2/h \int_a^b [2m(V-E)]^{\frac{1}{2}} dx + \exp 2/h \int_a^b [2m(V-E)]^{\frac{1}{2}} dx]^{-1}$$

If the barrier region above V_0, the difference between the barrier

Figure 22. Barrier from Which the Tunnelling Coefficient Was Determined (---) and Proton Transfer Barrier Determined by Scheiner (——) (35).

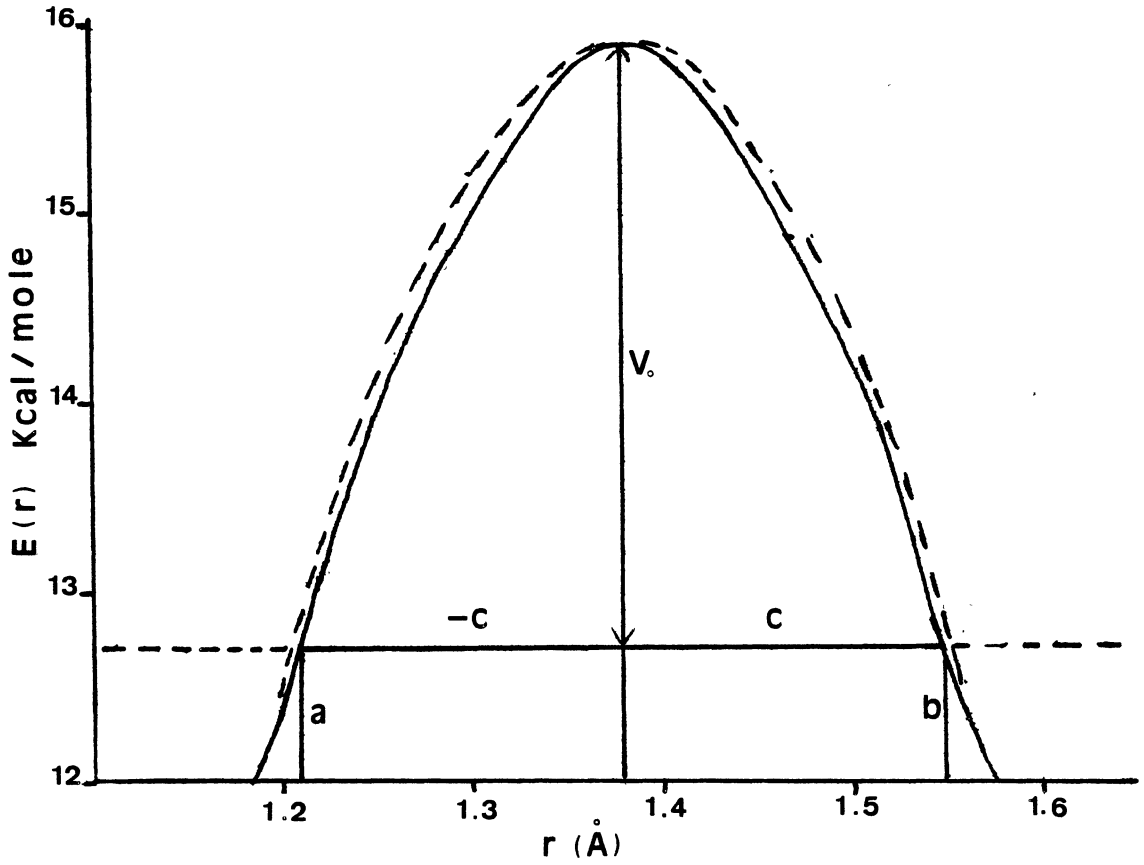
16
15
14
13
12
E(r) Kcal / mole
V₀
-c
c
a
b
1.2
1.3
1.4
1.5
1.6
r (Å)

height and the zero point energy (see Figure 22) is assumed to be parabolic, then the integrals in equation 3.7 can be done analytically,

$$(3.8) \quad I = \int_a^b [2m(V-E)]^{\frac{1}{2}} dx = (2mV_0)^{\frac{1}{2}} c\pi/2$$

c being the distance from the middle of the barrier to the turning point (see Figure 22). The proton and deuteron tunnelling coefficient calculated from the above procedure was 0.03 and .005, respectively. The oscillator frequency calculated from the curvature in the Morse potential is 3500 cm^{-1} which gives the hopping frequency of the proton (deuteron) in a one dimensional chain as 105 cm^{-1} (17.5 cm^{-1}), i.e. 3500 cm^{-1}*0.03. In the specific case of cubic ice the proton has three different one dimensional channels open for proton transfer. Therefore, the hopping frequency for the proton in ice should be around 300 cm^{-1} and 53 cm^{-1} for the deuteron hopping frequency. Because the upper limit of this frequency is expected to be around a period of the O-O lattice vibration (200 cm^{-1}), and, in fact, J. F. Nagle (36) has estimated from conductivity data that the hopping frequency is 47 cm^{-1}, one can conclude that proton transfer via tunnelling through the proton transfer barrier is certainly a possibility and crossing over the barrier is not the only way the proton can migrate through the crystal. Therefore, it is unlikely that the activation energy determined for the ethylene oxide clathrate hydrate is the energy needed to traverse the proton transfer barrier. The only thing that the preceeding calculation has done is to instill some confidence in the proton tunnelling mechanism in cubic ice but has not shed any light whatsoever on proton migration rates in clathrate hydrates. Inference from some recent

experimental results in cubic ice (27) might give some insights into what the activation energy determined in the ethylene oxide clathrate hydrate represents.

From the change in the infrared spectra of cubic ice samples which had been irradiated with 1.7 MeV electrons and subsequently annealed to 130 K, it was concluded that an equilibrium was established between the mobile protons in the sample and the protons that had been trapped in shallow L defect wells. This type of equilibrium was suggested by M. Kunst and J. M. Warman (38). If this is the case for cubic ice, then generalizing these results to clathrate hydrates, which presumably have a much greater i-defect concentration, one might postulate that the activation energy determined for the ethylene oxide clathrate hydrate is in some way dependent upon the energy needed to escape out of a shallow L defect trap. Such a mechanism is outlined in the following section.

(3.9) $2H_2O = H_3O^+ + OH^-$; ΔH_1^0 ionization step

(3.10) $[H_3O^+L] = H_3O^+ + L^-$; ΔH_2^0 escape step

(3.11) $[H_3O^+] = [H_3O^+L]/[L^-]\exp(\Delta S_2^0/R)\exp(-\Delta H_2^0/RT)$

(3.12) $[H_3O^+] = 1/[OH^-]\exp(\Delta S_1^0/R)\exp(-\Delta H_1^0/RT)$

Combining equations 3.11 and 3.12,

(3.13) $[H_3O^+L][OH^-]/[L^-] = \exp(\Delta S^1/R)\exp(-\Delta H^1/RT)$

where ΔS^1 is $\Delta S_1^0 - \Delta S_2^0$ and ΔH^1 is $\Delta H_1^0 - \Delta H_2^0$.

At equilibrium, $[H_3O^+]$ is equal to $[OH^-] - [H_3O^+L]$ and $[L^-]eq$ is equal to $[L^-] - [H_3O^+L]$. The concentration of L defects can be estimated by using equation 3.14 which was taken from reference 39, page 160.

$$(3.14)\quad [L^-] = 24.9\exp((-7.84\ \text{Kcal/mole})/RT)$$

From van't Hoffs equation (3.15-16) the equilibrium constants can be calculated if a reference point is known.

$$(3.15)\quad d\ \ln K/dT = \Delta H/RT$$

$$(3.16)\quad \ln\left(K(T_2)/K(T_1)\right) = -\Delta H/R[1/T_2 - 1/T_1]$$

The reference point is supplied by J. M. Warman and co-workers (32) in which they determined that K_2 (the equilibrium constant for the dissociation of the complex $[H_3O^+L]$) at 268 K was $[L^-]/6$ or 1.67E-6. They estimated at 268 K that the complex $[H3O^+L]$ concentration was six times the concentration of protons which was estimated to be 3.5E-10. Therefore, the hydroxide ion concentration should be the sum of the complex concentration and the proton concentration at 268 K or 2.45E-9M. The equilibrium constant for the ionization step can then be estimated from the hydroxide ion and proton concentrations and is 8.58E-19. Once the equilibrium constants have been determined at a temperature then the proton concentration can be determined at that temperature from the cubic polynomial in equation 3.17. This cubic polynomial was obtained by solving the equilibrium expression in equation 3.10 in terms of the known variables (K_1, K_2 and $[L^-]$) and the unknown proton concentration.

$$(3.17)\quad [H_3O^+]^3 + [H_3O^+]^2(K_2 + [L^-]) - [H_3O^+]K_1 - K_1K_2 = 0$$

The only parameters yet to be determined for the L defect trapping model is ΔH_1^0 (the ionization energy in cubic ice) and ΔH_2^0 (the binding energy of the complex H_3O^+L). The ionization energy in cubic ice is expected to be higher than the ionization energy of 13.5 Kcal/mole determined for liquid water (40). Measurements of the dc conductivity of ice (39) have estimated that this ionization energy

should be around 17 Kcal/mole. If 17 Kcal/mole is used as an estimate, then the proton concentration as a function of temperature can be calculated from van't Hoffs equation and Warmans estimate of the proton concentration of 3.5E-10 M at 288 K (see equation 3.19).

$$(3.19)\quad [H_3O^+](T_2) = 3.5E\text{-}10\exp(-\Delta H_1^0/2R^*[1/T_2-1/268])$$

At 155 and 130 K the proton concentration was determined to be 3E-15 and 1.5E-17 M, respectively. This proton concentration can then be used to estimate the number of protons present in a 1.75E-3 cm^3 ice sample. This sample volume is the volume of the cubic ice sample in which the conversion of D_2O into HOD was monitored spectroscopically (34). The estimated number of protons at 155 and 130 K was 3300 and 16 protons, respectively. The length of the linearized proton transfer chain was estimated to be 1.71E20 Å and the time that it took for one-fourth of the D_2O molecules to convert to HOD at 155 K was 144 seconds. As a proton moves through a site which contains a D_2O molecule, it converts the D_2O molecule into an HOD molecule and it can be estimated from the number of protons calculated above, that the proton must move at a minimum velocity of 9.1E05 cm/sec or a hopping frequency of 1100 cm^{-1}. The upper limit for this hopping frequency has already been placed at 200 cm^{-1}. Therefore, it can be concluded that the ionization energy of 17 Kcal/mole is too large because it underestimates the proton concentration at 155 K. From the hopping frequency upper limit, the upper limit of the ionization energy can be estimated by working the above procedure in reverse and the ionization energy that predicts a hopping frequency of 200 cm^{-1} was found to be ∿15 Kcal/mole. Therefore, an ionization energy of 15 Kcal/mole appears to be a value which is

more consistent with the proton transfer data of Collier and co-workers (34) and was used instead of the ionization energy of 17 Kcal/mole which was determined from the high temperature dc conductivity of ice. The binding energy of the complex $[H_3O^+L]$ has already been determined by Warman (38) and his value of 4.5 Kcal/mole was used as ΔH_2^0. In Table XIV the equilibrium concentration of the modelled specie are presented along with the proton concentrations that have been estimated from the proton transfer work of Devlin (34) in cubic ice. If the assumption is made that the hopping rate constant is proportional to the proton concentration, i.e. the ionic defect formation step in cubic ice is an equilibrium process, then the activation energy can be determined from an Arrhenius plot of $\ln[H_3O^+]$ versus 1/T. The results are presented in Figure 23. The activation energy determined from the L defect model is 7.46 Kcal/mole — not the observed activation energy of 9.5 Kcal/mole in pure cubic ice. However, the model does a reasonable job of predicting the observed rate data of base doped ice (see Table XV) if the assumption is made that the effect of base doping is to increase and stabilize the concentration of shallow traps at a minimum value of 1×10^{-8} M. The observed and predicted activation energies for base doped ice are 3.5 Kcal/mole. It must be concluded at this time that the L defect trapping model does not offer any new insights into the proton transfer mechanism in pure cubic ice and it is doubtful that it can be used to model the observed proton transfer rates in ethylene oxide clathrate hydrate because the parameters are less well defined in the clathrate hydrates than they are in cubic ice. A cursory attempt was made to fit the rate data obtained for the ethylene oxide clathrate hydrate to the L defect trapping model by

TABLE XIV

L DEFECT TRAP IN PURE CUBIC ICE

Temp (K)	OH^-	H_3O^+	L^-	H_3O^+L	K_2	K_1
268	2.5×10^{-9}	3.5×10^{-10}	1.0×10^{-5}	2.1×10^{-19}	1.7×10^{-6}	8.6×10^{-19}
155	3.3×10^{-14}	3.1×10^{-14}	2.2×10^{-10}	1.9×10^{-15}	3.5×10^{-9}	1.0×10^{-27}
150	1.5×10^{-14}	1.4×10^{-14}	9.4×10^{-11}	6.1×10^{-16}	2.2×10^{-9}	2.0×10^{-28}
145	6.1×10^{-15}	5.9×10^{-15}	3.8×10^{-11}	1.7×10^{-16}	1.3×10^{-9}	3.6×10^{-29}
140	2.4×10^{-15}	2.2×10^{-15}	1.4×10^{-11}	4.6×10^{-17}	7.4×10^{-10}	5.6×10^{-30}
135	8.8×10^{-16}	8.7×10^{-16}	5.0×10^{-12}	1.1×10^{-17}	4.0×10^{-10}	7.6×10^{-31}
130	3.0×10^{-16}	3.0×10^{-16}	1.6×10^{-12}	2.3×10^{-18}	2.1×10^{-10}	8.9×10^{-32}
125	9.3×10^{-17}	9.3×10^{-17}	4.9×10^{-13}	4.3×10^{-19}	1.1×10^{-10}	8.7×10^{-33}
120	2.7×10^{-17}	2.6×10^{-17}	1.3×10^{-13}	7.0×10^{-20}	5.0×10^{-11}	7.0×10^{-34}
115	6.8×10^{-18}	6.7×10^{-18}	3.1×10^{-14}	9.6×10^{-21}	2.2×10^{-11}	4.6×10^{-35}
110	1.5×10^{-18}	1.5×10^{-18}	6.6×10^{-15}	1.1×10^{-21}	8.9×10^{-12}	2.3×10^{-36}
105	3.0×10^{-19}	3.0×10^{-19}	1.2×10^{-15}	1.1×10^{-22}	3.4×10^{-12}	8.8×10^{-38}
100	4.9×10^{-20}	4.0×10^{-20}	1.8×10^{-16}	7.9×10^{-24}	1.1×10^{-12}	2.4×10^{-39}

ΔH_1^0 = 15 Kcal/mole.

ΔH_2^0 = 4.5 Kcal/mole.

$[L^-] = 1\times10^{-8}$ M.

Figure 23. Arrhenius Behavior of the Hopping Step in Pure Cubic Ice Determined by Devlin (A) (34) and Arrhenius Behavior Predicted by the L Defect Trapping Model in Pure Cubic Ice (B).

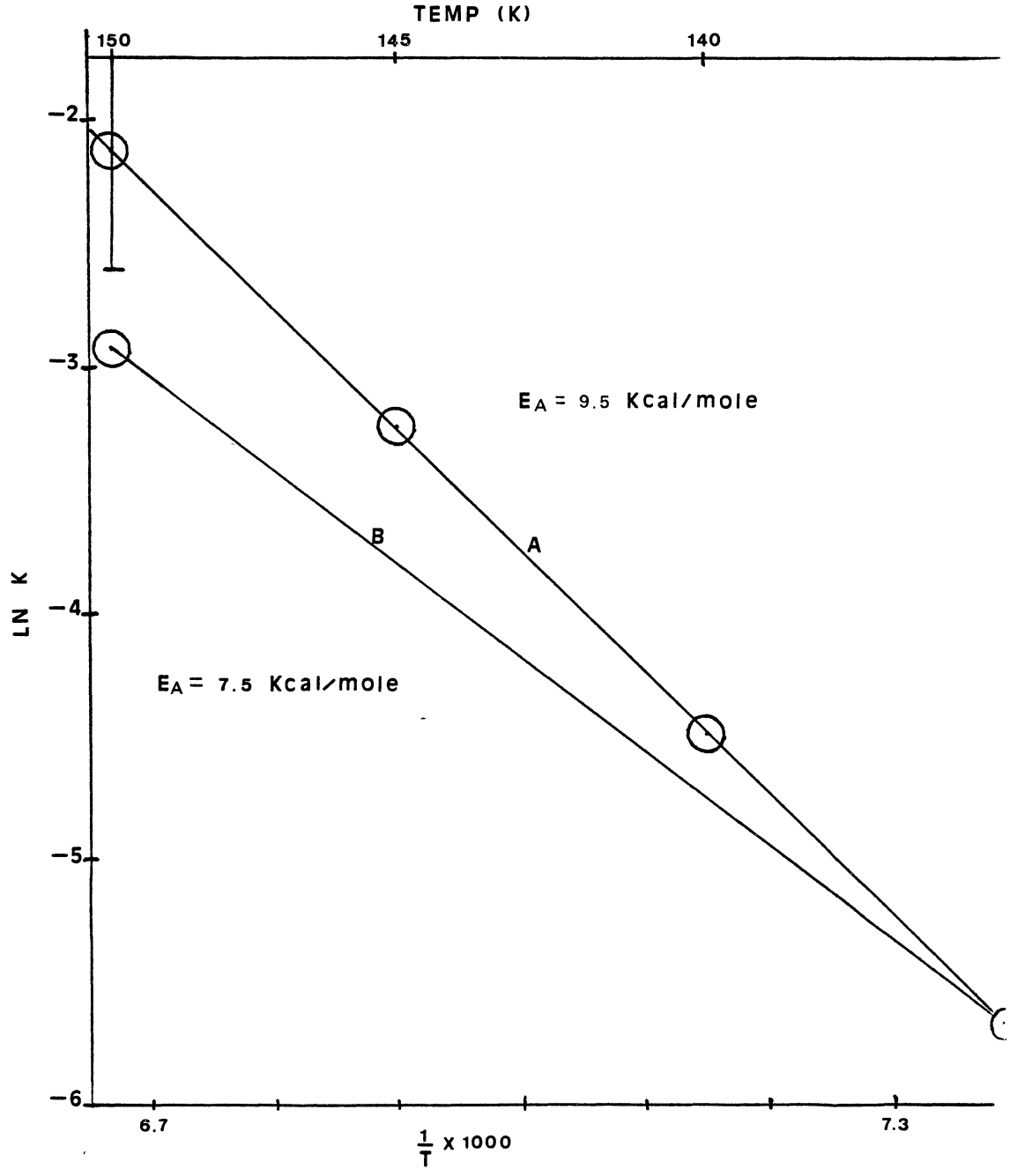
TEMP (K)
150
145
140
-2
-3
-4
-5
-6
LN K
E_A = 9.5 Kcal/mole
E_A = 7.5 Kcal/mole
A
B
6.7
7.3
$\frac{1}{T}$ X 1000

TABLE XV

L DEFECT TRAP IN BASE DOPED CUBIC ICE

Temp (K)	OH^-	H_3O^+	L^-	H_3O^+L	K_2	K_1
268	2.5×10^{-9}	3.5×10^{-10}	1.0×10^{-5}	2.1×10^{-7}	1.7×10^{-6}	8.6×10^{-19}
155	6.3×10^{-14}	1.6×10^{-14}	1.0×10^{-8}	4.7×10^{-14}	3.5×10^{-9}	1.0×10^{-27}
150	3.4×10^{-14}	6.0×10^{-15}	1.0×10^{-8}	2.8×10^{-14}	2.2×10^{-9}	2.0×10^{-28}
145	1.0×10^{-14}	2.0×10^{-15}	1.0×10^{-8}	1.6×10^{-14}	1.3×10^{-9}	3.6×10^{-29}
140	9.0×10^{-15}	6.2×10^{-16}	1.0×10^{-8}	8.4×10^{-15}	7.4×10^{-10}	5.6×10^{-30}
135	4.4×10^{-13}	1.7×10^{-16}	1.0×10^{-8}	4.3×10^{-15}	4.0×10^{-10}	7.6×10^{-31}
130	2.1×10^{-15}	4.3×10^{-17}	1.0×10^{-8}	2.0×20^{-15}	2.1×10^{-10}	8.9×10^{-32}
125	9.1×10^{-16}	9.5×20^{-18}	1.0×10^{-8}	9.0×10^{-16}	1.1×10^{-10}	8.7×10^{-23}
120	3.8×10^{-16}	1.9×10^{-18}	1.0×10^{-8}	3.7×10^{-16}	5.0×10^{-11}	7.0×10^{-34}
115	1.4×10^{-16}	3.2×10^{-19}	1.0×10^{-8}	1.4×10^{-16}	2.2×10^{-11}	4.6×10^{-35}
110	5.1×10^{-17}	4.5×10^{-20}	1.0×10^{-8}	5.1×10^{-17}	8.9×10^{-12}	2.3×10^{-26}
105	1.6×10^{-17}	5.4×10^{-21}	1.0×10^{-8}	1.6×10^{-17}	3.4×10^{-12}	8.8×10^{-38}
100	4.6×10^{-18}	5.2×10^{-22}	1.0×10^{-8}	4.6×10^{-18}	1.1×10^{-12}	2.4×10^{-39}

ΔH_1^0 = 15 Kcal/mole

ΔH_2^0 = 4.5 Kcal/mole

$[L^-] = 1\times10^{-8}$ M.

assuming that all of the parameters were the same between cubic ice and clathrate hydrates except for the L defect formation energy. Davidson (14) has determined that the sum of the L defect formation energy and the energy to mobilize the L defect should be 7.7 Kcal/mole. This is considerably lower than the corresponding energy in ice of 13.2 Kcal/mole. In ice, the L defect formation energy is 7.84 Kcal/mole; therefore, one would expect the L defect formation energy in the clathrate hydrate to be between 2.5 and 4.5 Kcal/mole. These results are presented in Table XVI where the predicted activation energy is around 7.5 Kcal/mole and the proton concentration is much too low to predict the observed rate data.

At this point a detailed mechanism which explains the observed rate data in ethylene oxide clathrate hydrate has not been developed. It can only be speculated that the relatively low activation energy obtained in the hydrate might be the energy needed for the proton to escape out of a shallow trap. It is also uncertain if this shallow trap is caused by an intrinsic defect such as the L defect or an extrinsic defect such as a contaminant. To summarize, the information obtained from the rate data of the ethylene oxide clathrate hydrate follows: 1) The ionization energy in the ethylene oxide clathrate hydrate should be the same or slightly higher than the ionization energy in cubic ice because the hydrogen bond lengths are slightly longer in the hydrate than they are in cubic ice (cubic ice 2.75 Å; clathrate hydrate 2.77 Å). This means that the ionization energy in clathrate hydrates should be greater than 15 Kcal/mole. 2) The activation energy determined in the temperature range between 100-120 K is not directly related to the ionization energy as would be expected

TABLE XVI

L DEFECT TRAP FOR CLATHRATE HYDRATES

Temp (K)	OH^-	H_3O^+	L^-	H_3O^+L	K_2	K_1
268	2.6×10^{-8}	3.2×10^{-11}	1.4×10^{-3}	2.7×10^{-8}	1.7×10^{-6}	8.6×10^{-19}
155	1.8×10^{-12}	5.6×10^{-16}	1.2×10^{-5}	1.8×10^{-12}	3.5×10^{-9}	10×10^{-27}
150	8.7×10^{-13}	2.4×10^{-16}	7.0×10^{-6}	8.7×10^{-13}	2.2×10^{-19}	2.0×10^{-28}
145	3.9×10^{-12}	9.3×10^{-17}	5.3×10^{-6}	3.8×10^{-13}	1.3×10^{-9}	3.6×10^{-29}
140	1.6×10^{-13}	3.5×10^{-17}	3.4×10^{-6}	1.6×10^{-13}	7.4×10^{-10}	5.6×10^{-30}
135	6.4×10^{-14}	1.2×10^{-17}	2.2×10^{-6}	6.4×10^{-14}	4.0×10^{-10}	7.6×10^{-31}
130	2.3×10^{-14}	3.8×10^{-18}	1.3×10^{-6}	2.3×10^{-14}	2.1×10^{-10}	8.9×10^{-32}
125	7.0×10^{-15}	1.1×10^{-18}	7.6×10^{-7}	7.9×10^{-15}	1.1×10^{-10}	8.7×10^{-33}
120	2.4×10^{-15}	2.9×10^{-19}	4.2×10^{-7}	2.4×10^{-15}	5.0×10^{-11}	7.0×10^{-34}
115	6.8×10^{-16}	6.7×10^{-20}	2.2×10^{-7}	6.8×10^{-16}	2.2×10^{-11}	4.6×10^{-35}
110	1.7×10^{-16}	1.4×10^{-20}	1.1×10^{-7}	1.7×10^{-16}	8.9×10^{-12}	2.3×10^{-36}
105	3.7×10^{-17}	2.4×10^{-21}	5.2×10^{-8}	3.7×10^{-17}	3.4×10^{-12}	8.8×10^{-38}
100	6.9×10^{-18}	3.5×10^{-22}	2.2×10^{-8}	6.9×10^{-18}	1.1×10^{-12}	2.4×10^{-39}

ΔH_1^0 = 15 Kcal/mole.

ΔH_2^0 = 4.5 Kcal/mole.

$[L^-]$ = exp-3.5/RT.

from results obtained in cubic ice. The relatively low activation energy of 4.5 Kcal/mole is indicative of a shallow trapping mechanism — not the deep traps of the hydroxide ions. 3) If the proton concentration in the ethylene oxide clathrate hydrate was a result of a thermal equilibrium, then the entropy change associated with ion defect formation in the clathrate hydrate must be greater than the corresponding change in cubic ice because, in a temperature region where the proton migration through the ice crystal was stopped because of lack of ionic defects (< 120 K), the D_2O half life was on the order of 9 minutes at 120 K in the ethylene oxide clathrate hydrate. If this is not the case, then an anomalously high non-equilibrium concentration of protons must have been incorporated into the hydrate with crystallization.

Evans Holes in the Ethylene Oxide Clathrate Hydrate

Evans holes have been observed in the infrared and Raman spectra of various materials (41-43). They are narrow frequency regions of enhanced transmission where mixing of modes occur with the absorption minimum a sharp band superimposed on a broad band. The infrared spectra of the ethylene oxide clathrate hydrate in which Evans holes were obtained is presented in Figures 24-25 along with some spectra in which positive (non-resonance) bands were obtained. The assignment of the bands which were causing the holes is presented in Table XVII. These resonance phenomena have been described by J. C. Evans in the following manner (42). Let E_1^0 be the unperturbed energy of the sharp band while E_2^0 is the unperturbed energy of the broad band. Ψ_1^0 and

Figure 24. Evans Holes in the Ethylene Oxide Clathrate Hydrate.
A - 10 K; B - 20 K; C - 30 K; D - 40 K; E - 50 K;
F - 60 K; G - 70 K; H - 80 K; I - 90 K; J - 100 K;
K - 110 K; L - 120 K; and M - 130 K.

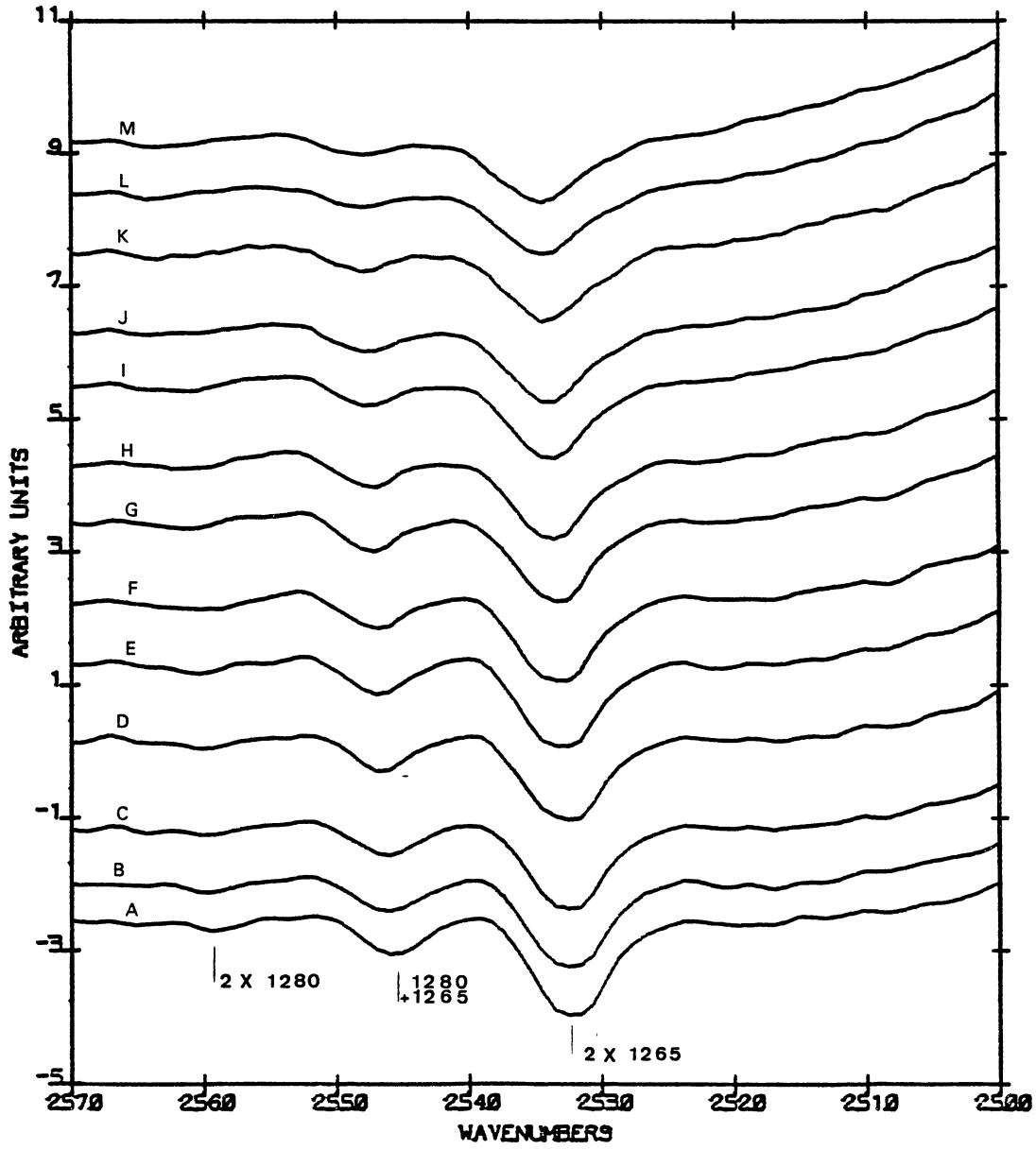
11
9
7
5
3
1
-1
-3
-5
M
L
K
J
I
H
G
F
E
D
C
B
A
ARBITRARY UNITS
2 X 1280
1280
+1265
2 X 1265
2570
2560
2550
2540
2530
2520
2510
2500
WAVENUMBERS

Figure 25. Positive (Non-resonance) Peaks in the Ethylene Oxide Clathrate Hydrate. A - 10 K; B - 20 K; C - 30 K; D - 40 K; E - 50 K; F - 60 K; G - 70 K; H - 80 K; I - 90 K; J - 100 K; K - 110 K; and L - 120 K.

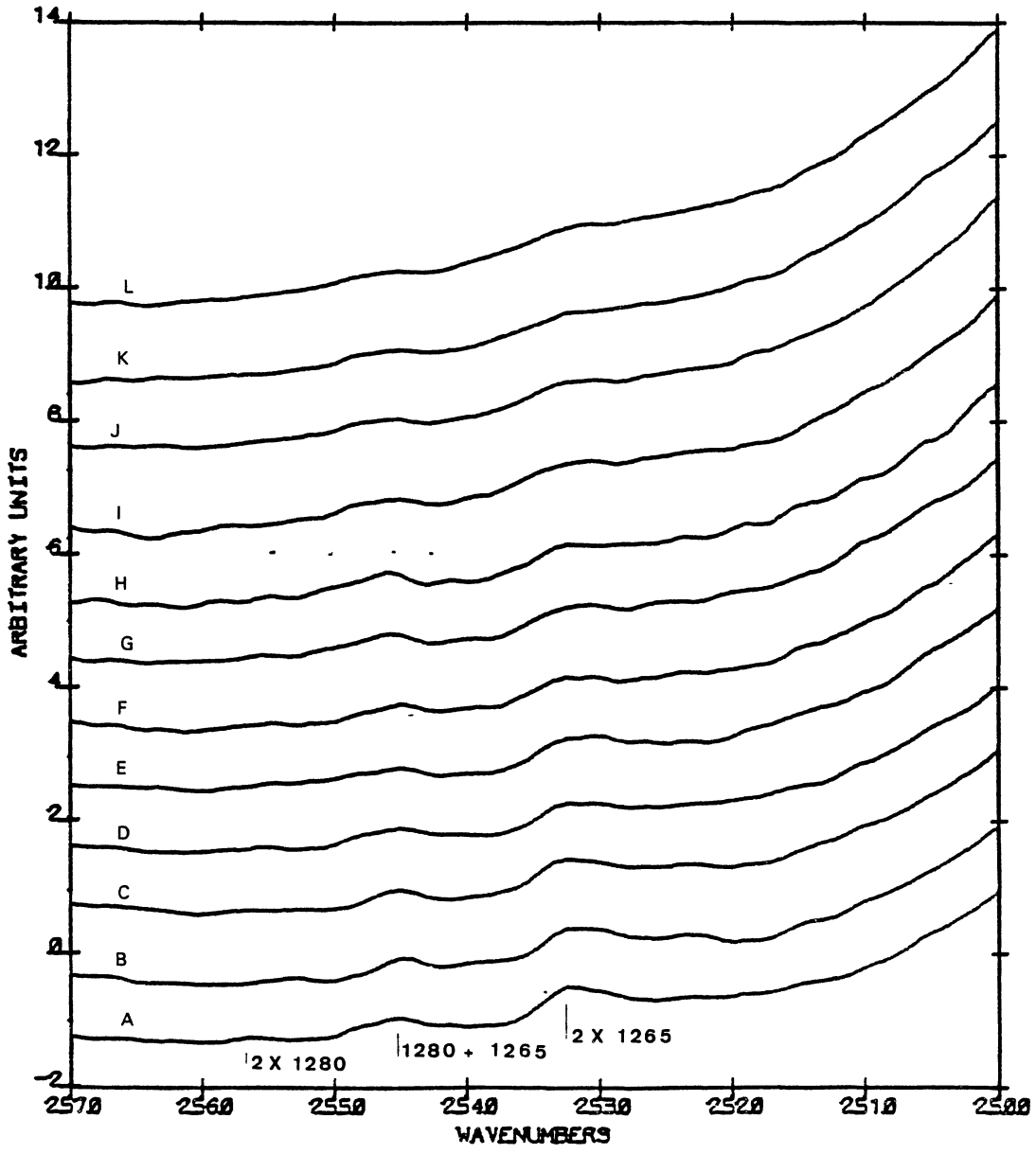
14
12
10
8
6
4
2
0
-2
ARBITRARY UNITS
L
K
J
I
H
G
F
E
D
C
B
A
2 X 1280
1280 + 1265
2 X 1265
2570
2560
2550
2540
2530
2520
2510
2500
WAVENUMBERS

TABLE XVII

ASSIGNMENT OF EVANS HOLES

ν (cm^{-1})	Assignment	$\Delta\nu$ (cm^{-1})	Remarks
2559	2 x 1279.5	0	Overtone of ν_3 from small cage
2546	1279.5 + 1265.5	1	Combination of ν_3 from small and large cage
2533	2 x 1265.5	2	Overtone of ν_3 from large cage
2433	1279.5 + 1154	-0.5	Combination of ν_3 from small cage and ν_{11}, ν_{14} from small cage.
2423	1279.5 + 1145	-1.5	Combination of ν_3 from small cage and ν_{11}, ν_{14} from large cage.
2410	1265.5 + 1145	-0.5	Combination of ν_3 from large cage and ν_{11}, ν_{14} from large cage.

Ψ_2^0 are the unperturbed wavefunctions associated with E_1^0 and E_2^0, respectively. If Ψ_1^0 and Ψ_2^0 have the same symmetry and $E_1^0 \cong E_2^0$, then first order perturbation theory can be used to study the interaction between these wavefunctions. The different Ψ's must be of the same symmetry because their subspaces must overlap in order for an intersection to exist between them. This interaction Hamiltonian is given by equation 3.21 in which all of the off-diagonal terms are incorporated in H^1, i.e. $(Y_1^0/H^1/Y_1^0) = 0$ and $(Y_1^0/H^0/Y_2^0) = 0$. The perturbed wavefunctions can be written as linear combinations of the zero order wavefunctions (Ψ_1^0, Ψ_2^0) and are given by equations 322-23.

$$(3.21) \quad H = H^0 + H^1$$

$$(3.22) \quad \Psi_1 = a\Psi_1^0 - b\Psi_2^0$$

$$(3.23) \quad \Psi_2 = b\Psi_1^0 + a\Psi_2^0$$

The perturbed or new energies are given by equation 3.24 where Δ is equal to $[\delta^2 + 4W_{12}^2]^{\frac{1}{2}}$ and W_{12} is the off-diagonal matrix element of the secular equation, i.e. $(Y_1^0/H^1/Y_2^0)$ while δ is equal to $E_1^0 - E_2^0$.

$$(3.24) \quad E_1 \text{ or } E_2 = 1/2(E_1^0 + E_2^0) \pm 1/2\Delta$$

If the intensity of the broad band (I_2) is much greater than the intensity of the sharp band (I_1) then equation 3.25 holds.

$$(3.25) \quad I_1/I_2 = b^2/a^2$$

The constants a and b can be determined from $(\Psi_1^0/H/\Psi_1)$ which is equal to $E_1(\Psi_1^0/\Psi_1)$ and the fact that Ψ_1 and Ψ_2 are normalized wavefunctions.

$$(3.26) \quad a = [(\Delta+\delta)/2\Delta]^{\frac{1}{2}}; \quad b = [(\Delta-\delta)/2\Delta]^{\frac{1}{2}}$$

Evans has used the above equations to compute a fictitious band envelope for W = 10 cm^{-1} and a half band width for E_2^0 of 150 cm^{-1}. His results are shown in Figures 26 and 27. It should be noted that the negative band is always closer to the broad band maximum while the positive peaks are perturbed further from it in the Evans theory. If the two bands are coincident then the new band envelope will have only a single minimum and not the derivative behavior seen when the bands are not coincident (see Figure 27). However, the holes that are seen in the ethylene oxide clathrate hydrate do not appear as the derivative bands that Evans theory would have predicted. This behavior can be explained if the assumption is made that the E band in the ethylene oxide clathrate hydrate is really the very broad combination band of the hydrate lattice instead of the isolated HOD or D_2O band. The slope of this lattice combination band is nearly zero in the Evans hole region and the hole profile should be very similar to what is observed when E_1^0 is coincident with E_2^0, i.e. only a single minimum should be observed.

The temperature dependence of the Evans holes is shown in Figure 28 and it should be noted that with an increasing temperature the holes move in the same direction as the bands from which they are originated as they should (toward higher frequencies), while the non-resonance positive peaks do not seem to follow this temperature dependence. One would have to wonder if the positive peaks are being affected by an anharmonic distortion, whereas the holes are not affected by this distortion. This situation could arise if the positive non-resonance bands are the combination modes of the ethylene oxide V_3 band (see

Figure 26. Evans Hole (b) Predicted from Theory If the Interacting Bands (a) Are Non-coincident.

Figure 27. Evans Hole (b) Predicted from Theory If the Interacting Bands (a) Are Coincident.

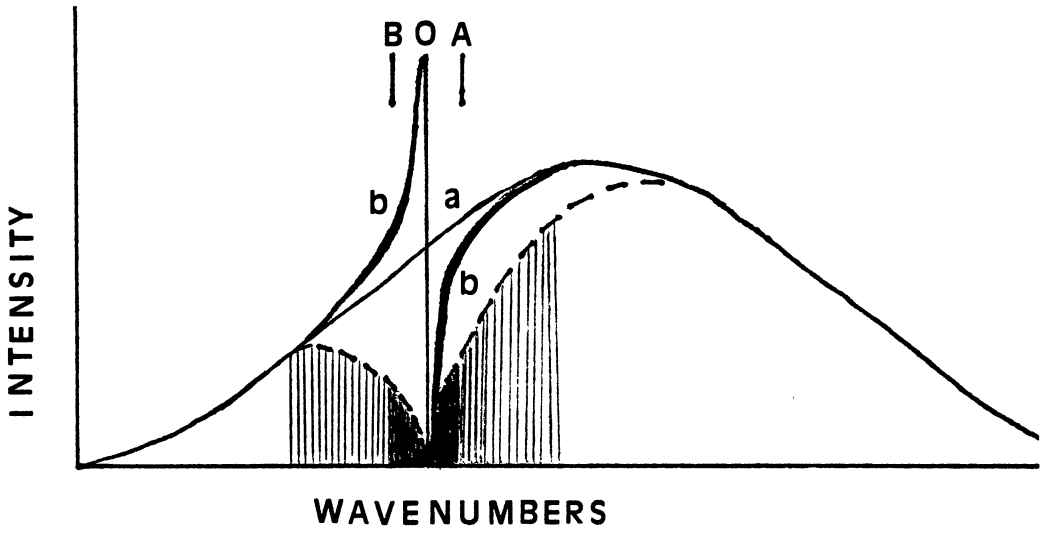
B O A
b
a
b
INTENSITY
WAVENUMBERS

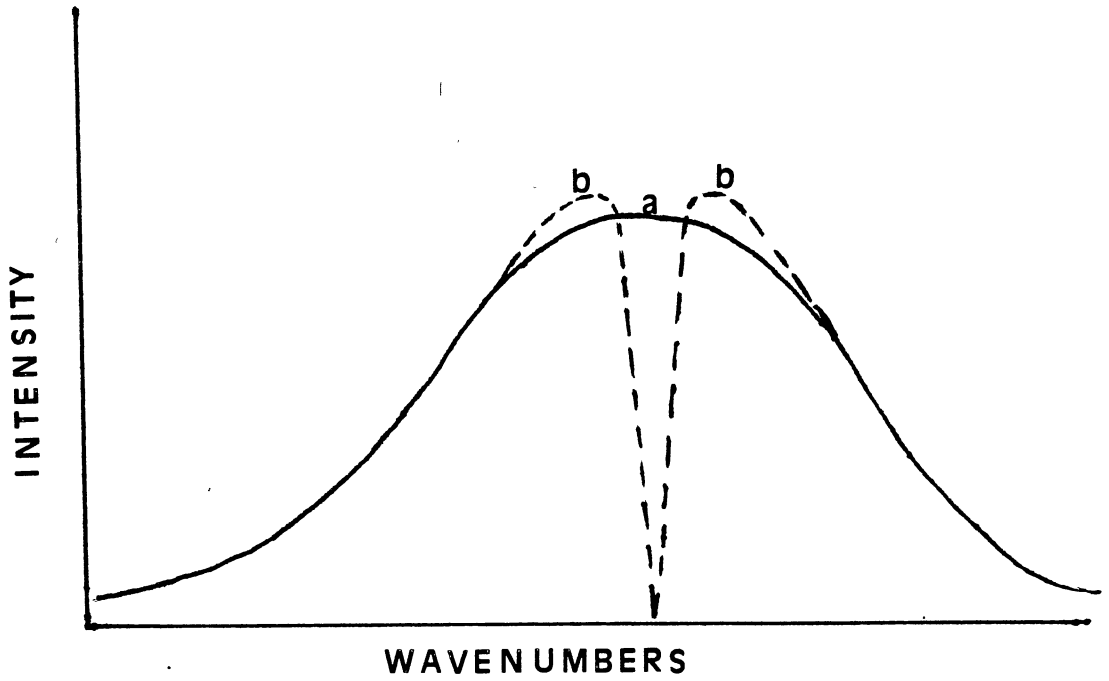
b
a
b
INTENSITY
WAVENUMBERS

Figure 28. Comparison of the Evans Holes and Positive Peaks Obtained in the Ethylene Oxide Clathrate Hydrate. A - positive peaks at 10 K; B - Evans holes at 10 K; C - positive peaks at 100 K; and D - Evans holes at 100 K.

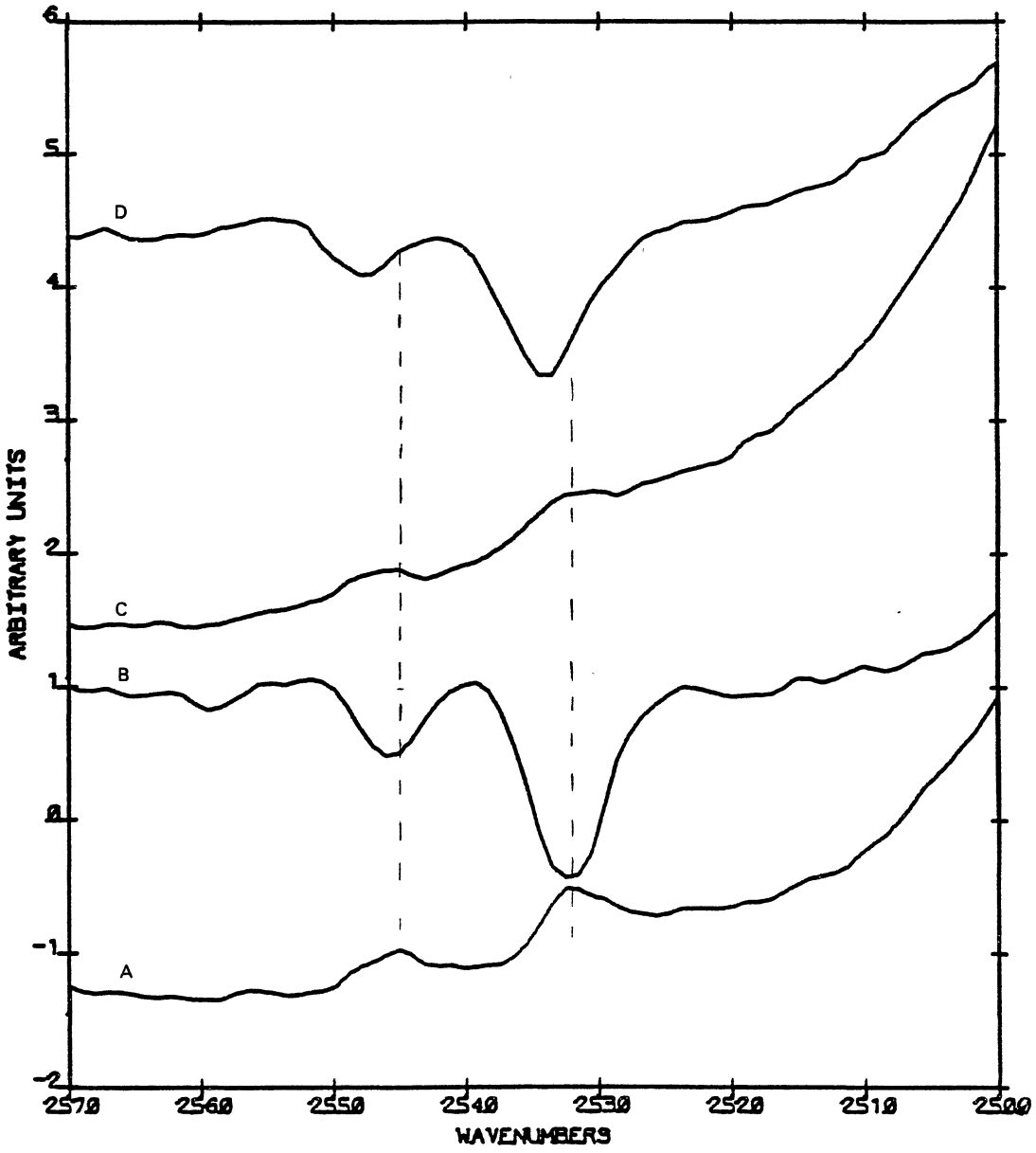
6
5
4
3
2
1
0
-1
-2
ARBITRARY UNITS
D
C
B
A
2570
2560
2550
2540
2530
2520
2510
2500
WAVENUMBERS

Table XVII), where the positive band at 2532 cm^{-1} would be the overtone of the ethylene oxide molecules in the large cage, while the band at 2556 cm^{-1} would be the overtone of the V_3 band from the ethylene oxide molecule in the small cages. The band at 2545 cm^{-1} would be the combination band of the V_3 mode from the small-caged ethylene oxide molecules with the V_3 mode of the large-caged ethylene oxide molecules. Another aspect that is puzzling at this point is the dependence of sample preparation upon the formation of Evans holes. Samples with higher concentrations of ethylene oxide appeared to produce samples with Evans holes, whereas samples with a lesser concentration of ethylene oxide had positive non-resonance bands in the infrared spectrum. However, it should be noted this observation has not been proven in any type of quantitative manner.

Chemical Effects of Irradiation of the Ethylene Oxide Clathrate Hydrate

The ethylene oxide clathrate hydrate was irradiated at 80 K with 1.7 MeV electrons from a Van de Graaff generator for 25 minutes to give a total dosage of ∿1E22 eV/g radiation (37). The results of the radiolysis are presented in Figures 29-36. It is believed that some of the ethylene oxide molecules inside the cages decomposed into different products with radiolysis and have remained inside the cages. An obvious product is CO (Figure 37) whose characteristic frequency of 2136 cm^{-1} eliminates consideration of most other possible molecules. The temperature dependence of the infrared absorption of the CO molecule (Figure 38) gives credence to the conclusion that the products are still enclathrated. The difference between the after irradiation

Figure 29. Comparison of the Before (A) and After (B) 1.7 MeV Electron Radiation of the Ethylene Oxide Clathrate Hydrate at 10 K.

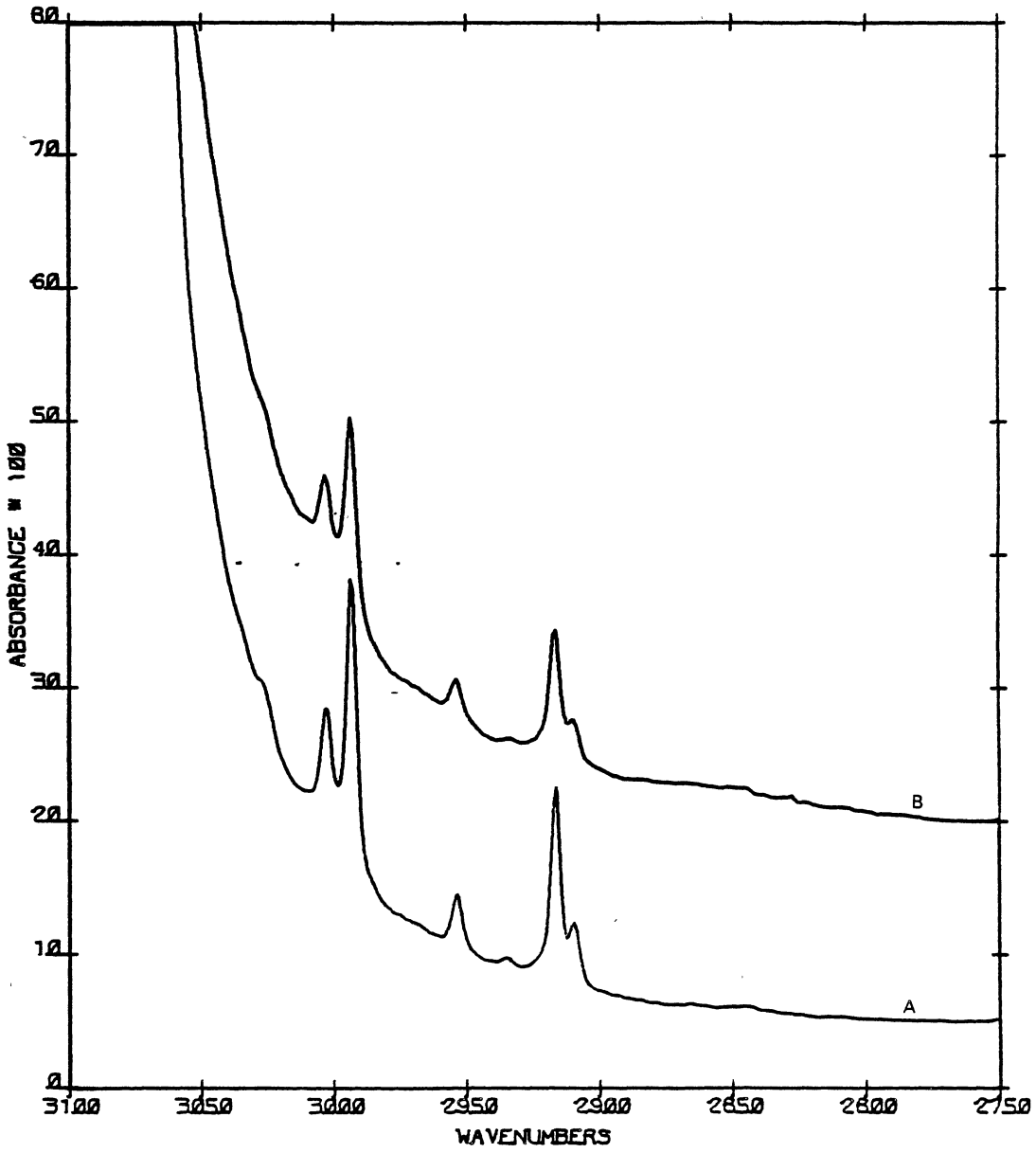
80
70
60
50
40
30
20
10
0
ABSORBANCE * 100
3100
3050
3000
2950
2900
2850
2800
2750
WAVENUMBERS
B
A

Figure 30. Comparison of the Before (A) and After (B) 1.7 MeV Electron Radiation of the Ethylene Oxide Clathrate Hydrate at 10 K.

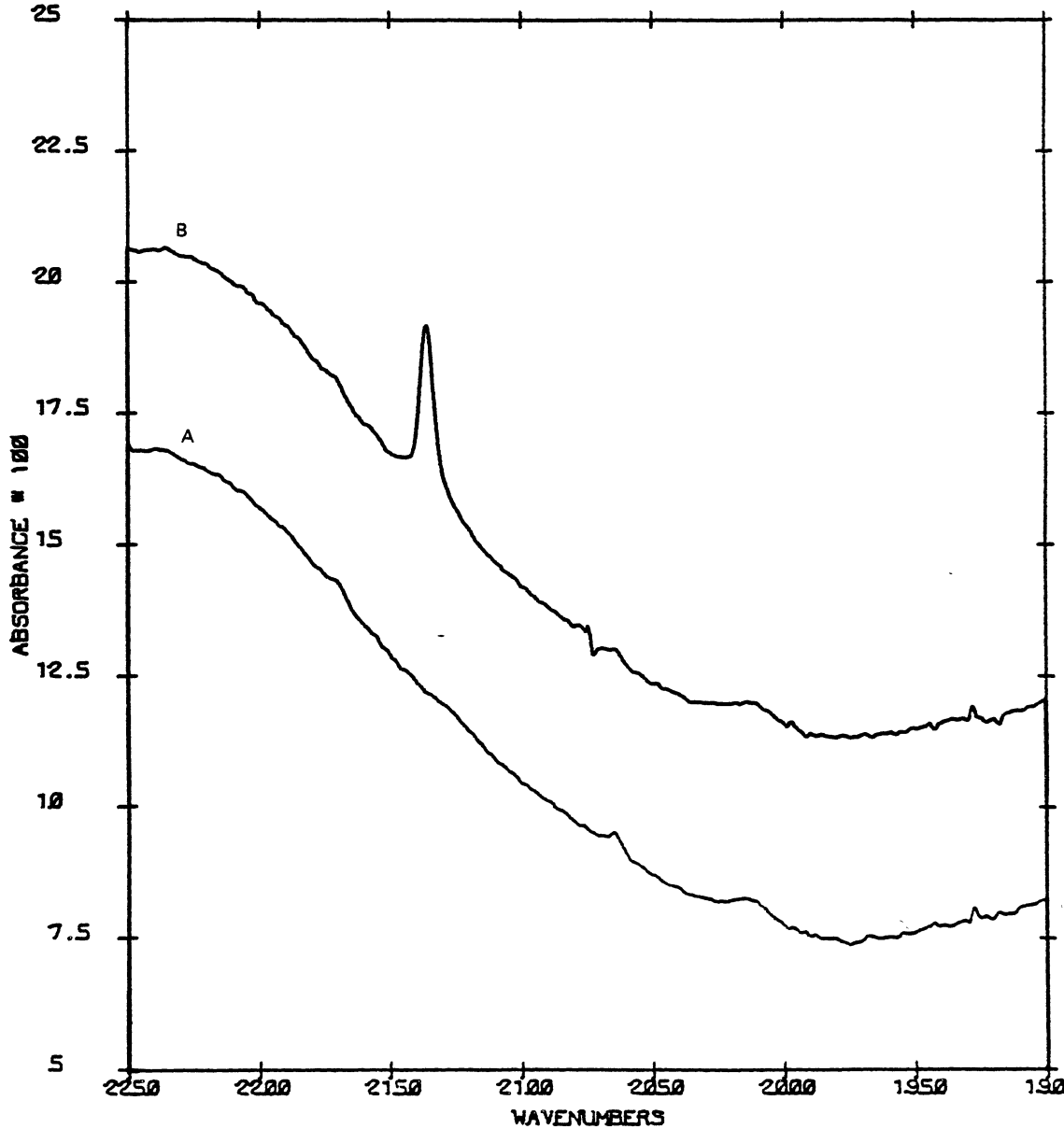
25
22.5
20
17.5
15
12.5
10
7.5
5
ABSORBANCE * 100
B
A
2250
2200
2150
2100
2050
2000
1950
1900
WAVENUMBERS

Figure 31. Comparison of the Before (A) and After (B) 1.7 MeV Electron Radiation of the Ethylene Oxide Clathrate Hydrate at 10 K.

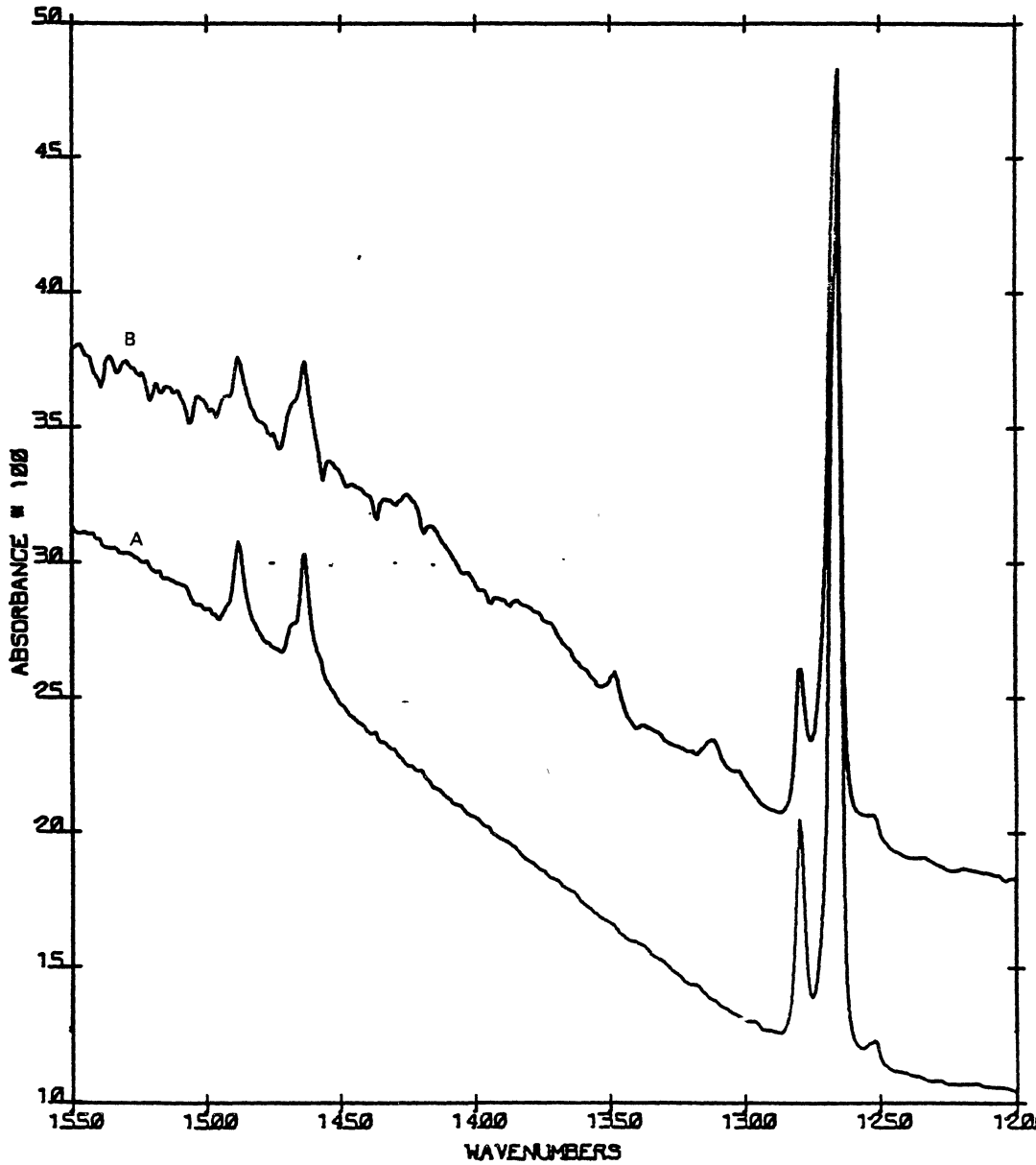
50
45
40
35
30
25
20
15
10
ABSORBANCE = 100
B
A
1550
1500
1450
1400
1350
1300
1250
1200
WAVENUMBERS

Figure 32. Comparison of the Before (A) and After (B) 1.7 MeV Electron Radiation of the Ethylene Oxide Clathrate Hydrate at 10 K.

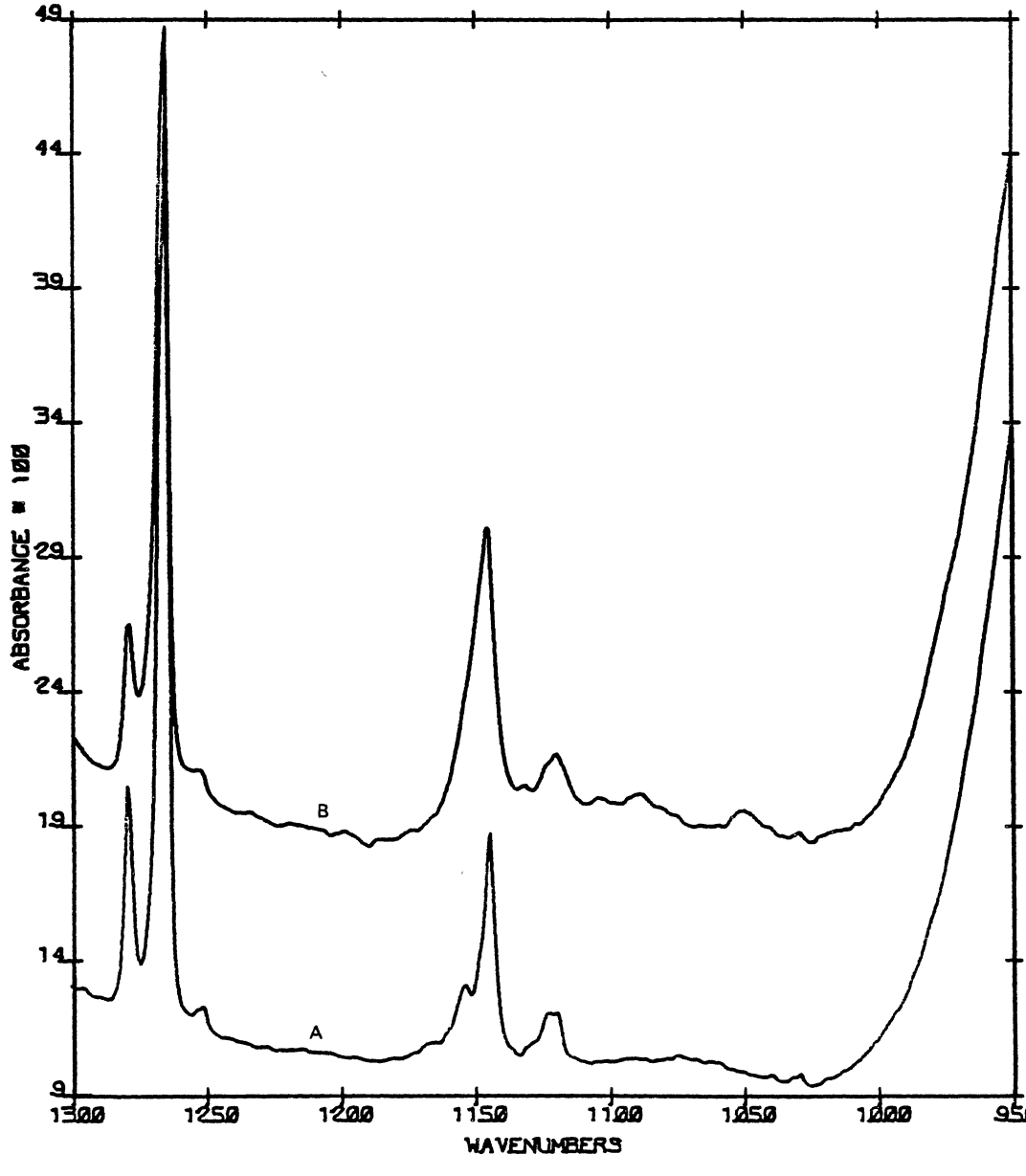
49
44
39
34
29
24
19
14
9
ABSORBANCE * 100
B
A
1300
1250
1200
1150
1100
1050
1000
950
WAVENUMBERS

Figure 33. Subtraction of the Before Irradiation Spectrum from the After Irradiation Spectrum.

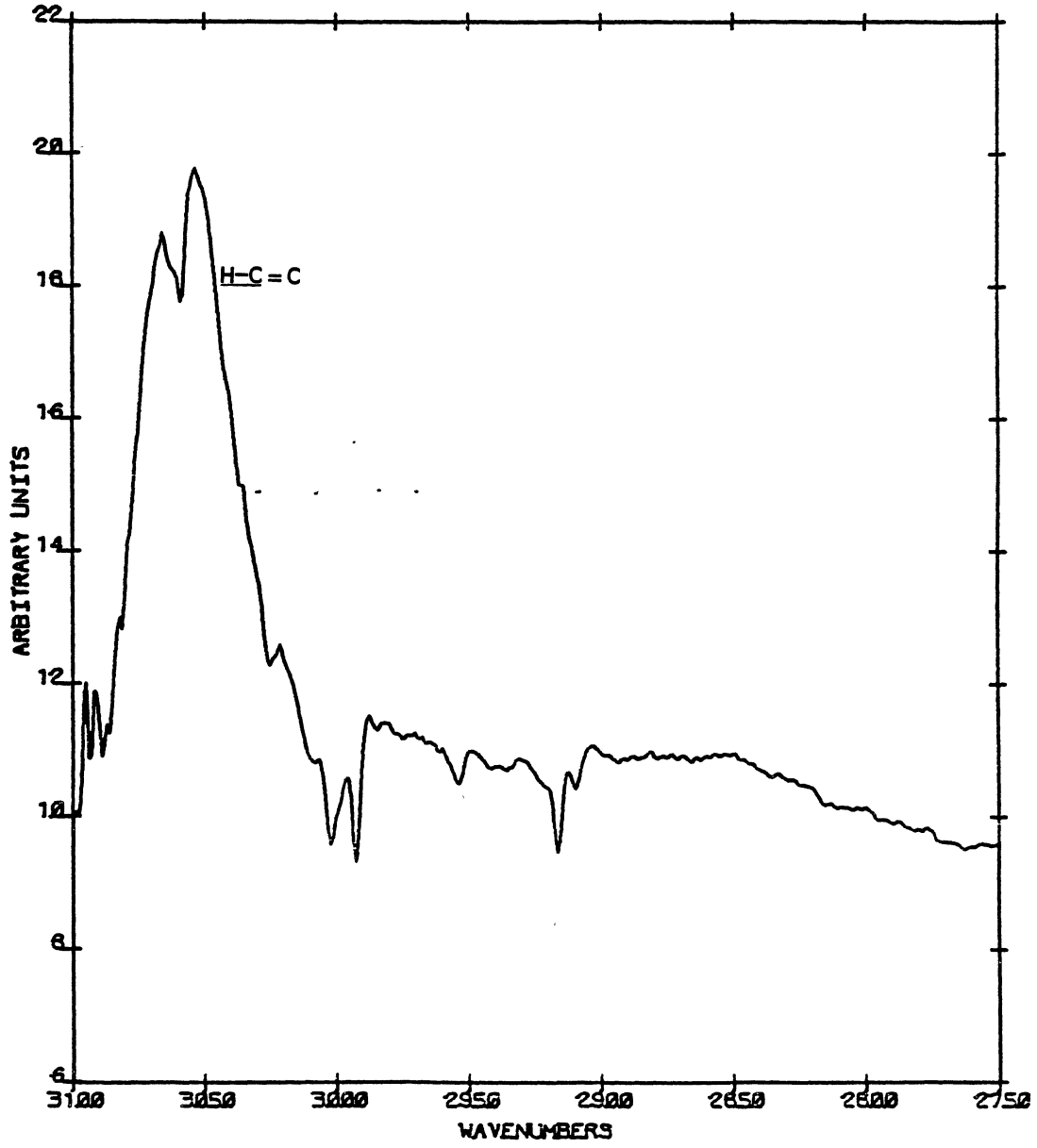
22
20
18
16
14
12
10
8
6
H–C = C
ARBITRARY UNITS
3100
3050
3000
2950
2900
2850
2800
2750
WAVENUMBERS

Figure 34. Subtraction of the Before Irradiation Spectrum from the After Irradiation Spectrum.

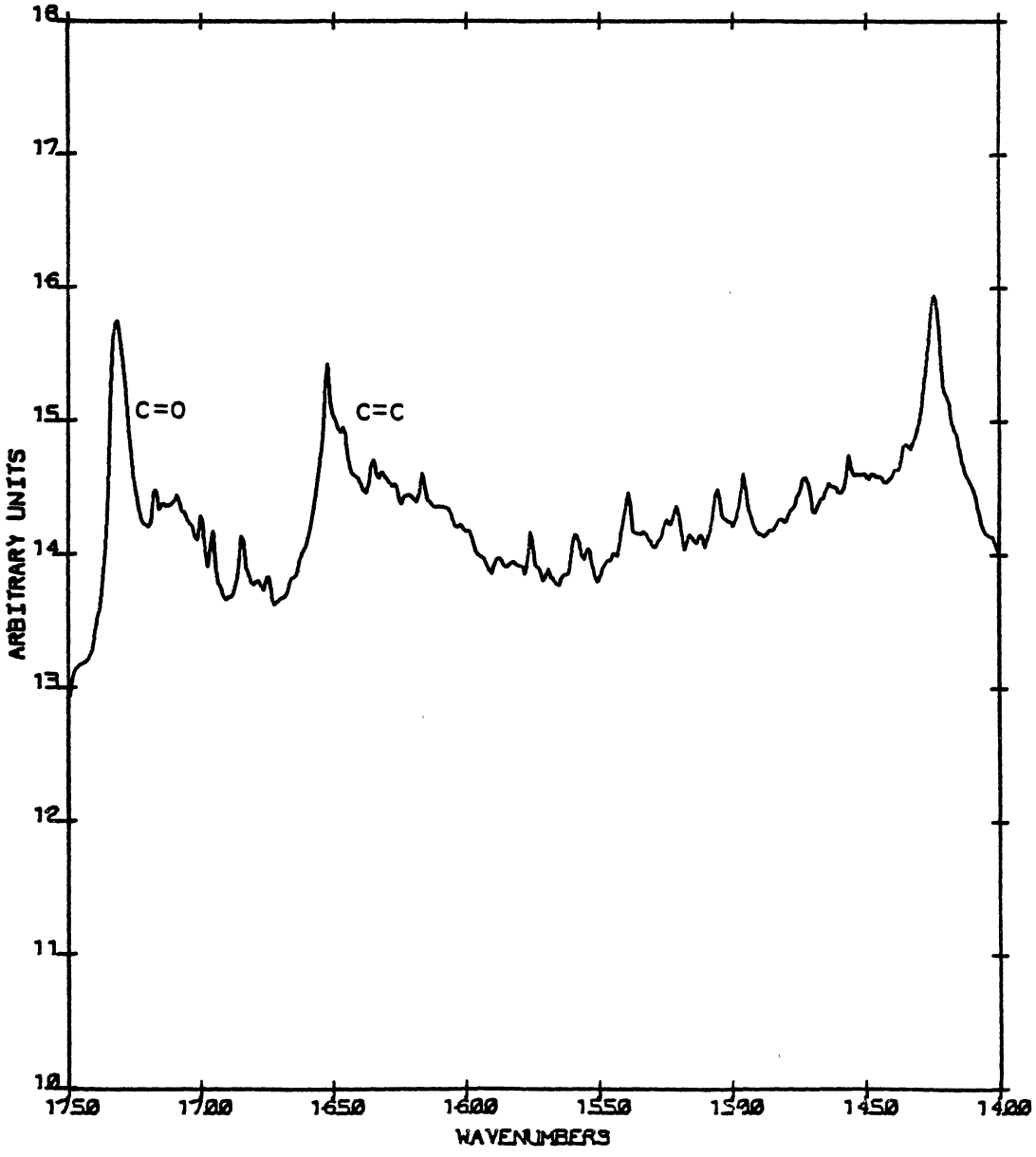
18
17
16
15
14
13
12
11
10
ARBITRARY UNITS
C=O
C=C
1750
1700
1650
1600
1550
1500
1450
1400
WAVENUMBERS

Figure 35. Subtraction of the Before Irradiation Spectrum from the After Irradiation Spectrum.

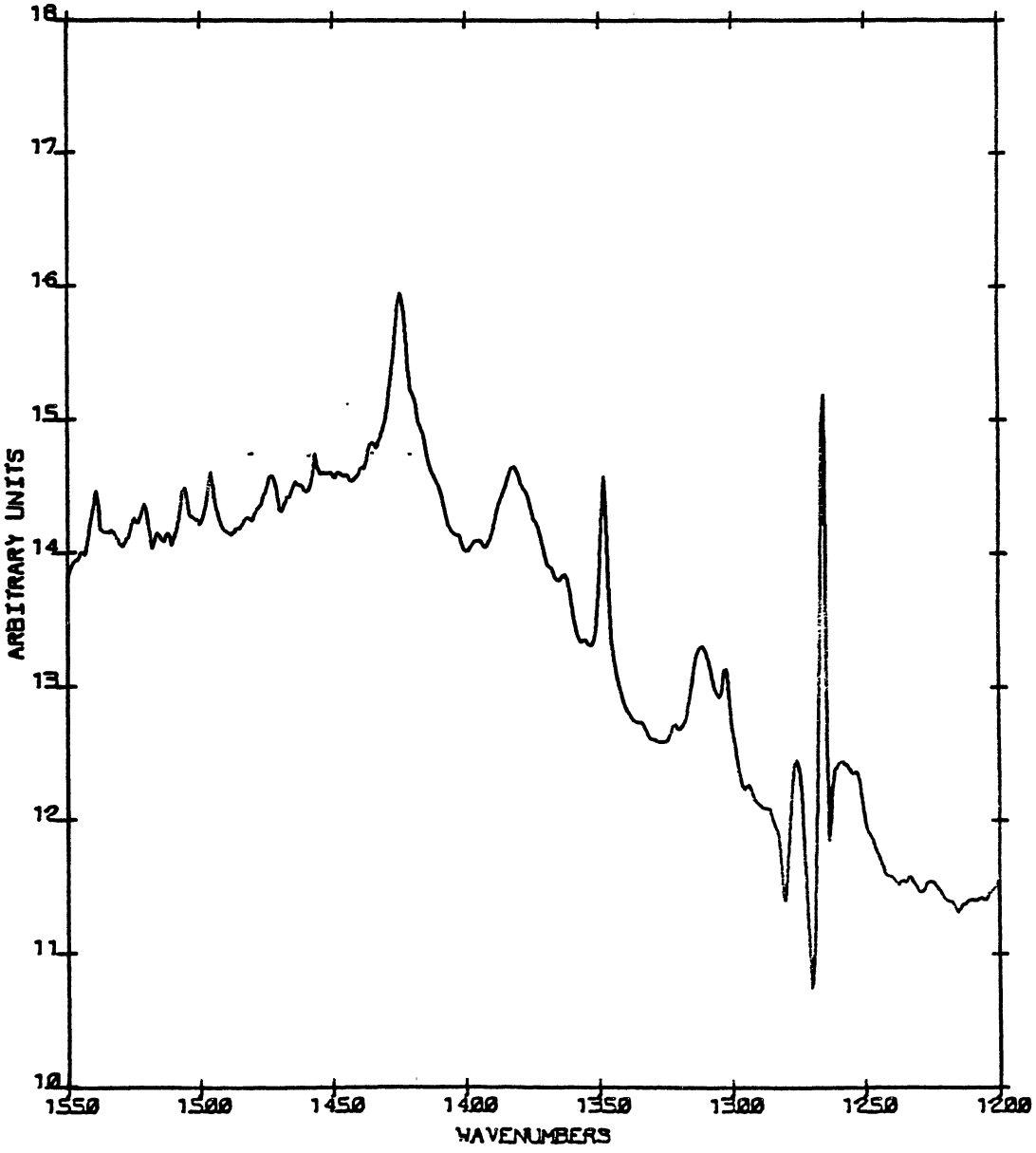
18
17
16
15
14
13
12
11
10
ARBITRARY UNITS
1550
1500
1450
1400
1350
1300
1250
1200
WAVENUMBERS

Figure 36. Subtraction of the Before Irradiation Spectrum from the After Irradiation Spectrum.

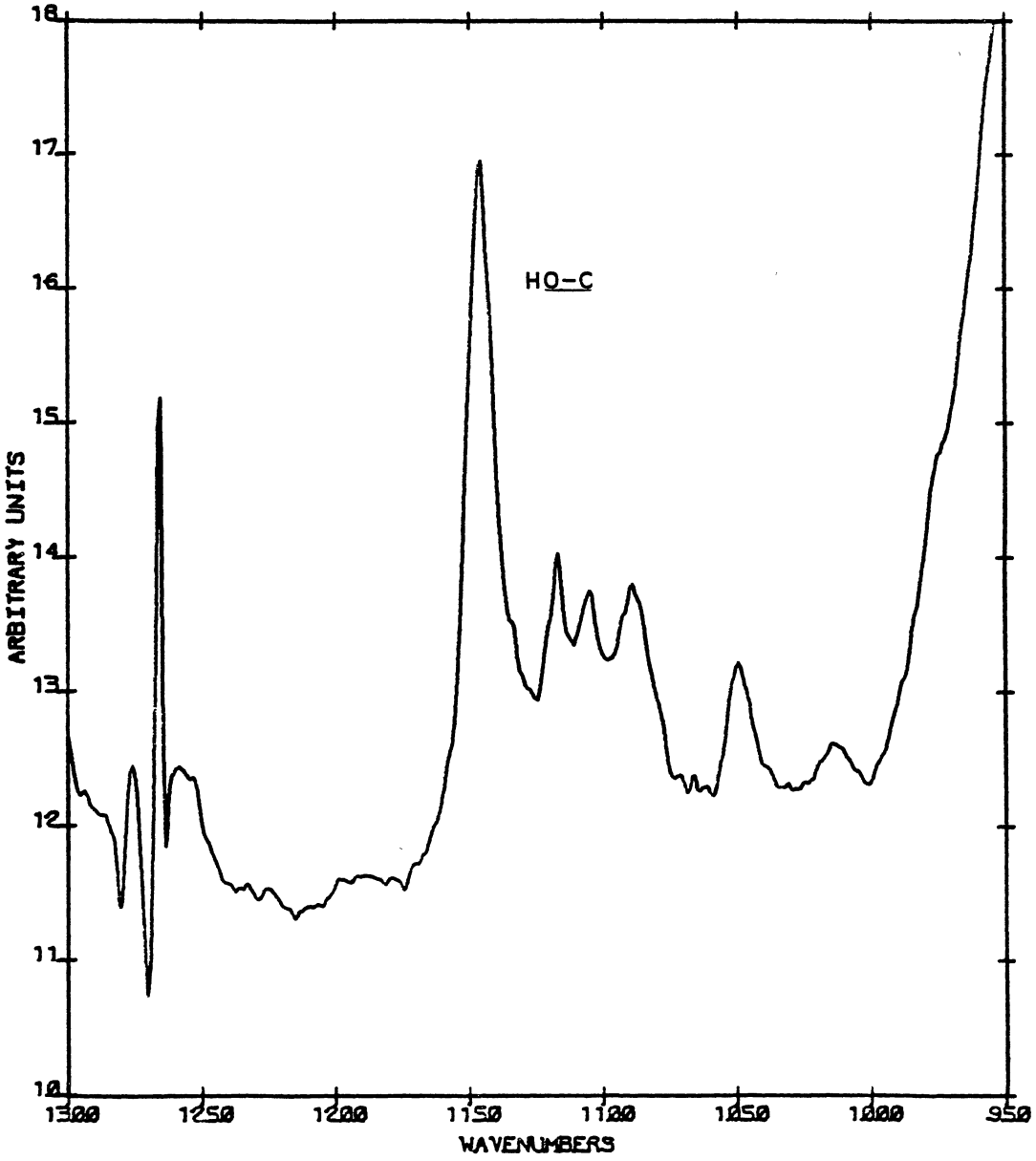
HQ-C
ARBITRARY UNITS
WAVENUMBERS
18
17
16
15
14
13
12
11
10
1300
1250
1200
1150
1100
1050
1000
950

Figure 37. Carbon Monoxide Enclathrated at 10 K.

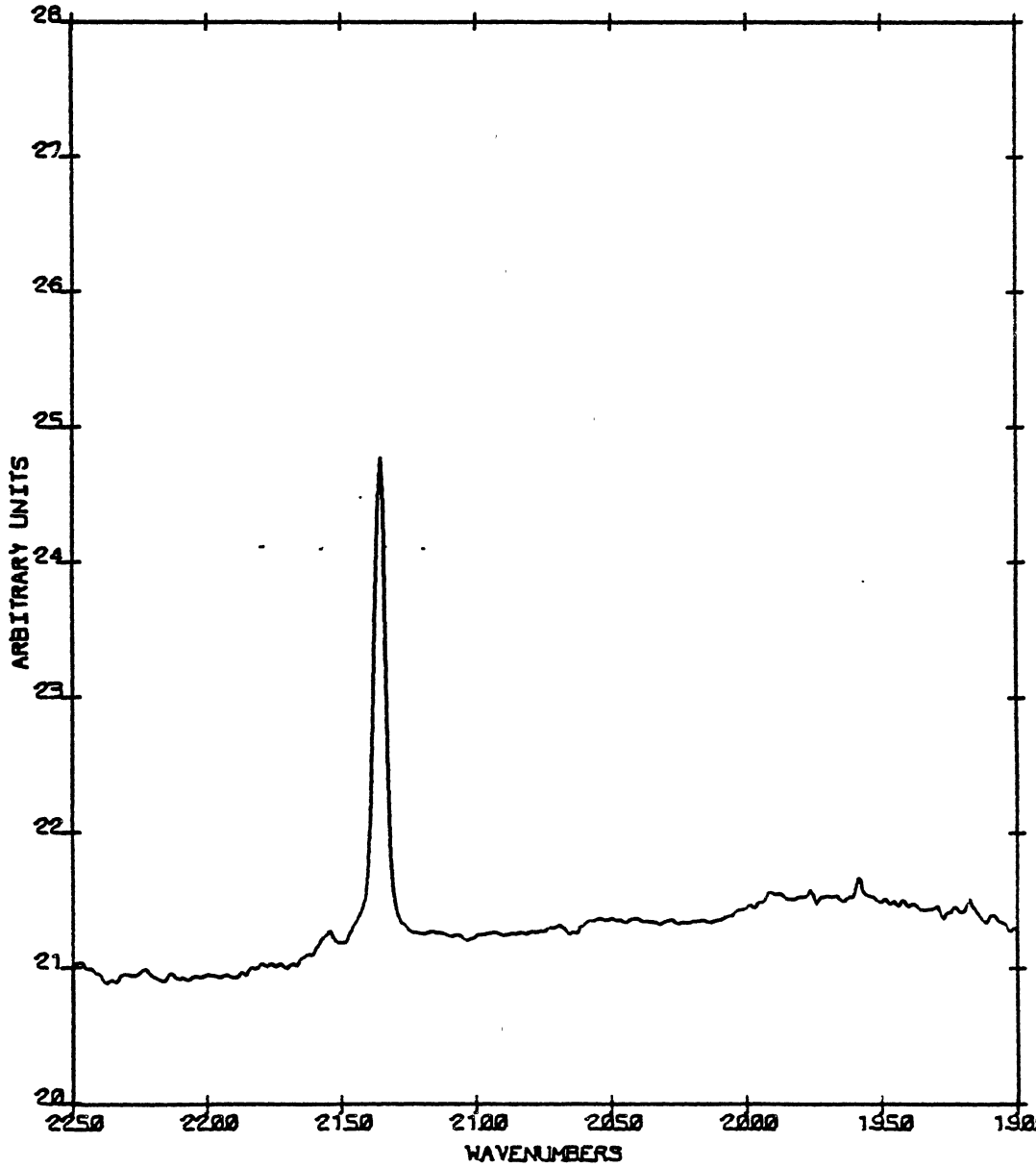
28
27
26
25
24
23
22
21
20
ARBITRARY UNITS
2250
2200
2150
2100
2050
2000
1950
1900
WAVENUMBERS

Figure 38. Carbon Monoxide Enclathrated. A - 130 K; B - 120 K; C - 110 K; D - 100 K; E - 90 K; F - 80 K; and G - 10 K.

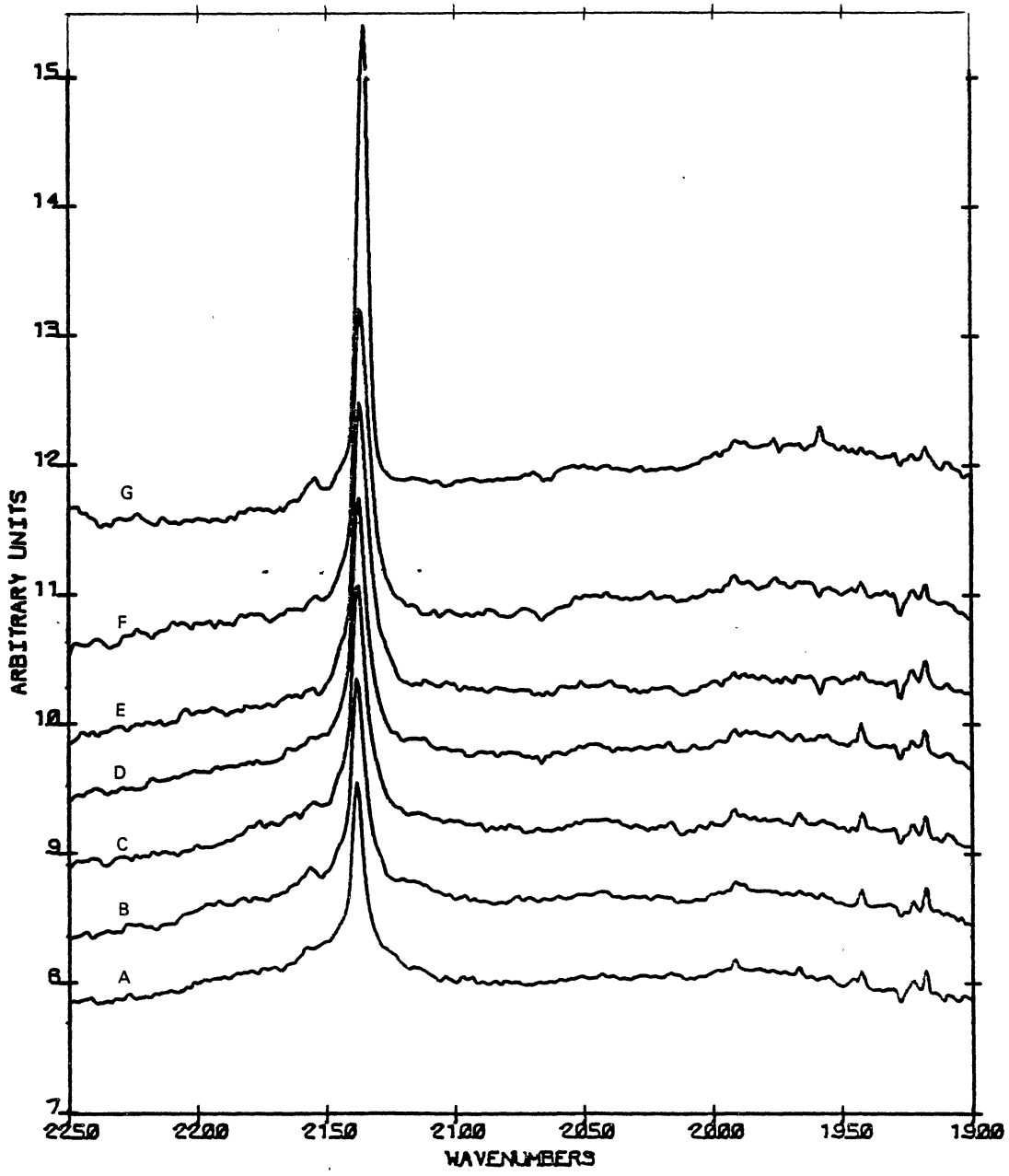
ARBITRARY UNITS
15
14
13
12
11
10
9
8
7
G
F
E
D
C
B
A
2250
2200
2150
2100
2050
2000
1950
1900
WAVENUMBERS

and before irradiation spectra (see Figures 33-36) can be used to deduce what functional groups the products have. The following functional groups were determined from the characteristic frequencies: 1) C-H alkenes (3020-3080 cm^{-1}, Figure 33); 2) C=O carbonyl (1690-1760 cm^{-1}, Figure 34); 3) C=C alkene (1640-1680 cm^{-1}, Figure 34); and 4) C-O alcohol (1080-1300 cm^{-1}, Figure 36). Some of the possible products are: 1) $H_2C=CH_2$; 2) $H_2C=C=O$; and 3) CH_3CH_2OH. Other products whose identities are known with reasonable certainty are CO and CO_2 (Figures 39 and 37, respectively). The irradiated sample was warmed to 130 K with only minor changes in the infrared spectrum. The CO_2 peak split into a doublet at about 120 K (see Figure 39) and some of the product bands in the low frequency region (1000-1400 cm^{-1}) sharpened after annealing. Almost without exception the product bands did show some intensity enhancement with cooling, indicating that the products may have been enclathrated.

The real reason for irradiating ethylene oxide clathrate hydrates with 1.7 MeV electrons was not to do interesting organic chemistry, but to obtain in the ethylene oxide clathrate hydrate the coupled HOD infrared spectrum. From the radiolysis work on cubic ice it was inferred that coupled HOD could be obtained in the clathrate hydrate if the radiolysis was done at a temperature sufficiently low so that the Bjerrum defects could not cross the rotational bond breaking barrier. The mobility of the L defects in both the clathrate hydrate and ice is an activated process. Therefore, if the L defects are not mobile (there is not enough energy available for them to cross the bond breaking barrier), and it is noted that only a Bjerrum defect migration through a coupled HOD site can uncouple the HOD, then the

Figure 39. Carbon Dioxide Generated After Irradiation of 1.7 MeV Electrons at 10 K.

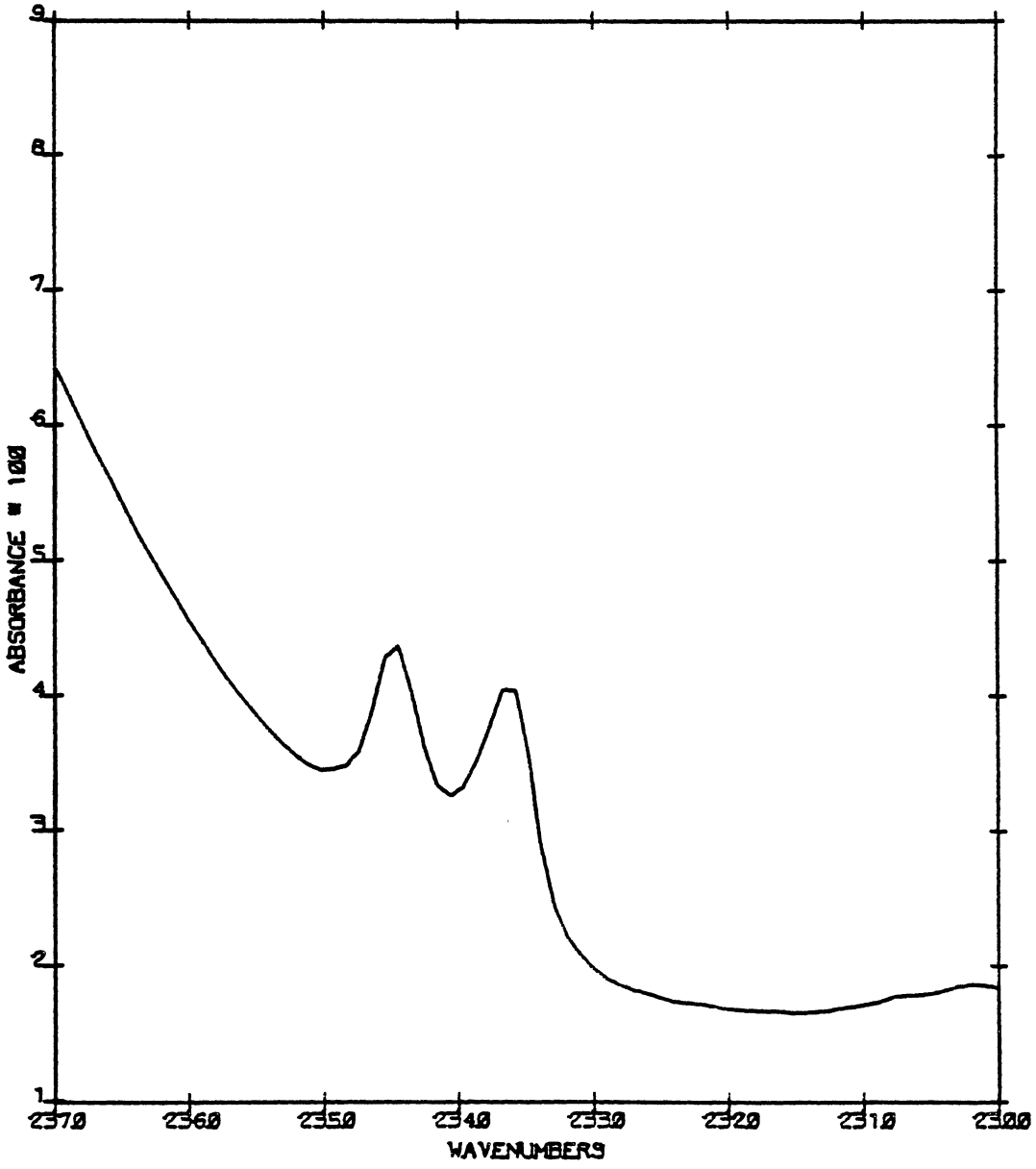
9
8
7
6
5
4
3
2
1
ABSORBANCE = 100
2370
2360
2350
2340
2330
2320
2310
2300
WAVENUMBERS

conclusion can be made that, if coupled HOD is formed at a temperature in which L defects are not mobile, coupled HOD will be the final product (see Chapter III, proton transfer kinetics of ethylene oxide clathrate hydrate). In cubic ice this temperature is below 130 K so the first clathrate hydrate sample was irradiated at 80 K. Isolated HOD was the only product and it was concluded that the barrier to Bjerrum defect migration is sufficiently low in the ethylene oxide clathrate hydrate to allow these defects to be mobile at temperatures as low as 80 K. A much lower irradiation temperature of 30 K was tried with success. The infrared spectrum of coupled HOD in the ethylene oxide clathrate hydrate at 10 K is presented in Figure 40. It should be noted that in moving the sample from the Van de Graaff generator to the infrared spectrometer the sample temperature temporarily reached a maximum in temperature of 60 K. When the sample was annealed to a temperature of 50 K and recooled to 10 K there was little change in the coupled HOD spectrum, but when the sample was annealed to 90 K and recooled to 10 K the residual D_2O in the irradiated sample had converted to coupled HOD while the coupled HOD was converting to isolated HOD (see Figure 40). The conversion of D_2O to coupled HOD can be ascribed to the proton hopping step, whereas the conversion of coupled HOD into isolated HOD is just the Bjerrum defect migration step which uncouples the coupled HOD. Therefore, in the temperature range between 50 and 90 K both the hopping step and Bjerrum defect migration step are occurring simultaneously and are maintaining an approximately steady state concentration of coupled HOD — a phenomenon which happens naturally in pure cubic ice at 140 K (see Figure 41).

Figure 40. Coupled HOD Generated in the Ethylene Oxide Clathrate Hydrate by Irradiation of 1.7 MeV Electrons at 10 K. A - before annealing; B - annealed at 50 K; C - annealed at 90 K; D - annealed at 110 K; and E - annealed at 120 K.

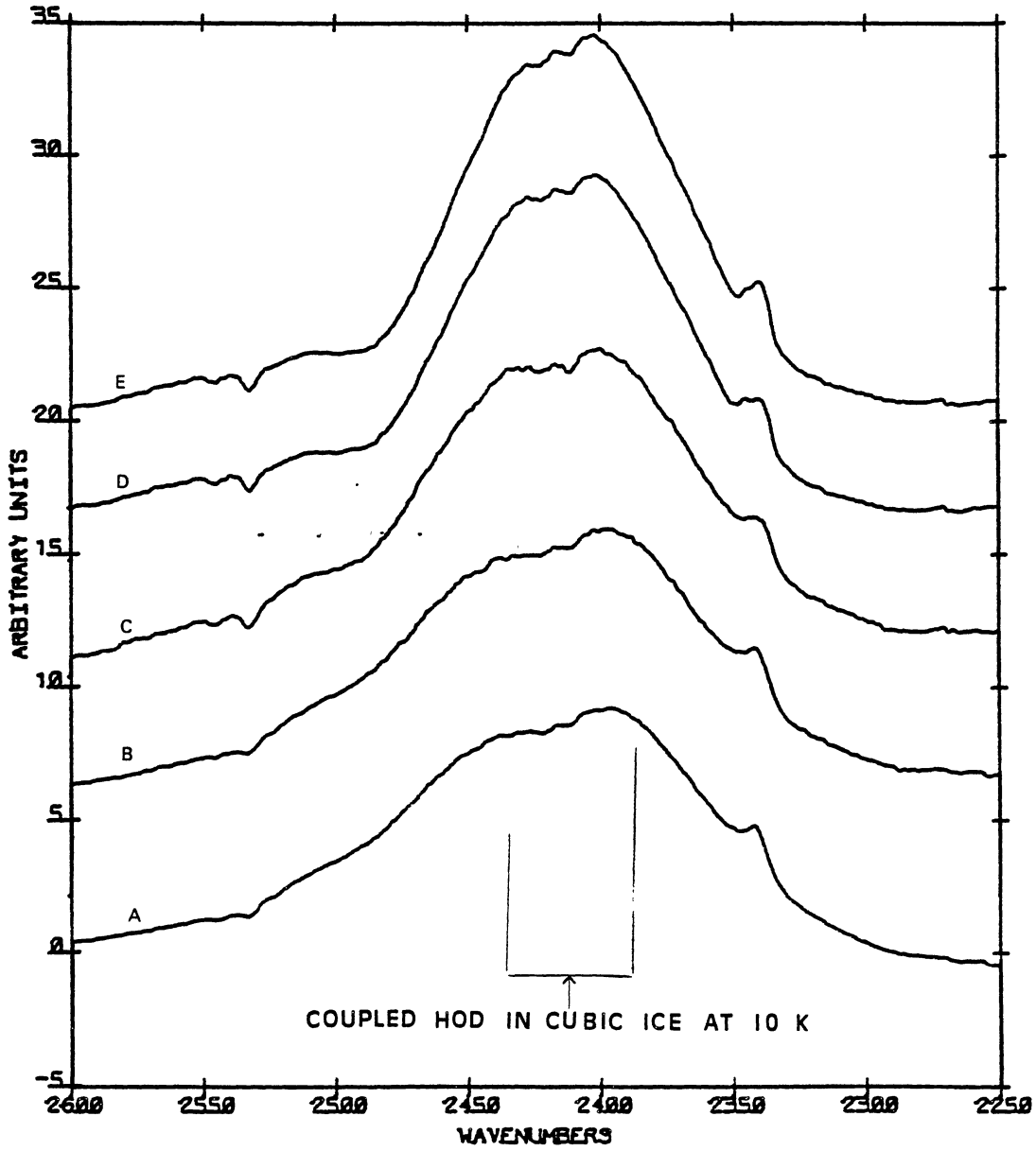
35
30
25
20
15
10
5
0
-5
ARBITRARY UNITS
E
D
C
B
A
COUPLED HOD IN CUBIC ICE AT 10 K
2600
2550
2500
2450
2400
2350
2300
2250
WAVENUMBERS

Figure 41. Coupled HOD Generated in Cubic Ice by Irradiation of 1.7 MeV Electrons at 10 K. A - before annealing with 45% of the HOD subtracted and 25% of the D_2O; B - annealed at 140 K with 50% of the HOD subtracted and 20% of the D_2O; C - annealed again at 140 K with 55% of the HOD subtracted and 18% of the D_2O.

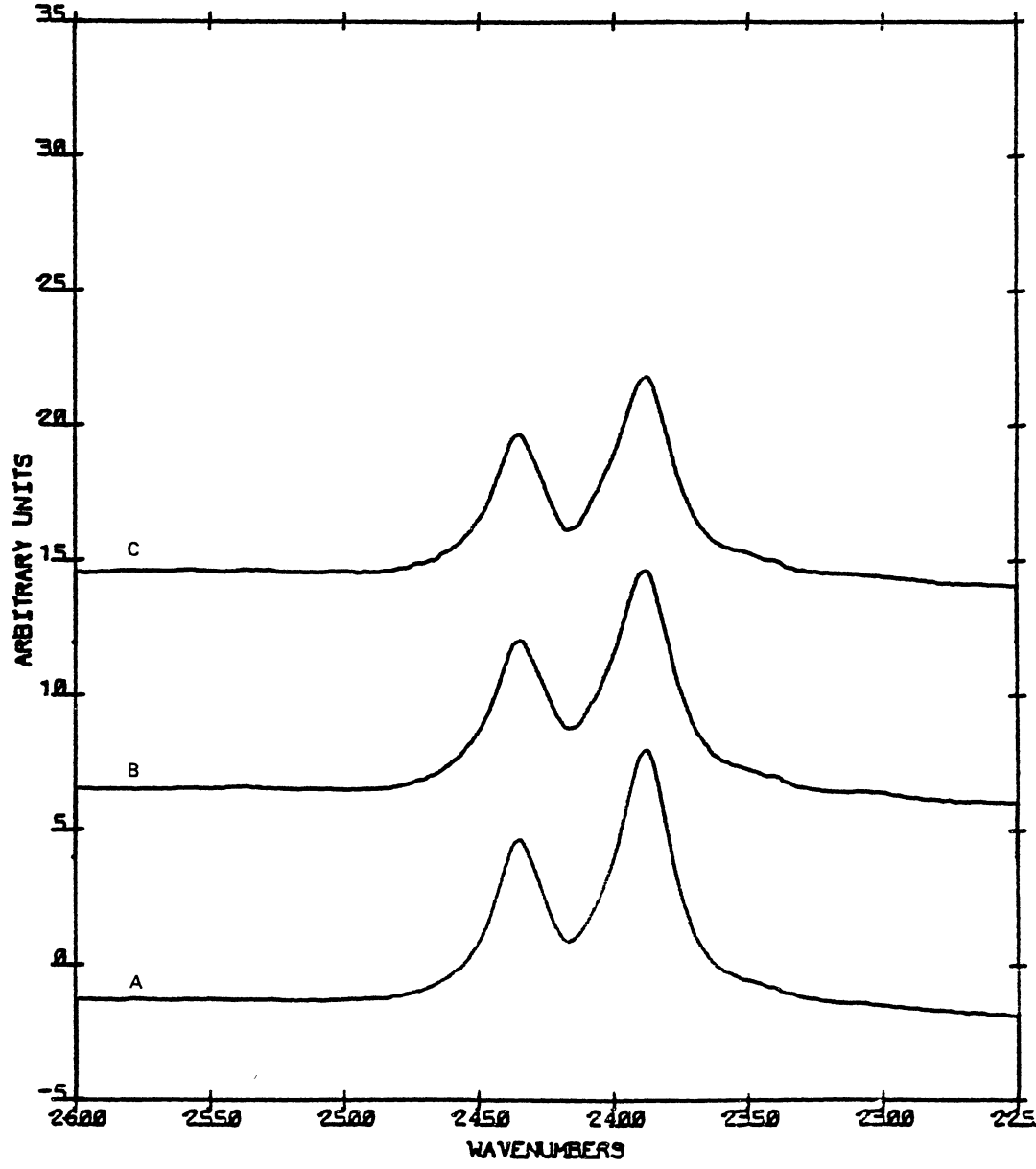
35
30
25
20
15
10
5
0
-5
ARBITRARY UNITS
C
B
A
2600
2550
2500
2450
2400
2350
2300
2250
WAVENUMBERS

CHAPTER IV

OTHER CLATHRATE SPECTRA

In this chapter the information obtained on other clathrate hydrates besides the ethylene oxide clathrate hydrate is presented along with some trends applicable to clathrate hydrates in general.

Hydrogen Sulfide Clathrate Hydrate

The infrared spectra of the H_2S clathrate hydrate is presented in Figures 42-45. The dramatic increase in the intensity of the H_2S bands with cooling along with the value of the isolated HOD frequency confirms the clathrate hydrate structure. Figures 46-47 compare the observed change in the 1800 cm^{-1} band of the ethylene oxide clathrate hydrate as the sample is transformed from the amorphous mixture to the clathrate hydrate with the corresponding transformation in the H_2S clathrate hydrate. The change in the 1600 cm^{-1} band is almost identical in the two clathrate hydrates and adds some confidence to the conclusion that the H_2S clathrate hydrate was indeed obtained instead of an amorphous mixture of H_2S and water. It was not possible to isolate D_2O in the clathrate hydrate lattice without it converting to HOD as the sample was crystallized to the clathrate hydrate. It appeared as though the D_2O converted to HOD in the amorphous material instead of in the clathrate hydrate because conversion to HOD was complete before the sample had been annealed to the hydrate crystalli-

Figure 42. Hydrogen Sulfide Enclathrated. A - 130 K; B - 90 K; C - 80 K; D - 70 K; E - 50 K; and F - 30 K.

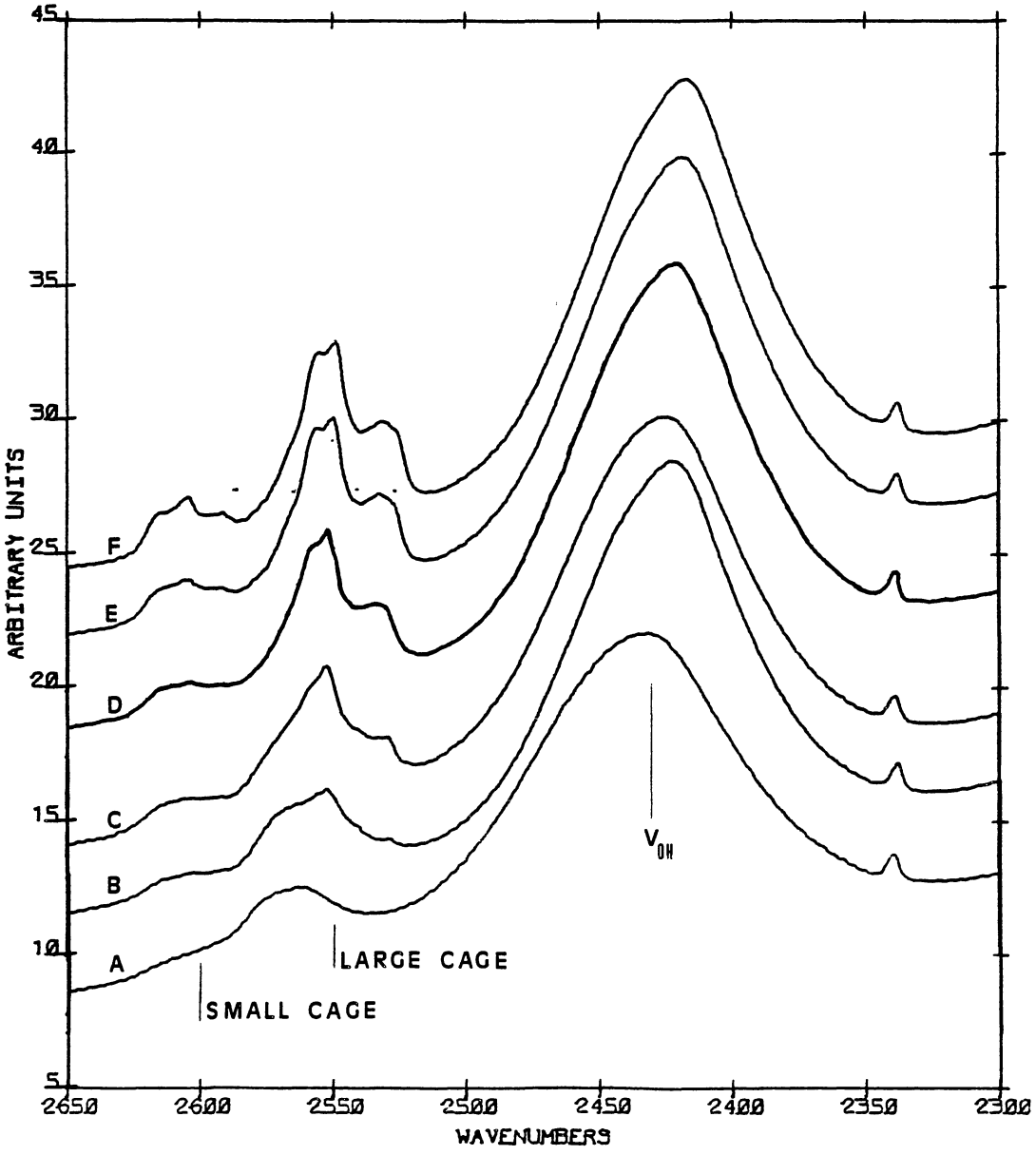
45
40
35
30
25
20
15
10
5
ARBITRARY UNITS
F
E
D
C
B
A
SMALL CAGE
LARGE CAGE
V_{OH}
2650
2600
2550
2500
2450
2400
2350
2300
WAVENUMBERS

Figure 43. Hydrogen Sulfide Enclathrated. A - 130 K; B - 80 K; C - 50 K; and D - 10 K.

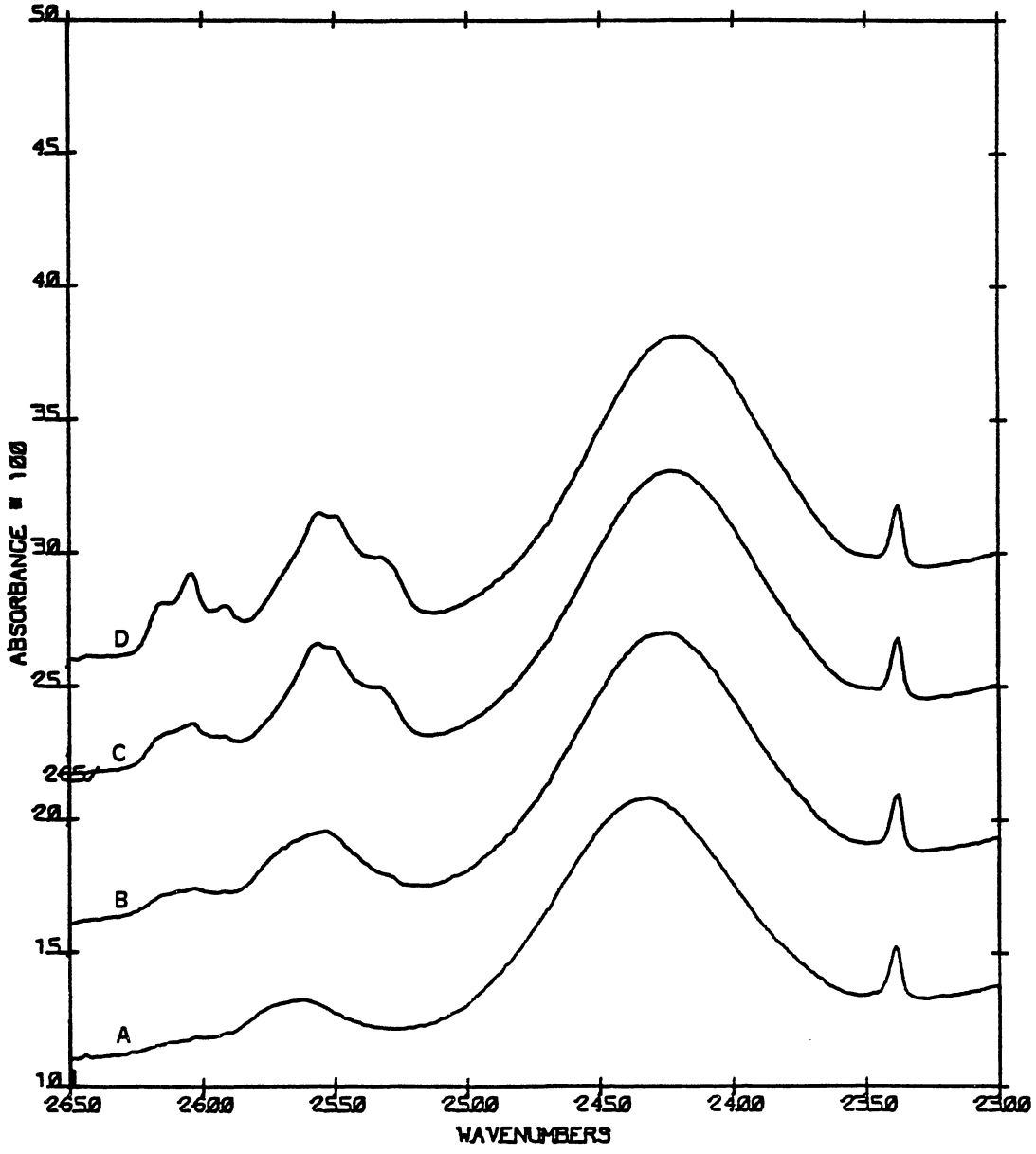
50
45
40
35
30
25
20
15
10
ABSORBANCE * 100
D
C
B
A
2650
2600
2550
2500
2450
2400
2350
2300
WAVENUMBERS

Figure 44. Hydrogen Sulfide Enclathrated with Some Conversion to Cubic Ice. A - 10 K; B - 15 K; C - 20 K; D - 25 K; and E - 30 K.

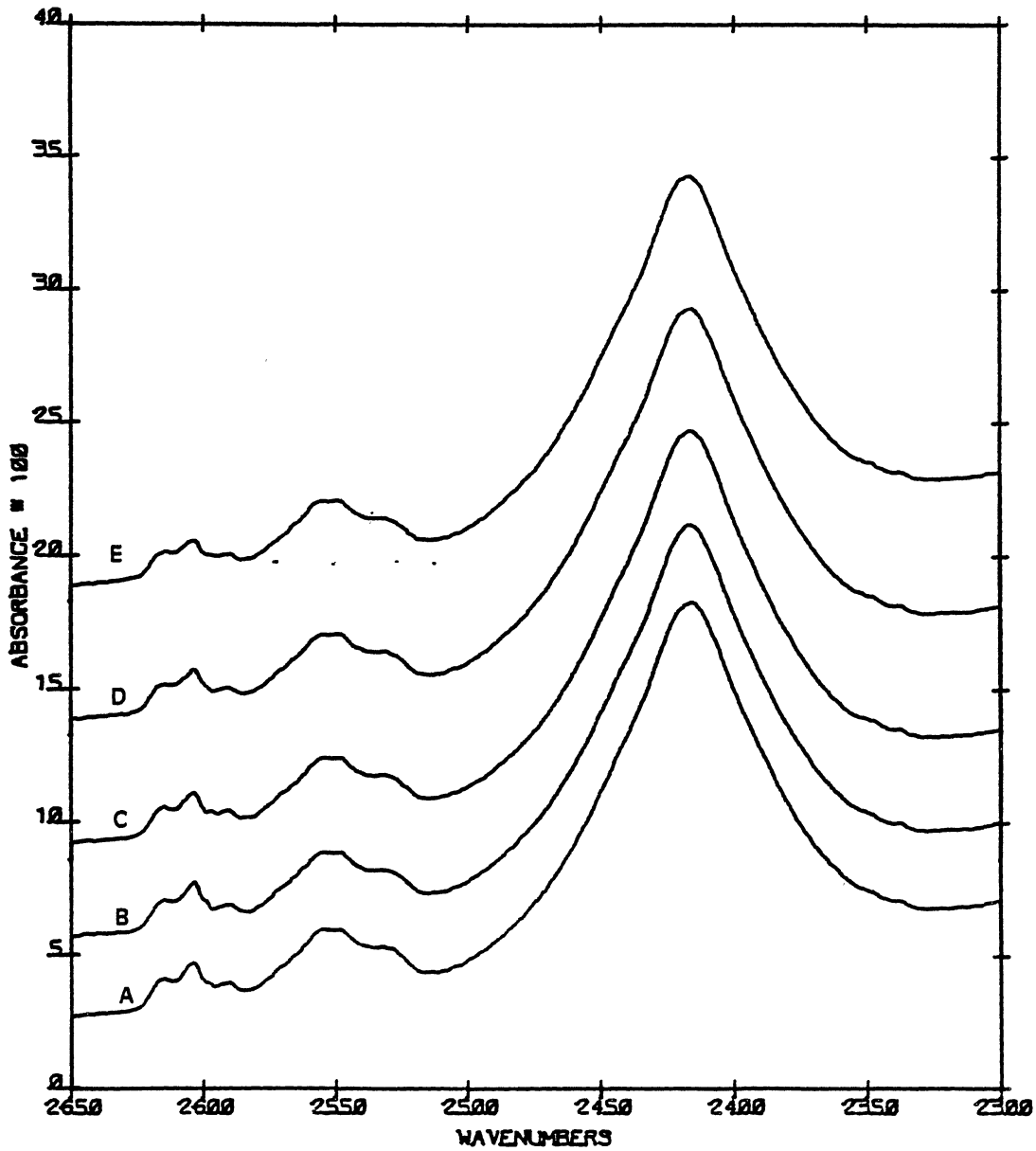
40
35
30
25
20
15
10
5
0
ABSORBANCE * 100
E
D
C
B
A
2650
2600
2550
2500
2450
2400
2350
2300
WAVENUMBERS

Figure 45. Hydrogen Sulfide Enclathrated. A - 130 K; B - 80 K; C - 50 K; and D - 10 K.

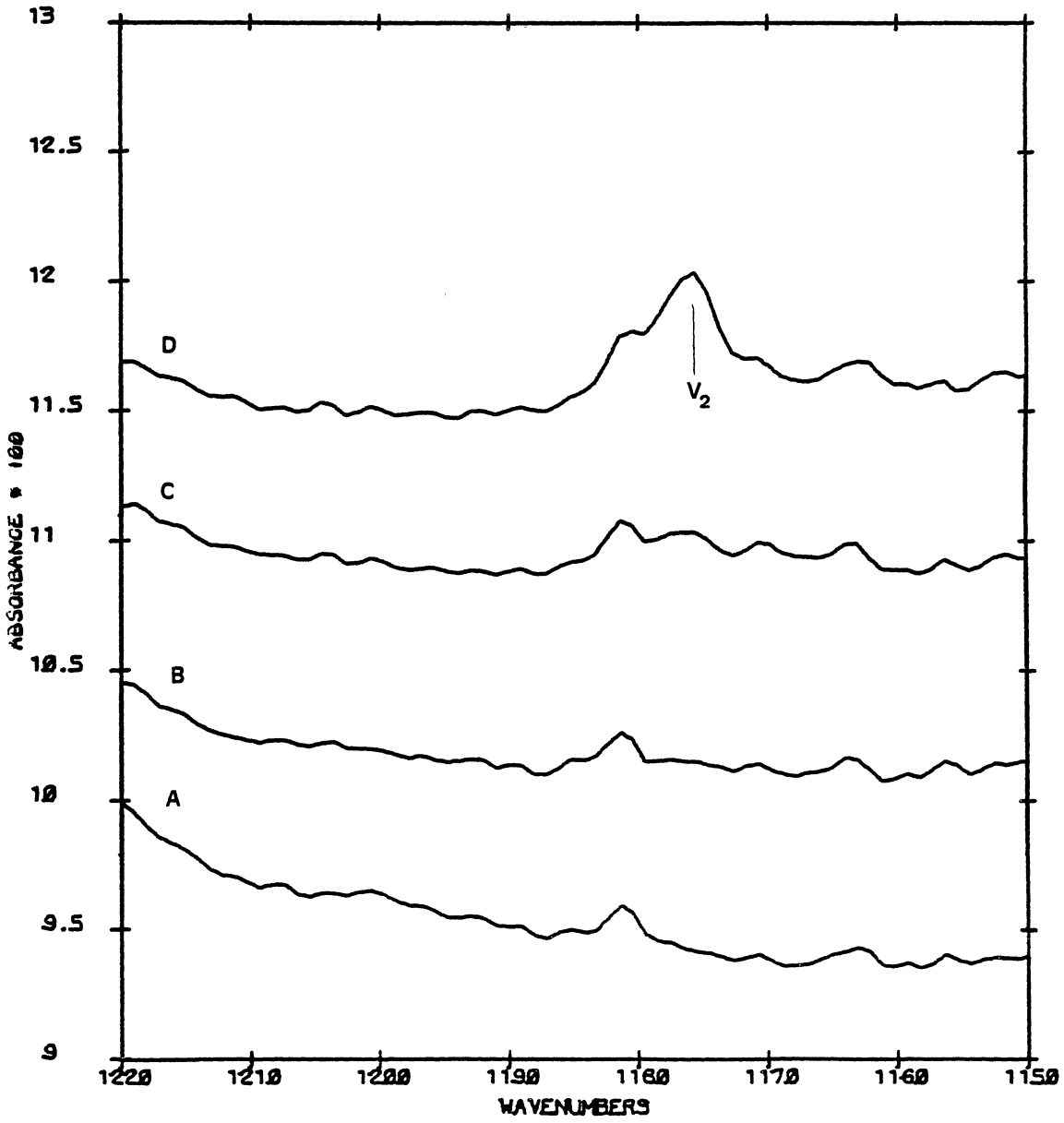
13
12.5
12
11.5
11
10.5
10
9.5
9
ABSORBANCE * 100
D
C
B
A
V_2
1220
1210
1200
1190
1180
1170
1160
1150
WAVENUMBERS

Figure 46. Transition from the Amorphous Mixture of H_2S and Water to the H_2S Clathrate Hydrate at 10 K. A - amorphous mixture; B - H_2S clathrate hydrate; and C - subtraction of the amorphous mixture spectrum from the H_2S clathrate hydrate spectrum.

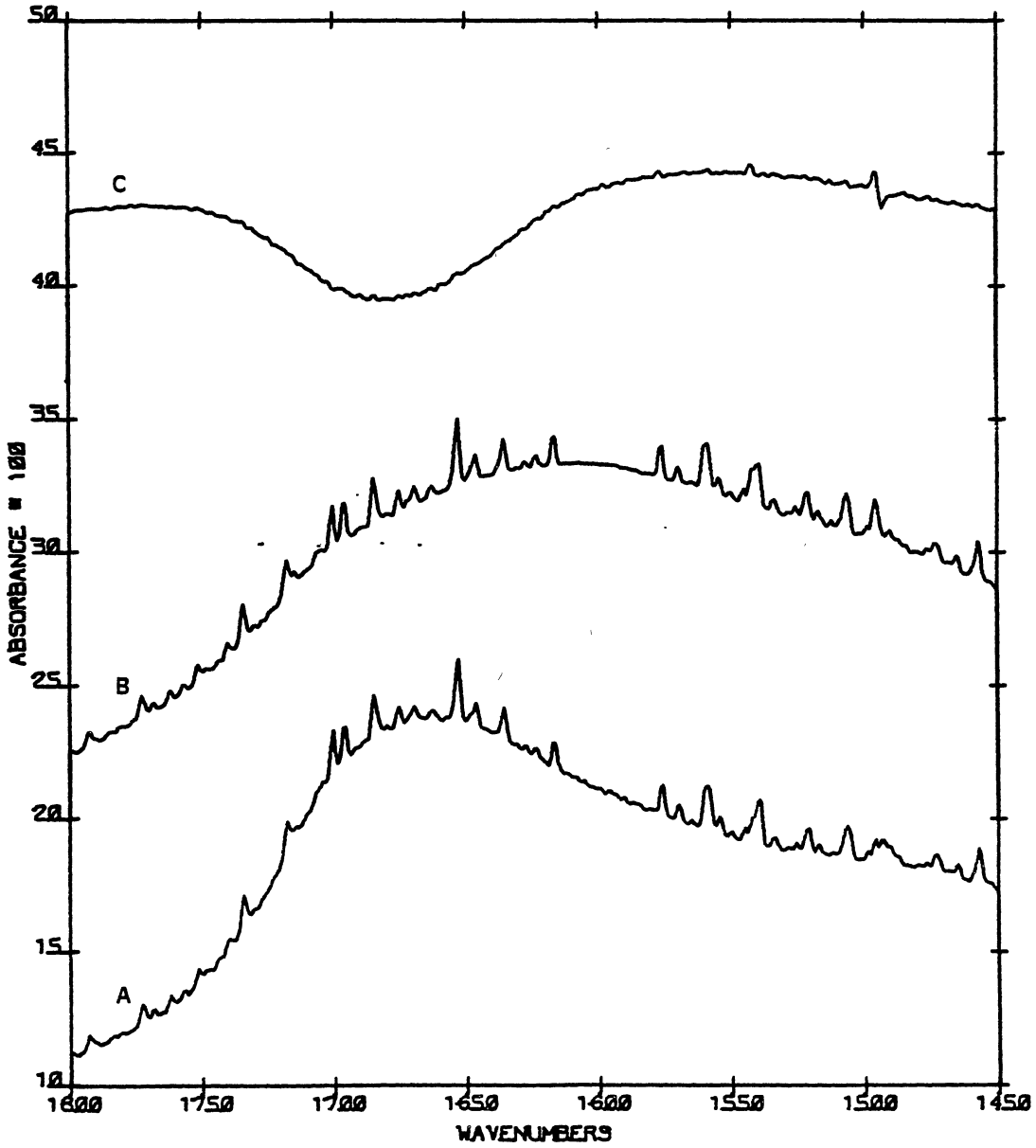
50
45
40
35
30
25
20
15
10
C
B
A
ABSORBANCE = 100
1800
1750
1700
1650
1600
1550
1500
1450
WAVENUMBERS

Figure 47. Comparison of the Transition from the Amorphous Mixture to the Clathrate Hydrate with Different Guest Molecules Enclathrated. A - subtraction from the H_2S clathrate hydrate; B - subtraction from the ethylene oxide clathrate hydrate; and C - subtraction from the SO_2 clathrate hydrate.

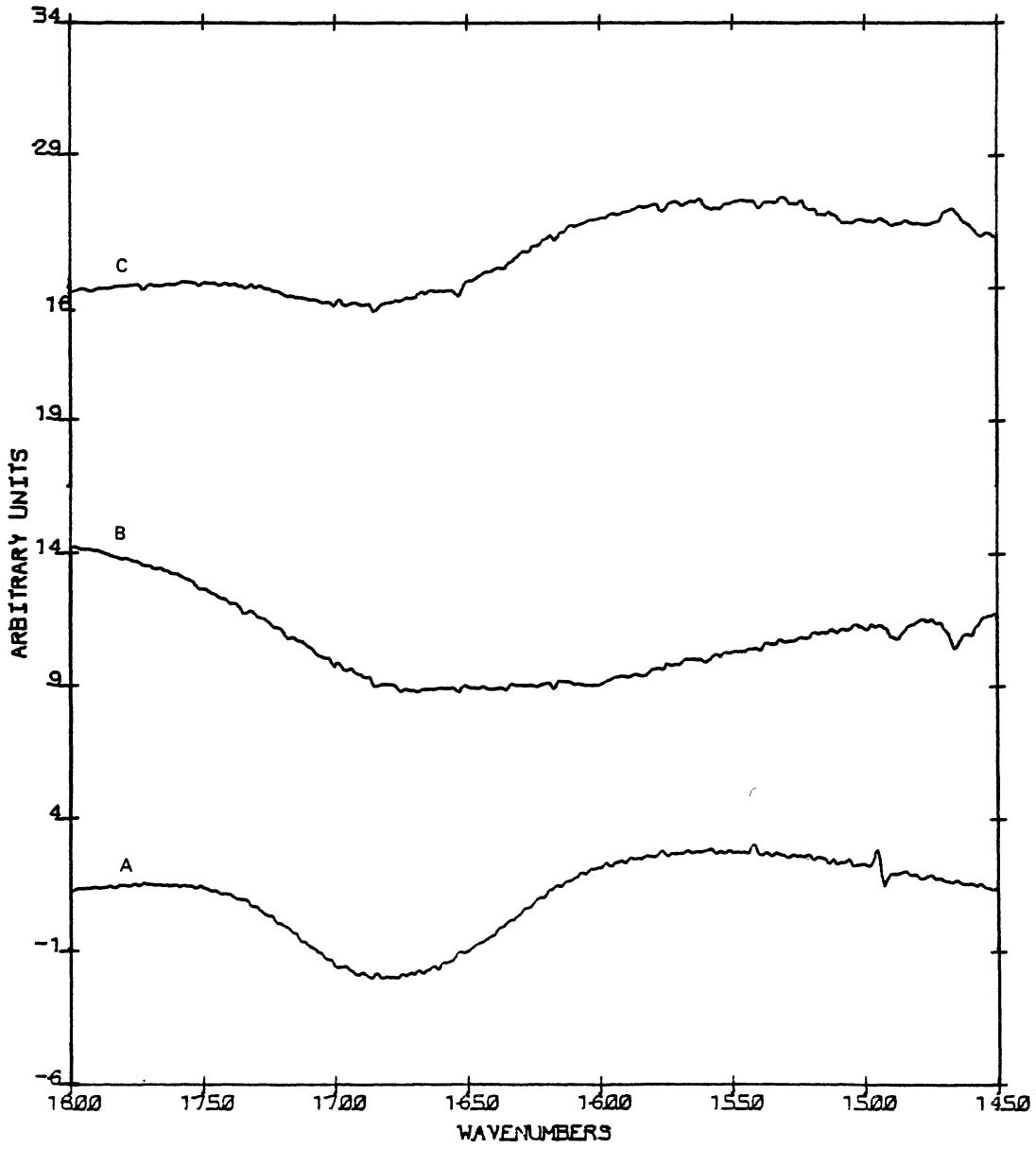
34
29
24
19
14
9
4
-1
-6
ARBITRARY UNITS
C
B
A
1800
1750
1700
1650
1600
1550
1500
1450
WAVENUMBERS

zation temperature of around 130 K. This is attributed to the acidity of the H_2S molecule in the amorphous samples of H_2O. However, it should be noted that D_2O conversion to HOD has been observed (37) in amorphous samples which have been irradiated with high energy electrons. It is believed that irradiation of amorphous samples with high energy electrons created ionic defects in the sample (H^+, OH^-) and the protons generated migration through the amorphous sample converting the D_2O molecules to HOD. In much the same way the conversion of the D_2O in the amorphous mixture of H_2S-D_2O-H_2O can be explained if the source of protons is attributed to the acidity of the H_2S molecules in the amorphous mixture.

The H_2S molecule has C_{2v} symmetry and one would expect three infrared active modes: 1) V_1 (symmetric stretch); 2) V_3 (asymmetric stretch); and 3) V_2 (bending deformation). The bending mode in the H_2S clathrate hydrate (Figure 45) is easily identified at 1175 cm^{-1} (gas phase 1182 cm^{-1} (44)); however, the assignment of the V_3 and V_1 modes is a little more complicated. In the gas phase the symmetric stretch is located at 2628 cm^{-1} while the antisymmetric stretch is at 2615 cm^{-1} (44) with a separation between the V_3 and V_1 modes of 13 cm^{-1}. From Davidson's dielectric measurements of the H_2S clathrate hydrate (14), it is possible to conclude that the H_2S molecule in the different cases have a high degree of mobility even at low temperatures (-10 K). Therefore, it would be surprising to see well defined H_2S peaks attributable to preferred orientations of the H_2S molecules in the cases. The broad relatively structureless bands (Figure 43) show the wide spectrum of orientations that the H_2S molecule has in the different cages. Figure 42 shows the effect that cooling the sample

has on the stretching modes of the H_2S molecules enclathrated in the different cages. As the sample temperature is decreased two broad band complexes emerge out of the background at different rates. The broad band complex centered at 2550 cm^{-1} reaches its maximum peak intensity at 70 K while the broad band complex centered at 2600 cm^{-1} does not reach its maximum peak intensity until 20 K. Because the separation in the ν_3 and ν_1 modes should be around 13 cm^{-1}, it is easy to believe that the bands centered at 2550 cm^{-1} and 2600 cm^{-1} are from molecules located in the two different type of cages of the clathrate hydrate, i.e. the large and the small cages. However, the question remains as to which band should be assigned to the large or small cage. One would expect that the encroachment of the small cage upon the H_2S molecules would be observable at a higher temperature than the encroachment of the large cage. Therefore, a tentative assignment might be that the band centered at 2550 cm^{-1} is from the H_2S molecules in the small cages while the band at 2600 cm^{-1} is from the H_2S molecules in the large cages. It should be noted that there are three times as many guest molecules in the large cages than in the small cages and the observed peak intensities would argue against this assignment. Figure 44 shows the effect that converting some of the clathrate hydrate to ice had on the observed peak intensities and the dramatic loss in the peak intensity of the 2550 cm^{-1} band would seem to confirm the first assignment with the stipulation that the H_2S molecules in the small cages are bonding to the cell wall as the temperature is decreased and this bonding dramatically increasing their absorption coefficient. This conflict in the assignment of the broad bands centered at 2600 and 2550 cm^{-1} can be resolved by forming

the type II mixed clathrate hydrate of THF and H_2S. The THF molecules will occupy the large cages in the type II clathrate hydrate, while H_2S can occupy the small cages. The small cages in the type II hydrate are almost identical to the small cages of the type I clathrate hydrate but the large cages are bigger, allowing larger molecules like THF to form clathrate hydrates. The infrared spectrum of the type II mixed clathrate hydrate of THF and H_2S is presented in Figures 48-50. The H_2S peaks at 2615 and 1602 cm^{-1} confirms the assignment that the broad band centered at 2600 cm^{-1} is from the H_2S molecules that are enclathrated in the small cages. This result was unexpected but does explain the observed intensities of the H_2S clathrate hydrate. One might postulate that the H_2S molecule in the large cages experiences a double well potential inside the cage which restricts its mobility at a higher temperature than the H_2S molecules in the small cage. This in turn, would explain the observed temperature dependence. Therefore, the band centered at 2550 cm^{-1} is from the large-caged molecule (the breadth of the band a superpositioning of the H_2S molecules in a wide spectrum of orientations), while the band centered at 2600 cm^{-1} is attributed to the H_2S molecules in the small cages (see Table XVIII).

The infrared spectrum of the D_2S clathrate deuterate is presented in Figure 51. The broad bands associated with the D_2S molecules that have been enclathrated in the large and small cages are apparent. Again, the broad band centered closer to the gas phase frequency of 1890 cm^{-1} is assigned to the D_2S molecules in the small cages, while the broad band centered around 1850 cm^{-1} is assigned to the D_2S molecules in the large cages.

Figure 48. Tetrahydrofuran and H_2S Mixed Type II Clathrate Hydrate. A - 150 K; and B - 10 K.

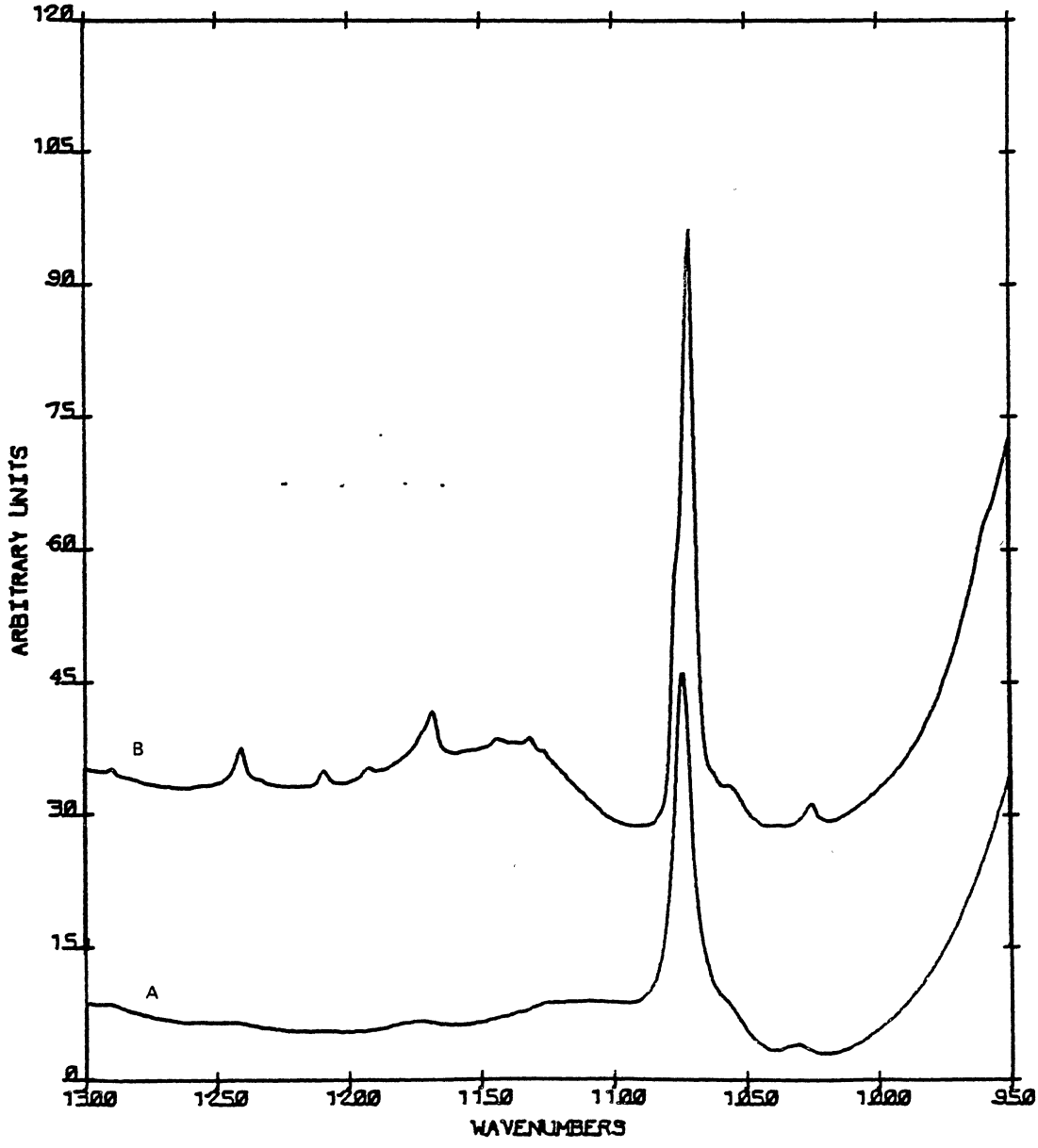
120
105
90
75
60
45
30
15
0
ARBITRARY UNITS
B
A
1300
1250
1200
1150
1100
1050
1000
950
WAVENUMBERS

Figure 49. Tetrahydrofuran and H_2S Mixed Type II Clathrate Hydrate at 10 K.

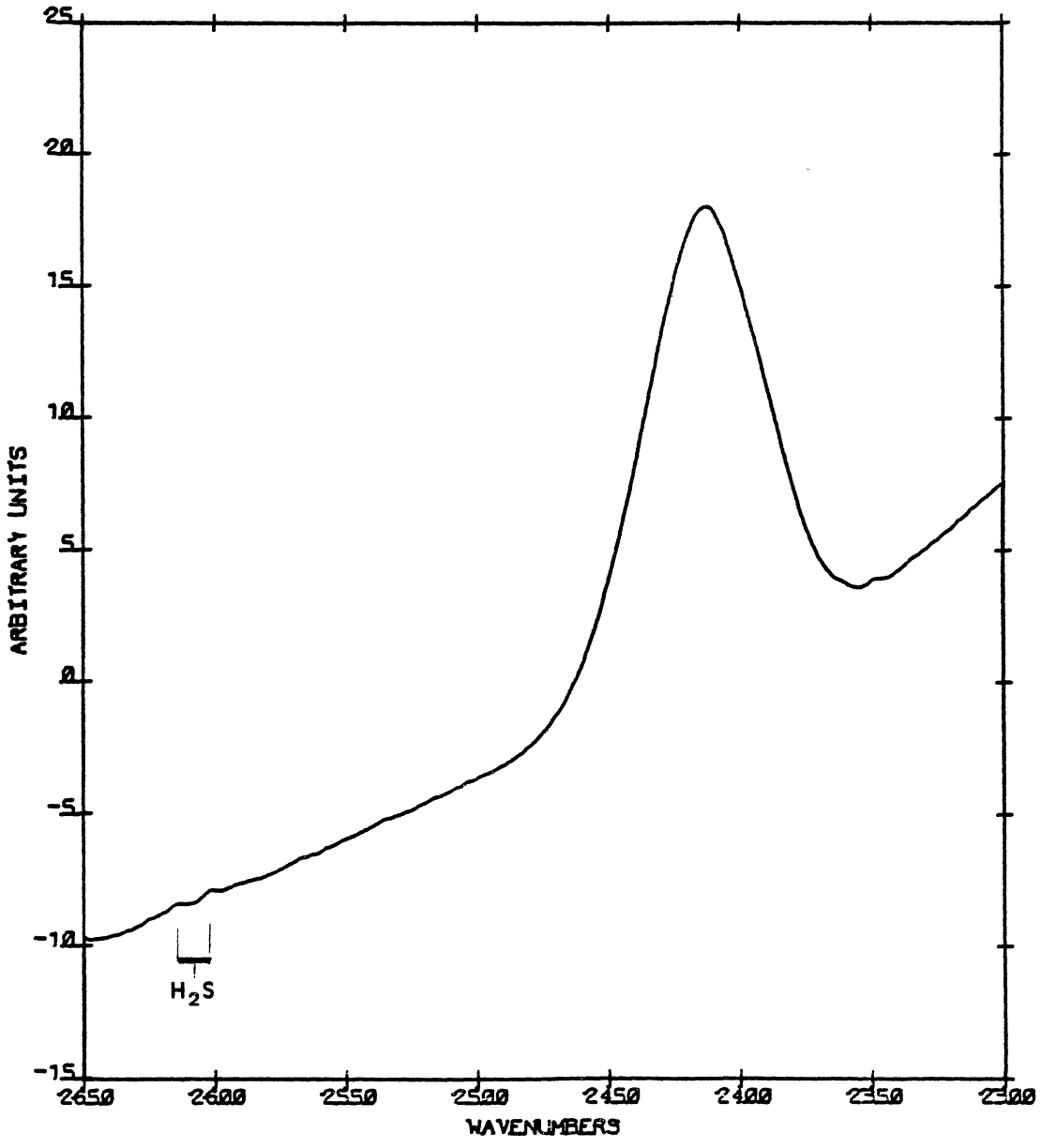
25
20
15
10
5
0
-5
-10
-15
ARBITRARY UNITS
H_2S
2650
2600
2550
2500
2450
2400
2350
2300
WAVENUMBERS

Figure 50. Subtraction of the THF-H_2S Mixed Type II Clathrate Hydrate at 150 K from 10 K. A - spectral region 2650-2580 cm^{-1}; and B - spectral region 2580-2510 cm^{-1}.

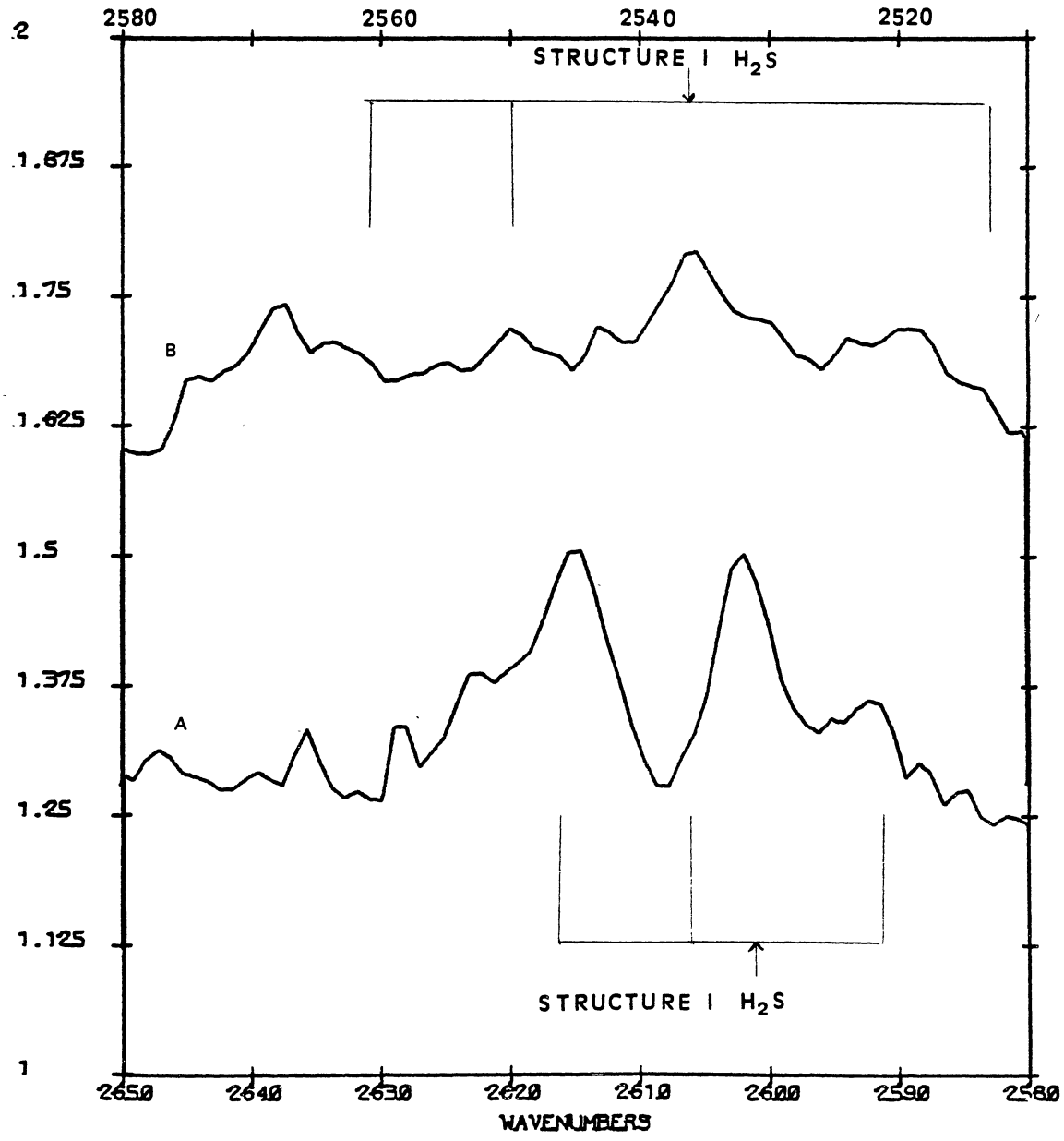
2580
2560
2540
2520
STRUCTURE I H_2S
2
1.875
1.75
1.625
1.5
1.375
1.25
1.125
1
B
A
STRUCTURE I H_2S
2650
2640
2630
2620
2610
2600
2590
2580
WAVENUMBERS

TABLE XVIII

H_2S CLATHRATE HYDRATE GUEST FREQUENCIES AT 10 K

ν (cm^{-1})	Assignment
2616	ν_3 small cage
2606	ν_1 small cage
2591	-
2561	ν_3 large cage
2550	ν_1 large cage
2513	-
1176	ν_2

Figure 51. Deuterium Sulfide Enclathrated in the Clathrate Deuterate at 10 K.

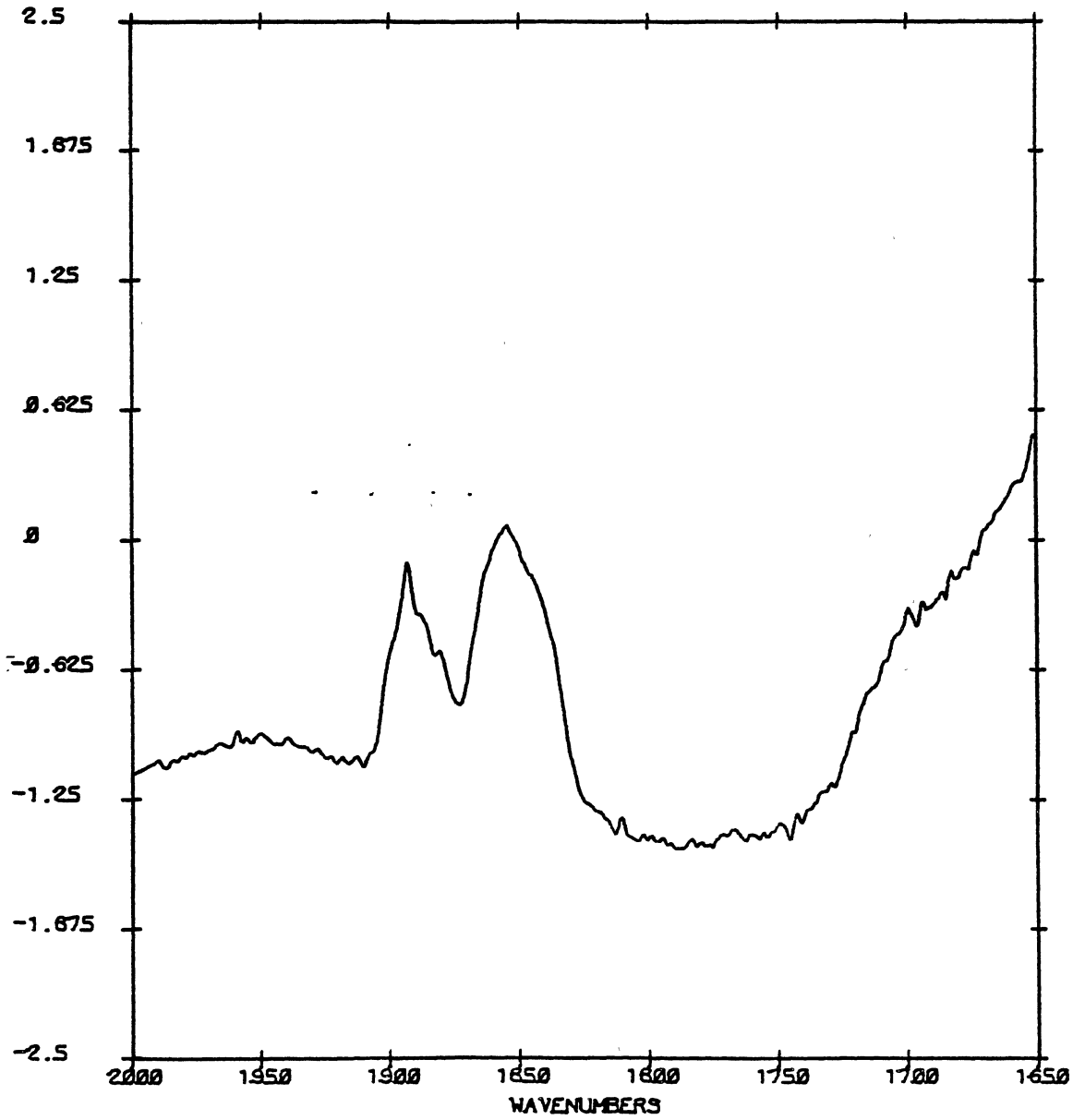
2.5
1.875
1.25
0.625
0
-0.625
-1.25
-1.875
-2.5
2000
1950
1900
1850
1800
1750
1700
1650
WAVENUMBERS

Sulfur Dioxide Clathrate Hydrate

The infrared spectra of the SO_4 clathrate hydrate is presented in Figures 52-56. The assignment of the SO_2 clathrate hydrate is presented in Table XIX. The antisymmetric stretch (V_3) of the SO_2 molecule in the clathrate hydrate gave a sharp singlet (FWHM = 12 cm) at 1339.5 cm^{-1} and the symmetric stretch (V_1) appeared as an even sharper singlet (FWHM = 8 cm^{-1}) at 1147 cm^{-1}. Superimposed on both the symmetric and the antisymmetric stretches was a very broad low frequency band which gave the V_3 and V_1 bands the appearance of having a slow decaying function or tail on the low frequency side of the band. The bending mode (V_2) at 517 cm^{-1} (FWHM = 7 cm) showed the most dramatic intensity enhancement upon cooling (see Figure 56). Formation of the SO_2 clathrate hydrate by epitaxial deposition was unsuccessful and the samples had to be annealed further to a temperature between 130-140 K before the clathrate hydrate would crystallize from the amorphous mixture of SO_2 and water to the clathrate hydrate crystalline structure. This transformation was determined by the peak enhancement and sharpening of the SO_2 fundamentals and combination bands, as well as the characteristic clathrate hydrate isolated O-D stretching frequency and the shift and broadening of the 1600 cm^{-1} band (see Figure 47). An interesting doublet appeared in the infrared spectrum of the SO_2 clathrate hydrate around 1025 cm^{-1} (see Figure 55) which is not observed in the gas phase or amorphous samples of SO_2 (45). The overtone of the bending mode (2 x 517 cm^{-1}) is in this region but the peculiar band shape of the doublet suggests that an Evans hole might be distorting the infrared spectrum in this region. An Evans hole is

Figure 52. Sulfur Dioxide Enclathrated at 10 K.

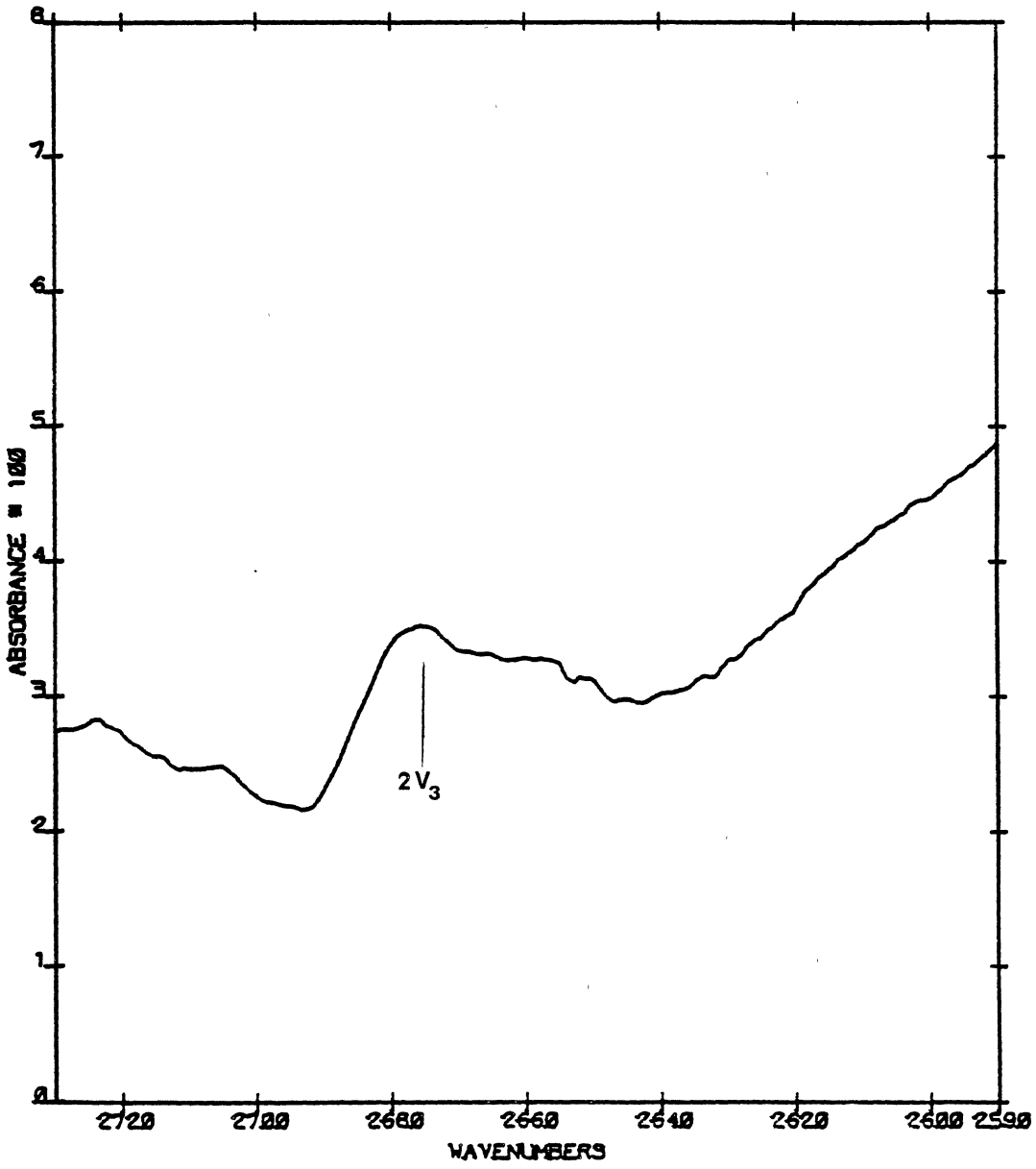
ABSORBANCE = 100
8
7
6
5
4
3
2
1
0
2720
2700
2680
2660
2640
2620
2600
2590
WAVENUMBERS
$2V_3$

Figure 53. O-D Stretching Absorption Spectrum of the SO_2 Clathrate Hydrate at 10 K.

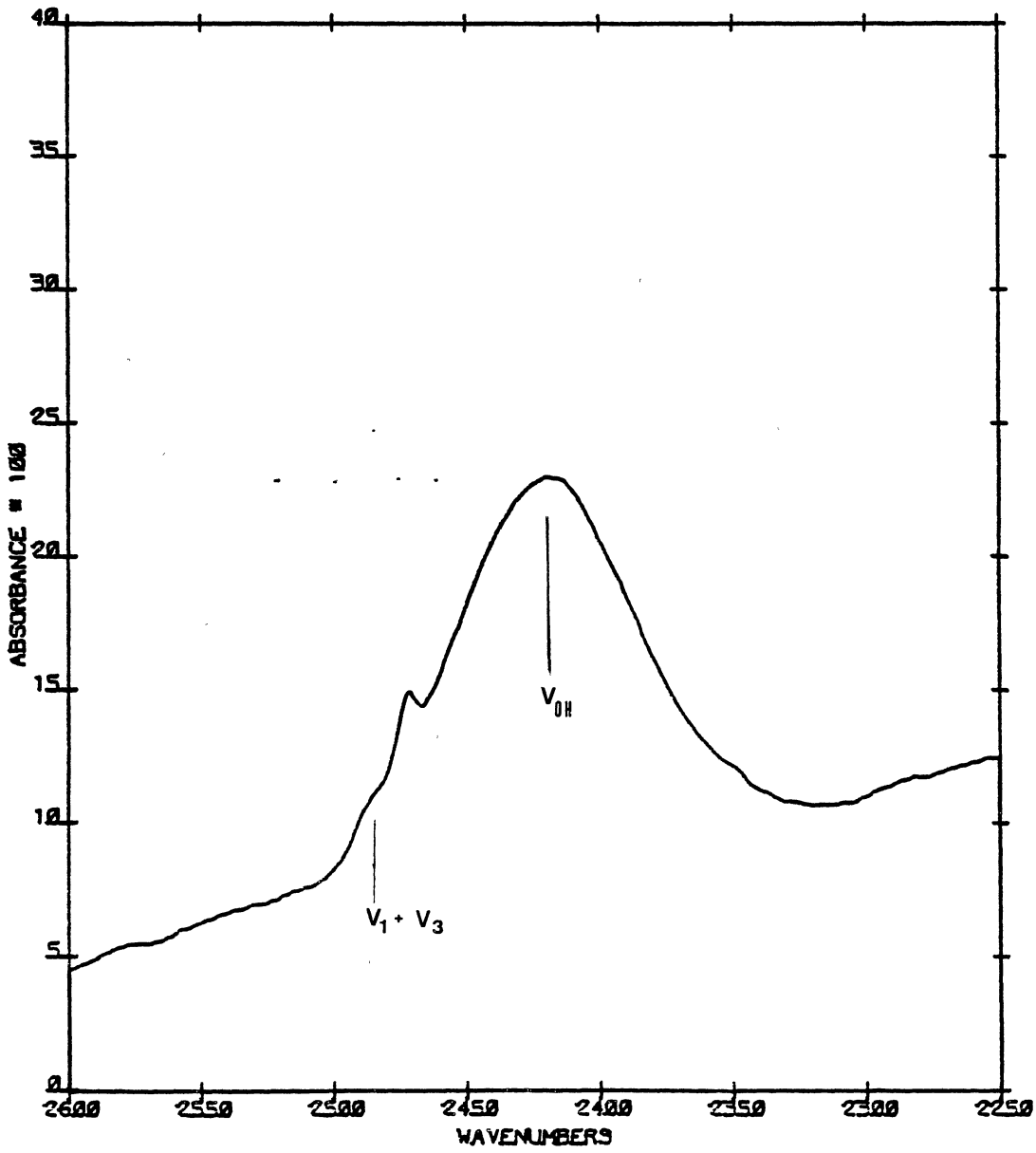
40
35
30
25
20
15
10
5
0
ABSORBANCE x 100
2600
2550
2500
2450
2400
2350
2300
2250
WAVENUMBERS
V_{OH}
$V_1 + V_3$

Figure 54. Sulfur Dioxide Enclathrated. A - 140 K; and B - 10 K.

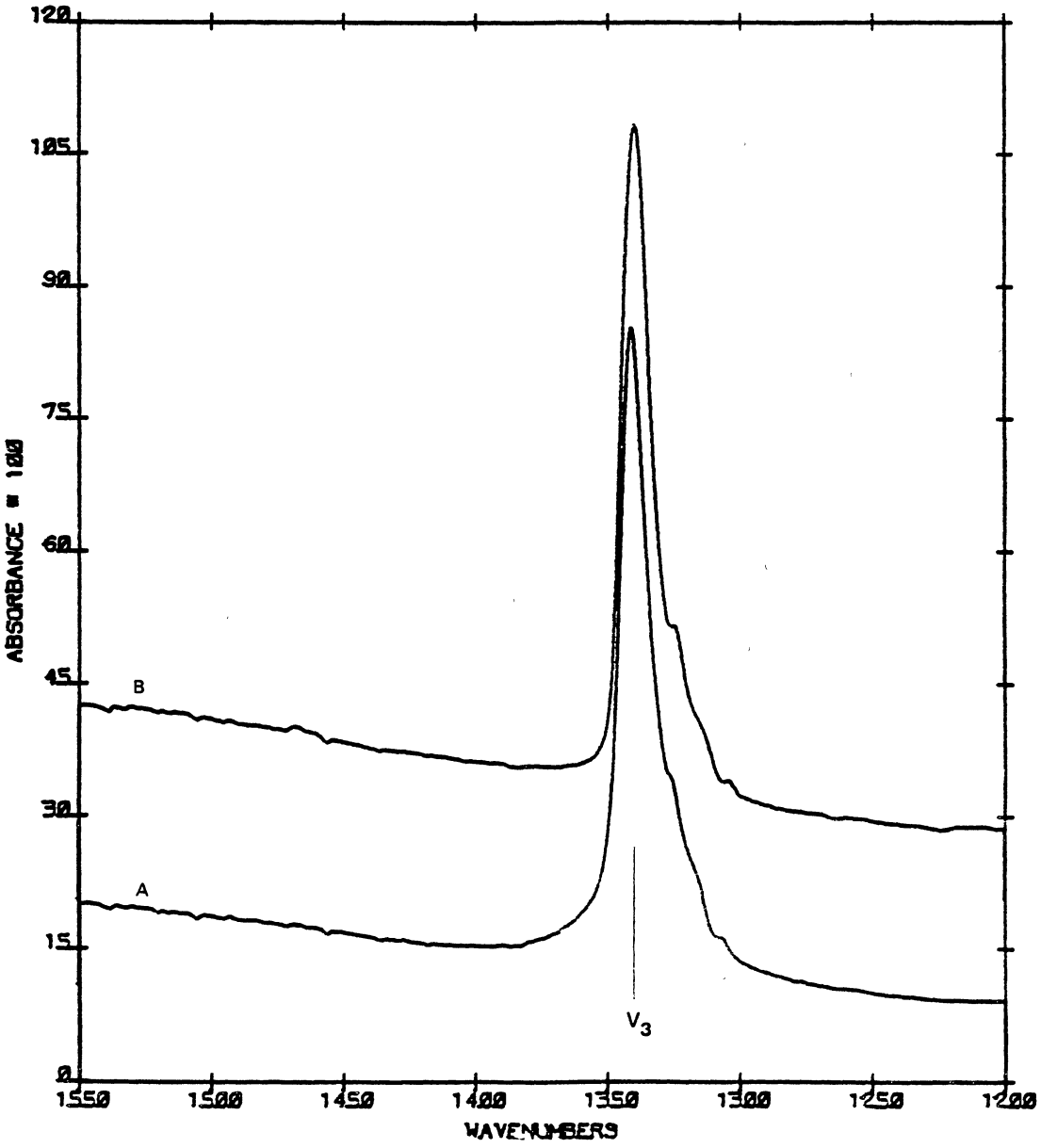
120
105
90
75
60
45
30
15
0
ABSORBANCE = 100
B
A
V_3
1550
1500
1450
1400
1350
1300
1250
1200
WAVENUMBERS

Figure 55. Sulfur Dioxide Enclathrated. A - 140 K; and B - 10 K.

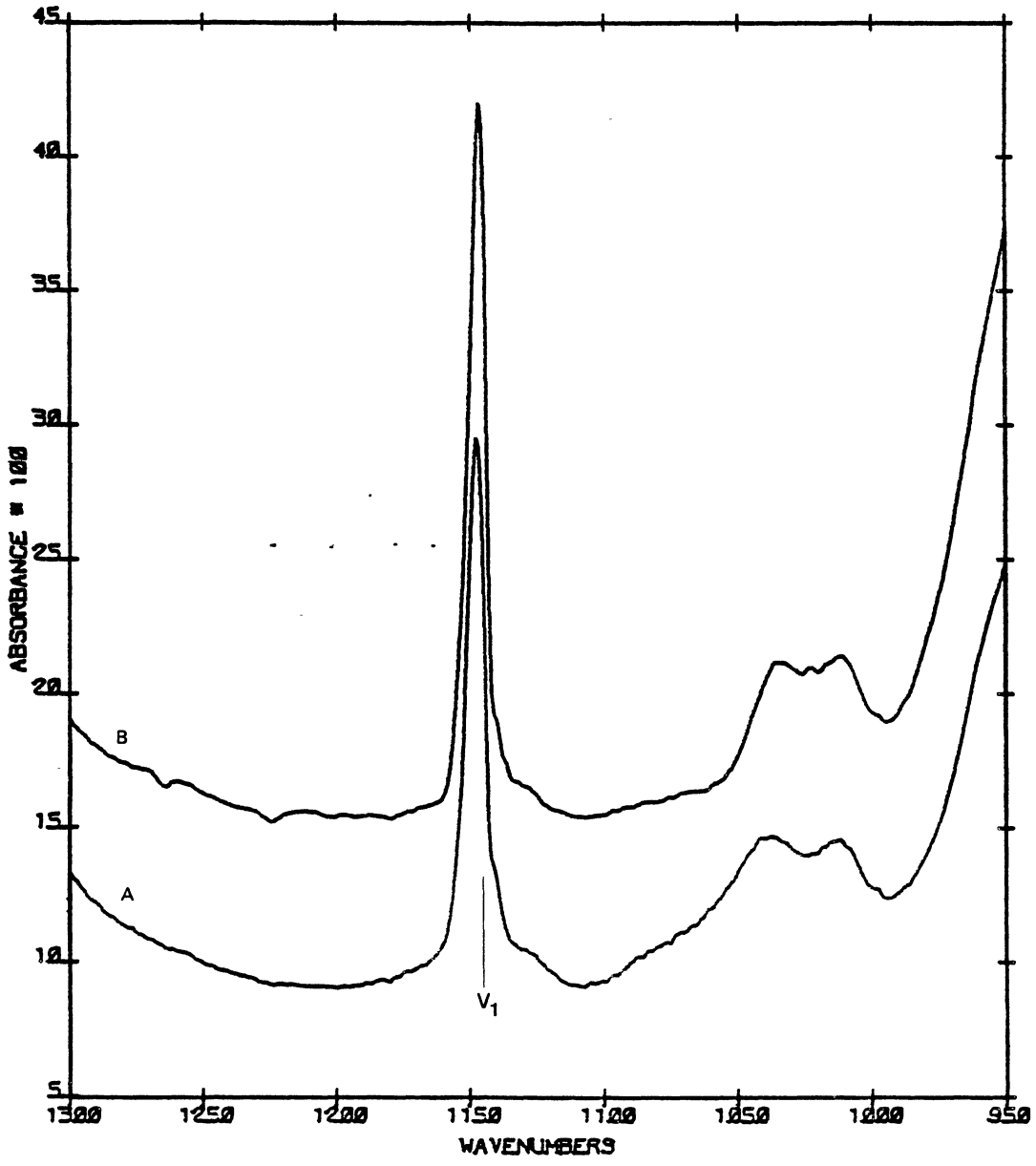
45
40
35
30
25
20
15
10
5
ABSORBANCE x 100
B
A
V_1
1300
1250
1200
1150
1100
1050
1000
950
WAVENUMBERS

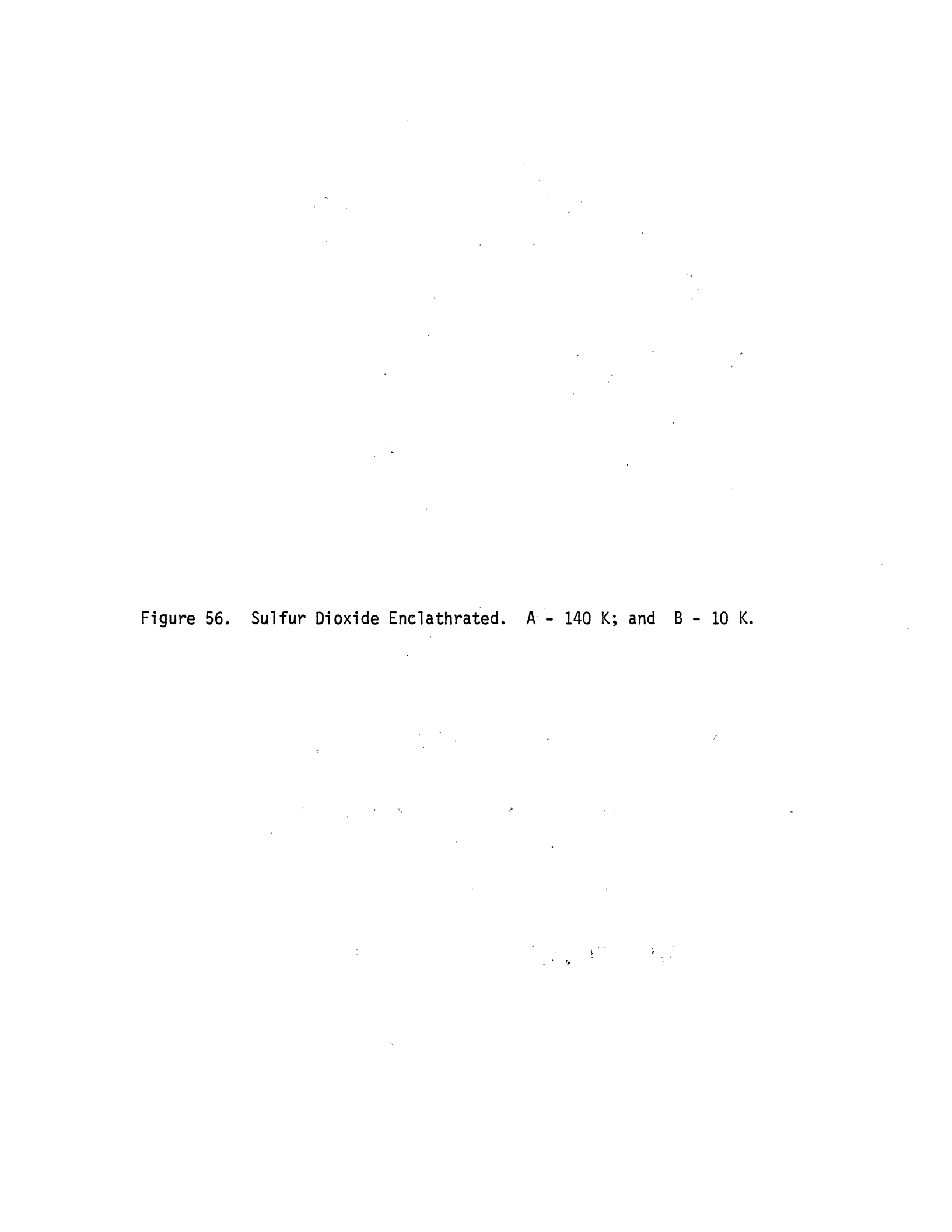

Figure 56. Sulfur Dioxide Enclathrated. A - 140 K; and B - 10 K.

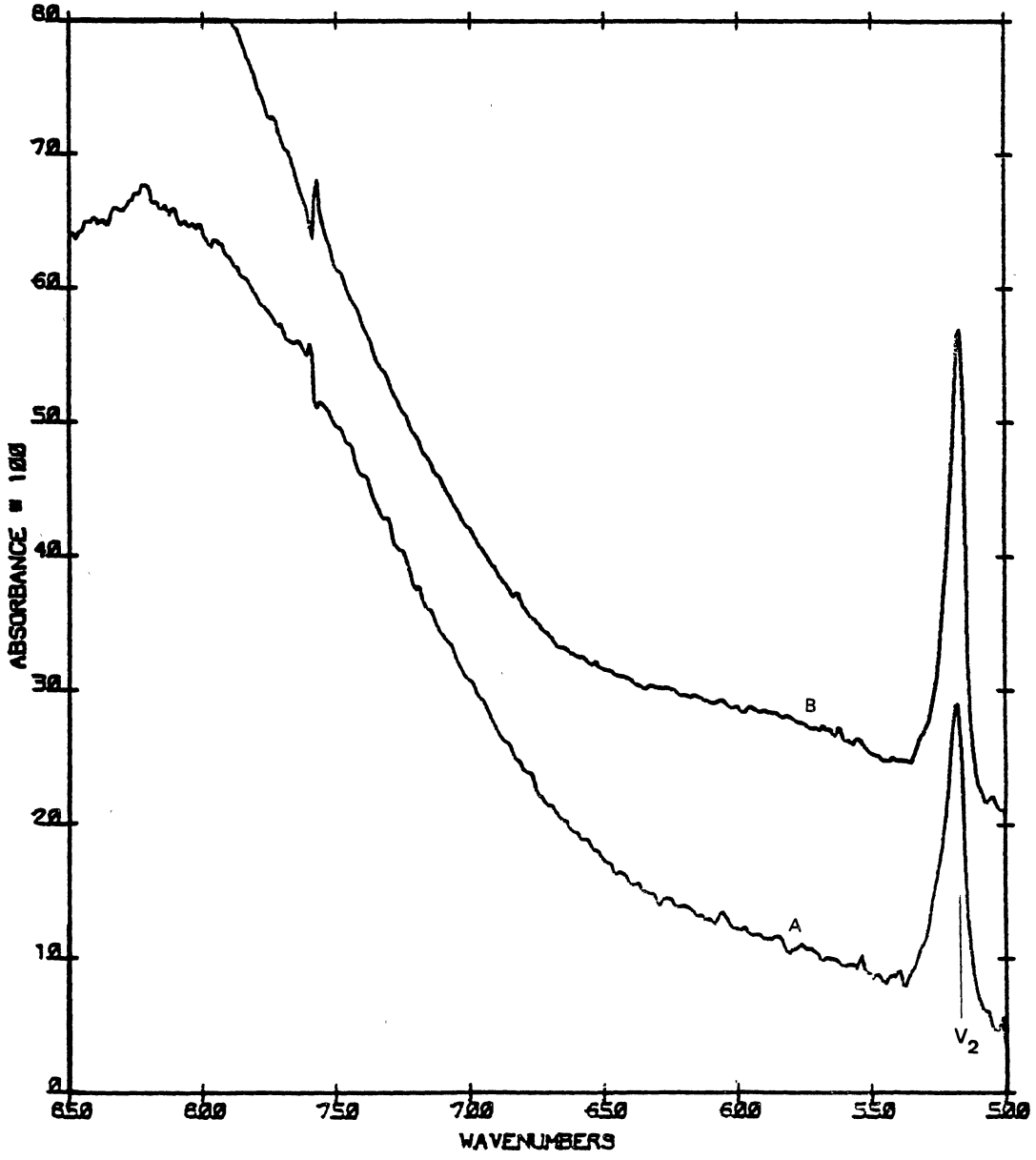
80
70
60
50
40
30
20
10
0
ABSORBANCE = 100
850
800
750
700
650
600
550
500
WAVENUMBERS
B
A
V_2

TABLE XIX

SO_2 CLATHRATE HYDRATE GUEST FREQUENCIES AT 10 K

ν (cm^{-1})	Assignment
2675	$2\ \nu_3$
2473	$\nu_1 + \nu_3$
1339	ν_3
1145	ν_1
1033	-
1011	-
517	ν_2

definitely observed at 2690 cm^{-1} and is probably caused by the overtone of the antisymmetric stretch (V_3) (see Figure 52), while a broad hole observed at 2635 cm^{-1} might be caused by the low frequency slowly decaying component of the antisymmetric stretch. The Evans hole at 2690 cm^{-1} almost certainly has to be in resonance with the combination mode of the clathrate hydrate lattice and not the isolated HOD molecules that are found in the hydrogen bonded network of the clathrate hydrate. This adds support to the interpretation that the observed shape of the Evans hole is from an E_2^o band that is essentially flat and that only a single minimum should be observed (see the Evans hole section in Chapter III).

Unfortunately, it was not possible to isolate D_2O into the hydrogen bonded chain of the SO_2 clathrate hydrate in order that a comparison between the proton migration rates in the SO_2 clathrate hydrate could be made to the proton migration rates obtained in the ethylene oxide clathrate hydrate. The same technique used to isolate the D_2O in the ethylene oxide clathrate hydrate (epitaxial deposition) was attempted with the SO_2-D_2O-H_2O vapor deposits with no success. One might suspect that the reorientation rates in the ethylene oxide clathrate hydrate are faster than they are in the SO_2 clathrate hydrate because the SO_2 clathrate hydrate would not form on a thin film of clathrate hydrate at 100 K. The sharp bands observed in the SO_2 clathrate hydrate infer that the SO_2 molecules in the cages have a small number of preferred orientations. Thus they are not isotropically oriented as is the case for the H_2S enclathrated molecule. However, it should be noted that there are no peaks that can be attributed to SO_2 enclathrated molecules in different cages as should be expected from the results of the

ethylene oxide and H_2S clathrate hydrates. One explanation might be that the sharp component of the SO_2 fundamentals are the SO_2 molecules in the small cages while the broad underlying band can be attributed to the SO_2 molecules in the large cages. However, this is mere speculation and more work in this area is needed.

Carbon Monoxide Clathrate Hydrate

The clathrate hydrate of carbon monoxide was formed by radiolysis of the ethylene oxide clathrate hydrate (see Chapter III, chemical effects of irradiation of the ethylene oxide clathrate hydrate). The CO molecule is a linear molecule with only one infrared active mode and is an ideal guest moelcule to study the degree of rotational mobility of the guest molecules in the cages of the clathrate hydrate. A comparison of the infrared spectrum between 130 and 10 K, of CO molecules that have been enclathrated is presented in Figure 38. At 10 K the half band width is only 6-7 cm^{-1} while the half band width at 130 K is approximately the same, however, it should be noted that a broad underlying band grows in as the sample temperature is raised. If the CO molecules were rotating in a fixed preferred orientation then high resolution peaks would be observed on either side of the 2136 cm^{-1} band. The peak at 2136 cm^{-1} should not be observed at all if the CO molecules rotated as they would in the gas phase — only the P and R branches would be observed and the O branch would be absent. Because the gas-phase like spectra was not observed, one can conclude that the CO molecules in the cages do not experience a gas like environment and the cell walls do effect the properties of the guest molecule in the cages. At temperatures around 130 K, one would expect that if

the molecules were freely rotating in the cage that the most probable rotational quantum number would be ∿4 and the maximum intensity in the vib-rotational envelope should be displaced on either side of the peak at 2136 cm^{-1} by ∿8 cm^{-1}. The CO band at 130 K does show a broad underlying band which might be attributed to this vib-rotational envelope. However, the strong intensity of the sharp peak at 10 K compared to the envelope intensity appears to argue against this interpretation. On the other hand, another interpretation would be that the CO molecules are not freely rotating in the cages but do have enough mobility in the cages to assume a wide spectrum of orientations at 130 K, thus the observed band broadening at 130 K. This interpretation of the observed infrared spectrum neglects the fact that the CO molecules in the two different type of cages should have different infrared spectra. Clearly more work needs to be done in this area so that a more exact assignment can be made.

General Trends Observed for the Clathrate Hydrates

The H_2S, SO_2 and the ethylene oxide clathrate hydrates all appeared to crystallize from the amorphous mixture to the clathrate hydrate at a temperature around 130 K. The isolated HOD frequency in the clathrate hydrate was impervious to the type of guest molecules enclathrated; thus, it could be used as an internal standard for clathrate hydrate crystallization. The lattice combination band around 1600 cm^{-1} shifted and broadened upon clathrate hydrate crystallization and was used as one guide in determining how complete the sample had crystallized from the amorphous mixture to the clathrate hydrate. The stretching bands

of the guest molecules in the clathrate hydrate shifted to higher frequencies as the temperature was raised while the isolated HOD band shifted to lower frequencies with higher temperatures. The guest molecules in the cages did not appear as "freely rotating" molecules but did assume a greater spectrum of orientations in the cages as the temperature was increased. It was possible to assign infrared bands from molecules that had been enclathrated in both type of cages for the H_2S and ethylene oxide clathrate hydrates and to speculate that in the SO_2 and CO clathrate hydrates, the contributions to the infrared spectrum from molecules in the different cages could not be neglected.

One might conclude from the above trends that the guest molecules have little effect upon the observed clathrate hydrate properties except for occupying space in the clathrate hydrate cages. It might be concluded that any clathrate hydrate could be formed by the method of vapor deposition and annealing, if the guest molecules could be contained in the amorphous mixture at the clathrate hydrate crystallization temperature of 130 K. However, the unsuccessful enclathration of CO_2 and ethane disproved the above conclusion. The boiling point of CO_2 is as high as ethylene oxide and the CO_2 clathrate hydrate was never formed from the vapor deposits of CO_2 and water even though the sample was annealed to 150 K. The amorphous sample converted to cubic ice at 150 K instead of crystallizing to the clathrate hydrate is expected. The unsuccessful preparation of the CO_2 and ethane clathrate hydrates might be attributed to the lack of a dipole moment in both of these molecules; whereas, all of the other successful guest molecules chosen had significant dipole moments (ethylene oxide being the most

polar). This interpretation is reinforced by the fact that the ethane-ethylene oxide mixed clathrate hydrate was indeed formed but as the ethylene oxide concentration was depleted the extent of formation of the clathrate hydrate decreased (46). Thus, one could conclude that clathrate hydrates with highly polar guest molecules form more readily than do clathrate hydrates with non-polar molecules.

CHAPTER V

CONCLUSIONS AND NEW AREAS OF PROPOSED RESEARCH

The first section of this chapter presents a list of different conclusions that can be made from the experimental research that was at the center of this thesis, while the concluding sections outlines different ideas that might be used to further understand the nature of clathrate hydrates.

Conclusions

1. Ethylene oxide clathrate hydrates can be formed by the method of vapor deposition and annealing.
2. The ring breathing mode of the ethylene oxide in the clathrate hydrate can be assigned. The band at 1290 cm^{-1} is the V_3 mode of the ethylene oxide molecules in the small cages, while the doublet at 1267 and 1265 cm^{-1} is from two preferred orientations of the ethylene oxide molecule in the large cages. The band at 1253 cm^{-1} splits into a doublet with high resolution and can be assigned as the isotopically shifted ethylene oxide molecules of the large cage.
3. It was possible to incorporate D_2O into the hydrogen bonded lattice of the ethylene oxide clathrate hydrate. The D_2O converted to HOD if the amorphous mixture of ethylene oxide-H_2O-D_2O was annealed to crystallize the sample to the clathrate hydrate, but if the

clathrate hydrate was grown epitaxially at 100 K, the clathrate hydrate could be formed with D_2O isolated in the lattice of the clathrate hydrate.

4. The half-life of the D_2O molecules in the ethylene oxide clathrate hydrate was only 9 minutes at 120 K. This is an unexpected behavior in the ethylene oxide clathrate hydrate because the same D_2O half-life in cubic ice was observed at a temperature around 150 K. This implies that the same concentration of protons in cubic ice at 150 K is present in the ethylene oxide clathrate hydrate at 120 K.

5. The activation energy determined from the hopping rate constant in the ethylene oxide clathrate hydrate was 4.5 ± 1.8 Kcal/mole.

6. An ionization energy of 15 Kcal/mole in pure ice is consistent with the proton transfer data obtained by Devlin and co-workers (9), and ionization energies greater than 15 Kcal/mole gave unreasonable hopping frequencies of the protons in pure ice.

7. The L defect trapping model could not fit the observed D_2O half-lives in pure ice to the predicted proton concentration of the model. However, the L defect trapping model was able to predict the observed activation energy in base doped cubic ice samples.

8. Evans holes were observed in the ethylene oxide clathrate hydrate and were attributed to the V_3 mode of the ethylene oxide molecule in both the small and alrge cages, while positive non-resonance bands were attributed to the overtone and combination modes of the ethylene oxide molecule in both the small and large cages.

9. Irradiation of the ethylene oxide clathrate hydrate with 1.7 MeV electrons transformed some of the ethylene oxide molecules in the cages to different products. It can be speculated from the observed change

in the infrared spectrum of irradiated samples that these products are: a) $CH_2=CH_2$; b) $CH_2=C=O$; c) CH_3-CH_2-OH; d) CO_2 and e) CO.

10. Irradiation of the ethylene oxide clathrate hydrate with 1.7 MeV electrons at 80 K converted all of the isolated D_2O in the sample to isolated HOD. Because in cubic ice the L defects are not mobile at 90 K while they are in the ethylene oxide clathrate hydrate at this temperature, one can deduce that the L defects in the ethylene oxide clathrate hydrate have a higher degree of mobility if the concentrations are nearly the same between the two crystals. From the comparison of Davidsons (4) activation energy for the reorientation of water molecules in the clathrate hydrate with ice (7.7 Kcal/mole for ethylene oxide clathrate hydrate; 13.2 Kcal/mole for ice), it appears as though both the L defect formation energy and the energy to mobilize the L defect might be lower in the clathrate hydrate than it is in ice.

11. A steady state concentration of coupled HOD was maintained in irradiated ethylene oxide clathrate hydrate at a temperature around 90 K. This phenomenon does not happen in pure cubic ice until temperatures around 140 K.

12. It was not possible to isolate D_2O in the clathrate hydrate lattice of the H_2S clathrate hydrate because the D_2O converted to HOD in the amorphous mixture. This conversion can be attributed to the formation of protons in the amorphous mixture by the acidic H_2S.

13. The enclathrated H_2S molecule in the small cages had a different infrared spectrum from the H_2S molecule which had been enclathrated in the large cages. The broad band centered at 2600 cm^{-1} was assigned to the H_2S molecule enclathrated in the small cages, while the band

centered at 2550 cm^{-1} was assigned to the H_2S molecule in the large cages.

14. The D_2S clathrate deuterate showed the same splitting of the D_2S molecule in the different cages as did the H_2S molecule.

15. Formation of the SO_2 clathrate hydrate grown epitaxially on a thin film of clathrate hydrate was unsuccessful. However, the SO_2 clathrate hydrate could be formed by the method of vapor deposition and annealing.

16. The infrared spectrum of the CO clathrate hydrate did not appear as a CO gas phase spectrum, indicating that the CO molecule had some restricted motion in the cages. It can be inferred from this observation that the CO molecule in the clathrate hydrate was not "freely rotating" inside the different cages, but probably had enough mobility at temperatures around 130 K to assume a wide spectrum of orientations inside the cages.

17. The O-D stretching mode of isolated HOD in the clathrate hydrate lattice was impervious to the type of guest molecule used and was an internal standard of clathrate hydrate crystallization.

18. The combination mode around 1600 cm^{-1} of the clathrate hydrate lattice shifted to lower frequency and broadened upon clathrate hydrate crystallization from the amorphous mixture.

19. The inability to form the CO_2 and ethane clathrate hydrate was attributed to the lack of a dipole moment in these molecules. One could infer from this result that the polar molecules will form clathrate hydrates more readily than non-polar molecules with the method of vapor deposition and annealing.

New Areas of Proposed Research

1. The proton transfer mechanism in the ethylene oxide clathrate hydrate might be determined by irradiation with high energy electrons and subsequent annealing.

2. The mixed clathrate hydrates of H_2S-ethylene oxide and SO_2-ethylene oxide would give added assurance that the H_2S and SO_2 clathrate hydrates were obtained.

3. Incorporation of D_2O into a type II clathrate hydrate and the subsequent kinetical analysis of the conversion of D_2O into HOD might supply the missing piece of information between the observed proton transfer rates of the type I clathrate hydrate and the proton transfer rates in the cubic ice.

4. A wide variety of polar and non-polar guest molecules could be enclathrated to determine what effect the dipole moments of the guest molecules have upon clathrate hydrate formation.

5. The isolation of D_2O in another type I clathrate hydrate and a comparison of its half-life in this hydrate with the observed half-life in the ethylene oxide clathrate hydrate might give some insights into the effect that the guest molecules have upon the proton transfer rates in clathrate hydrates.

BIBLIOGRAPHY

1. H. Davy, Phil. Trans. Roy. Soc. (London) 101, 1 (1811).

2. M. Faraday, Quart. J. Sci. 15, 71 (1823).

3. D. A. Wilms and A. A. van Haute, Proc. Int. Sump. Fresh Water Sea 3, 117 (1970).

4. D. W. Davidson, "Water, A Comprehensive Treatise", F. Franks, Ed., Plenum, New York, 1972, Chapter 2.

5. F. E. C. Scheffer and G. Meyer, Proc. Roy. Acad. Sci. Amsterdam 21, 1104 (1919).

6. G. A. M. Diepen and F. E. C. Scheffer, Rev. Trav. Chim. Pays-Bas 69, 593 (1950).

7. L. Pauling, Nature 57, 2680 (1935).

8. G. H. Cady, J. Phys. Chem. 87, 4437 (1983).

9. D. N. Glew and N. S. Rath, J. Chem. Phys. 44, 1710 (1966).

10. R. K. McMullan and G. A. Jeffrey, J. Chem. Phys. 42, 2725 (1965).

11. D. W. Davidson, Can. J. Chem. 49, 1224 (1971).

12. J. H. van der Waals and J. C. Platteeuw, Adv. Chem. Phys. 2, 1 (1959).

13. R. M. Barrer and A. V. J. Edge, Proc. Roy. Soc., Ser. A, 300, 1 (1967).

14. D. W. Davidson; S. K. Garg; S. R. Gough; R. E. Hawkins and J. A. Ripmeester, in press.

15. S. K. Garg; D. W. Davidson and J. A. Ripmeester, J. Magn. Resonance 15, 295 (1974).

16. D. G. Leaist; J. J. Murray; M. L. Post and D. W. Davidson, J. Phys. Chem. 86, 4175 (1982).

17. D. W. Davidson; S. K. Garg; S. R. Gough; R. E. Hawkins and J. A. Ripmeester, Can. J. Chem. 55, 3641 (1977).

18. S. R. Garg; B. Morris and D. W. Davidson, J. C. S., Faraday Trans. II, 68, 481 (1972).

19. D. W. Davidson and R. H. Cole, J. Chem. Phys. 19, 1484 (1951).

20. J. E. Bertie and D. A. Othen, Can. J. Chem. 51, 1159 (1973).

21. J. E. Bertie and D. A. Othen, Can. J. Chem. 50, 3443 (1972).

22. J. E. Bertie and S. M. Jacobs, Can. J. Chem. 55, 1777 (1977).

23. J. E. Bertie and S. M. Jacobs, J. Chem. Phys. 69, 4105 (1979).

24. J. E. Bertie and S. M. Jacobs, J. Chem. Phys. 68, 97 (1978).

25. J. E. Bertie and S. M. Jacobs, J. Chem. Phys. 77, 3230 (1982).

26. G. P. Johari, J. Chem. Phys. 74, 1326 (1981).

27. G. P. Johari and H. A. M. Chew, Nature 303, 604 (1983).

28. G. P. Johari and H. A. M. Chew, Phil. Mag. B 49, 281 (1984).

29. V. T. Aleksanyan; E. R. Razumova; A. P. Kurbakova and S. M. Shostakovskii, Opt. Spectrosc. 31, 369 (1971).

30. J. E. BNrtie and D. A. Othen, Can. J. Chem. 51, 1155 (1973).

31. K. B. Harvey; F. R. McCourt and H. F. Shurvell, Can. J. Chem. 42, 960 (1964).

32. A. H. Hardin and K. B. Harvey, Can. J. Chem. 49, 4114 (1971).

33. J. E. Bertie and J. P. Devlin, J. Chem. Phys. 79, 6340 (1983).

34. W. B. Collier; G. Ritzhaupt and J. P. Devlin, J. Phys. Chem. 88, 363 (1984).

35. S. Scheiner, J. Am. Chem. Soc. 103, 315 (1981).

36. J. F. Nagle and S. Tristram-Nagle, J. Membrane Biol. 74, 1 (1983).

37. J. P. Devlin and H. H. Richardson, J. Chem. Phys. 91, 3250 (1984).

38. M. Kunst and J. M. Warman, J. Phys. Chem. 87, 4093 (1983).

39. P. V. Hobbs, "Ice Physics", Clarendon Oxford, 1974.

40. Canady; Popee and Laidler, Can. J. Chem. 34, 1677 (1956).

41. J. C. Evans and N. Wright, Spectrochim. Acta 16, 352 (1960).

42. J. C. Evans, Spectrochim. Acta 16, 994 (1960).

43. J. R. Scherer; M. K. Go and S. Kint, J. Phys. Chem. 77, 2109 (1972).

44. A. Anderson; O. S. Binbrek and H. C. Tang, J. Raman Spectros. 6, 213 (1977).

45. P. A. Giguere and M. Falk, Can. J. Chem. 34, 1833 (1956).

46. J. P. Devlin, unpublished work.

APPENDIX A

VACUUM SYSTEM

The vacuum system used for clathrate hydrate preparation is shown in Figure 57. On the very left of the system is the H_2O reservoir (A) which was capped off from the system with a stopcock. Finger #1 (B) was used as a vacuum buffer from the rest of the system instead of storage and water was cryropump from the H_2O reservoir (A) into finger #2 (C) then shut off from the H_2O reservoir. In this manner contamination of the H_2O reservoir with the guest molecules was discouraged. From finger #2 (C) water vapor could be easily bled into bulb #1 (D) where the pressure in either bulb #1 (D) or #2 (E) could be read with manometer #1 (F). The scale for this manometer ranged from 0-1000 torr and manometer #2 (G) could be used if higher accuracy was desired but with only a range of 0-100 torr. Needle #1 (H) controlled the flow of gas out of bulb #1 (usually H_2O and various guest molecules) while needle #2 (I) controlled the flow of D_2O vapor out of bulb #2. The vacuum system was split in half by stopcocks which prevented contamination of the D_2O side of the system from the H_2O side. There were also three main lines connected to the cryrogenic cell to insure the removal of any contaminants from the cryrogenic cell or substrate. On the far right of the vacuum system the pressure was monitored by a Hastings thermocouple vacuum gauge (J) while the pressure maintained in the manifold (K) could be determined by the General Electric

Figure 57. Vacuum System Used for Clathrate Hydrate Preparation. A - H_2O reservoir; B - finger # 1; C - finger # 2; D - bulb #1; E - bulb #2; F - manometer #1; G - manometer #2; H - needle #1; I - needle #2; J - thermocouple vacuum gauge; K - manifold; L - ionization gauge; M - vacuum line to cryrogenic cell; N - vacuum line to pump; and O - D_2O reservoir.

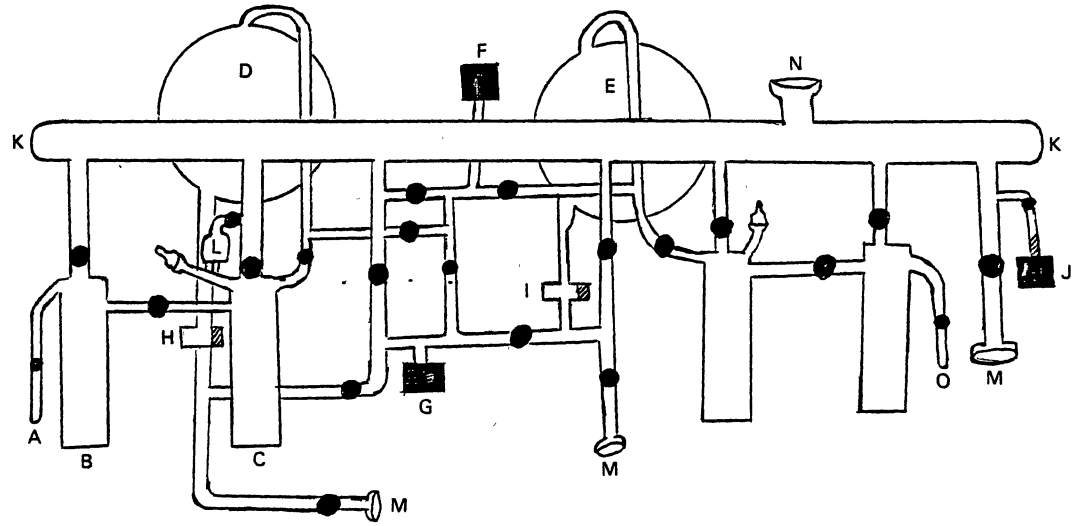
D
F
E
N
K
K
J
I
H
G
O
M
A
B
C
M
M

ionization gauge (L) located above finger #2. The thermocouple gauge was only able to read to a pressure of 1 micron, but the ionization gauge read many orders of magnitude above this and showed that the manifold maintained a pressure of about one tenth of a micron during deposition. However, most of the research reported in this thesis was made without the help of the ionization gauge because a malfunction in the gauge lead to its demise. The vacuum was maintained by a 3 stage diffusion pump in conjunction with a Welch duo sealed model 1402 roughing pump.

Digital Manometer System

The gas pressure in the different bulbs was monitored by a Validyne model CD223 Dual Channel Digital Manometer System. One channel was used to measure pressures in the 0-1000 torr range while the other channel was used to measure pressures in the 0-100 torr range. The 0-1000 torr manometer was calibrated using atmospheric pressure as a reference and then this manometer was used to calibrate the 0-100 torr manometer.

Needle Valves

The needle valves used in the vacuum system were the Whitey SS-22RS4-A type of micro-metering valves. Needle #1 was a straight pattern with a swagelok connection and O-ring stem seal while needle #2 was the identical valve except with an angle pattern. The calibration of the needle valve position with respect to the rate of pressure released from the different needle valves is shown in Figure 58.

Figure 58. Cryogenic Tip. A - substrate housing; B - D_2O flow tube; C - H_2O-guest vapor flow tube; D - CsI outside window; E - Aluminum window; F - thermocouple; G - CsI substrate; and H - cold side of the substrate housing.

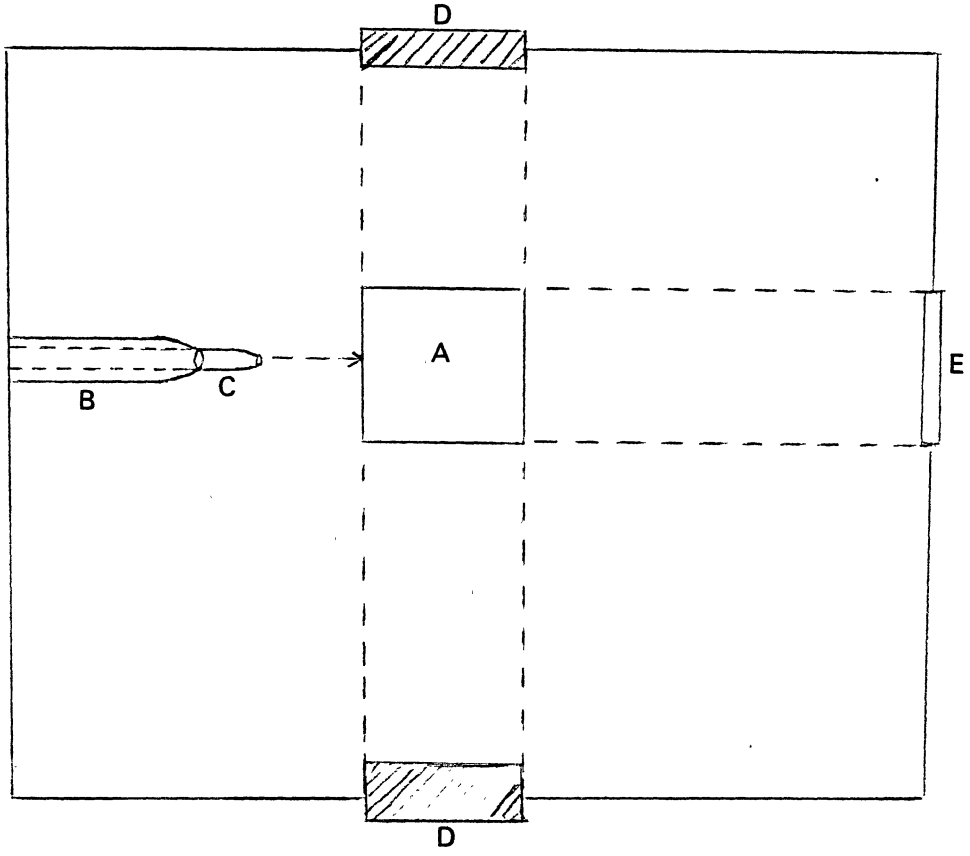
D
A
B
C
E
D

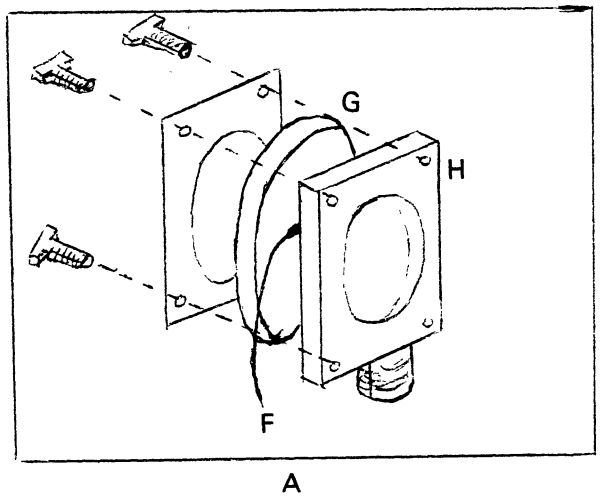
G
H
F
A

APPENDIX B

CLOSED-CYCLE REFRIGERATION SYSTEM

The closed-cycle refrigeration system used to cool samples to 10 K was a Displex closed-cycle refrigeration unit model CSA-202. This two stage refrigerature has an air cooled compressor instead of the water cooled compressor that is used by the model CSW-202 unit. At the base of the expander module is located the cryrotip which supports the copper substrate holder and CsI substrate (see Figure 59). The substrate and optical windows were CsI salt crystals which were polished and smoothed so that they were able to hold a vacuum and be optically transparent. The chromel vs gold iron thermocouple was connected between the substrate and the substrate holder (see Figure 59) and was connected on the cold side of the substrate, i.e. on the side in which the sample was deposited — the side with direct thermocontact to the cryrotip through the copper holder. The outside window opposite the deposition side of the substrate was made out of thin aluminum and was used to irradiate the sample with high energy electrons from a van de Graff generator.

Temperature Controller

The temperature was maintained to ± .5 K by an APD-B stepless controller with auxilary digital set point and temperature indicator.

Figure 59. Log of the Pressure Rate of the Various Bulbs Versus the Needle Valve Position Corresponding to the Bulb.

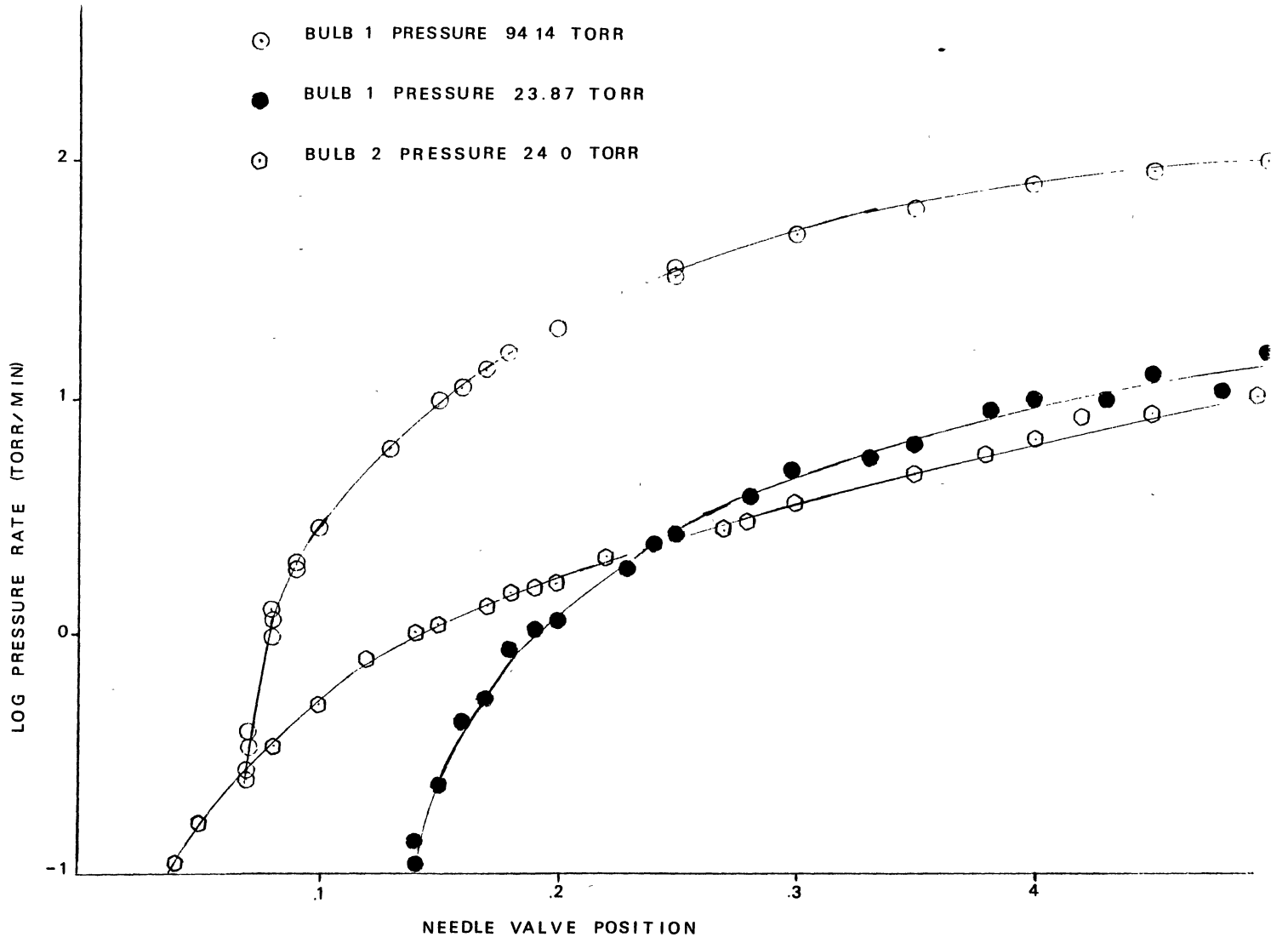
BULB 1 PRESSURE 94 14 TORR
BULB 1 PRESSURE 23.87 TORR
BULB 2 PRESSURE 24 0 TORR
LOG PRESSURE RATE (TORR/MIN)
2
1
0
-1
.1
.2
.3
4
NEEDLE VALVE POSITION

This temperature controller used zero crossing Thyristor (SCR) control and was also a proportionate controller with automatic reset and rate.

APPENDIX C

FOURIER TRANSFORMED INFRARED SPECTROMETER

The infrared spectrometer used was the Digilab FTS-2-C spectrometer. This is a single beam recording infrared spectrometer with a constant resolution between 0.1 and 0 cm^{-1} in the spectral range between 4000-450 cm^{-1}. The instrument has a Model 496A Michelson interferometer with a KBr beam splitter, an infrared source (Nernst graphite glowbar), a triglycine sulfate detector, an analog-to-digital converter, a data system with 8K of core memory, a 1.2 million word moving head disk, a digitally controlled plotter and a graphic and alphanumeric operator terminal. This particular spectrometer has the added feature that the sampling head can be evacuated and operates in a vacuum instead of nitrogen purged. All spectra were collected with triangular apodization and were computed from the average interferrograms via a fast fourier transform. The spectra were recorded with 2 cm^{-1} resolution except for spectra in which it was determined that higher resolution was necessary to differentiate unresolved bands.

VITA 2

Hugh Hill Richardson

Candidate for the Degree of

Doctor of Philosophy

Thesis: SPECTROSCOPIC DETERMINATION OF GAS-WATER INTERACTIONS IN CLATHRATE HYDRATES

Major Field: Chemistry

Biographical:

Personal Data: Born in Ft. Wayne, Indiana, November 19, 1954. Married August 1973; two sons ages 7 and 2.

Education: B.S., Oral Roberts University in 1979; M.S., Oklahoma State University in 1982; completed requirements for Doctor of Philosophy degree at Oklahoma State University in July, 1985.

Professional Experience: Graduate Teaching Assistant, Oklahoma State University, 1979-83; Graduate Research Assistant, 1983-84.

Memberships in Honorary and Professional Societies: American Chemical Society, Phi Lambda Upsilon (PLU) Honorary Fraternity and Tri Beta Biological Honorary Society.